AL-MUSTANSIRIYAH JOURNAL OF SCIENCE

VOL 1, DECEMBER 1976

College of SCIENCE, AL-MUSTANSIRIYAH UNIVERSITY BAGHDAD-IRAQ

CONTENTS

PRINTED BY THE UNIVERSITY OF MOSUL PRESS.

AL-MUSTANSIRIYAH JOURNAL OF SCIENCE

Volume 1, December 1976

College of science, Al-Mustansiriyah University Baghdad-Iraq.

Instructions for Authors:

1. Manuscripts should be Submitted in triplicate, they should be typewritten with double spacings. A margin of about 2.5 cm should be left onthe left hand side.
2. Both Arabic and English abstracts should be submitted, typed on separate sheets of paper.
3. The title of the Paper together with the name and address of the author (s) should be typed on a separate sheet. Name of author shouldbe written in full e.g Ahmed M. Ali.
4. Figures and illustrations should be drawn in black china ink on tracing Papers. Three photocopies of each diagram should also be submitted. Captions to figures should be written on the trace paper.
5. Tables should be arranged in such away so as to make them legible .
6. The same facts should not be given in tables and figures except when it is absoutely necessary to do so.
7. Reference numbers should be written between square brackets []. A list of referances should be given on a separate sheet of paper.
8. Where possible, Papers should follow the Pattern: Introduction, Experimental, Results and Discussion.

AL-MUSTANSIRIYAH JOURNAL OF SCIENCE 1976

Preface

The Board of Editors of (Al-Mustansiriyah Journal of Science) has the pleasure to introduce the first issue of this Journal to the scientific community in Iraq and the Arab World. It is hoped that this journal would be a positive contribution of Al-Mustansiriyah University to the development and progress of basic science in this part of the world.

The Journal accepts for publication original papers dealing with allfields of Science. All papers are refreed by national or international experts. Submitted papers are expected to be original, conciese and of high standard. The submission of a paper implies that it has not been submitted for publication elsewhere. The Journal also accepts for publication (Notes) and (Letters to the Editor).

The Board of Editors looks forward to the support of all scientists in Iraq and the Arab World in order to help in fulfilling its goals which are aimed to serve the progress of the nation.

The Board of Editors

POLAROGRAPHIC DETERMINATION OF MOLYBDENUM

Ahmed Khalil Ghonaim
Al-Mustansiriyah University, Faculty of Science,
Baghdad - Iraq

Received, 10 April, 1976

ABSTRACT

The polarographic behavior of Mo (VI) in solutions of CDTA* has been investigated. The effect of the pH of solution on both diffusion current and half-wave potential is studied. The half-wave potential is found independent on the CDTA concentration. The diffusion current is a linear function of the Mo (VI) concentration. A recommended method for the polarographic determination of Mo is proposed.

INTRODUCTION

The polarography of Mo (VI) and Mo (V) was always of interest. Ghonaim and Susic [1], reviewed the polarography of Mo in solutions of complexing and non-complexing agents till 1969. They also showed that Mo (VI) in the presence of DTPA is reduced at the M.D.E. giving rise to a well developed wave in the pH range 5.5-8. The half wave potential of the obtained wave is PH dependent and unaffected by the DTPA concentration. The linearity of the diffusion current with the Mo (VI) concentration was obtained up to 1.2 mM. They also succeeded to determine V in the presence of 10 folds of Mo (VI) in alkaline medium. Lassner[2], outlined an excellent review about Mo (VI) in the presence and absence of hydroxylamine, and Mo (V) with EDTA and other complexing agents and their applications in analytical chemistry.

Maximova and Staskova)[3] studied the behavior of Mo in solutions of acetic, citric, oxalic, nitriloacetic, phosphoric acids and in EDTA. The best defined waves are obtained in citric acid in the PH range (1.5-3.5), where the height of the waves remains constant. V and W have no interference effect.

---

* Cyclohexane diamine tetra acetic acid.

El-Inany and Veselinovic[4], utilized conc. H_2SO_4 in the presence and absenceof quinol and they showed that the height of the waves is proportional to the Mo concentration in the range from 1 mM to 14 mM. According to Zelinka *et.al.*[5], Mo (VI) in aqueous solutions of catechol , 3,4, dihydroxy benzene sulphonic acid, or tiron in the pH range 2-8 of chloroacetate, formate, acetate, pyridine or phosphate buffer yields two waves. 0.05 to 2 mM of Mo can be determined in 0.1 M catechol medium at pH 3.7 formate buffer by measuring the height of the first wave. The other two chelating agents are not satisfactory. The present work was carried out in order to recommend a method for the polarographic determination of Mo and to eliminate the interference of V and some other metals.

EXPERIMENTAL

Apparatus:

Lp 60a type polarograph (Czechoslovakia) was used for recording the polarograms. The polarographic cells used were those adopted specially for apparatus. An external saturated calomel electrode (S.C.E.) served as reference electrode. All experiments were performed at 25°C. The pH of the solutions was measured with a Beckman pH meter.

The capillary constans are : m = 3.2 gr/second, t = 4.5 sec./drop, while the mercury height is 20 cm.

Reagents:

Cyclohexane diamine tetra acetic acid (CDTA) was obtained from Fluka A.G. (Swiss). The stock solutions were prepared by dissolving the appropriate weights of sodium hydroxide just neccessary to dissolve in distilled water and diluted to 1 liter and molarity was checked by the recommended
diluted to 1 liter and the molarity was checked by the recommended methods.

All other chemicals used were reagent grade and used without further purification.

RESULTS AND DISCUSSION

Results:

Our experimental results indicates that Mo (VI) in the presence of CDTA gives one well-developed irreversible reduction wave due to an electron-transfer step involving one electron.

The reversibility of the electrode reactions wastested for each polarogram by determining the slopes of the curves of log $I_d - I/I$ vs the potential and checked by applying Tomes equation as rearranged by Meites[6]. The height of the wave is proportional to the square root of the mercury column which means that the reduction wave is diffusion controlled rather than rate controlled.

The effect of the pH of solution on the diffusion current and the half-wave potential of the obtained reduction waves was studied by recording the polarograms of 1 mM Mo (VI) and 15 mM CDTA using acetate buffer as supporting electrolyte. The pH was adjusted by the addition of NaOH or HCl.

At pH values less than 5, the diffusion current was found to be independent of the pH of solution. However, as the pH is increased, the diffusion current is decreased until it is completely diminished at pH higher than 7. This may be attributed to the fact that, as the pH is increased the number of the unreducible species are increased till pH about 7, where the Mo (VI)-(CDTA) complexes become totally inactive polarographically..

The half-wave potentials of theobtained reduction waves are also pH dependent, indicating the consumption of H_2 ions in the electrode reaction. From the slope of the line obtained by plotting $E_{1/2}$ vs pH, it is computed that one H^+ is participatingin the electrode reaction per Mo (VI) ion, since the slope is 0.085 V/pH unit and the average value of α n is 0.62 and applying the equation[7]:

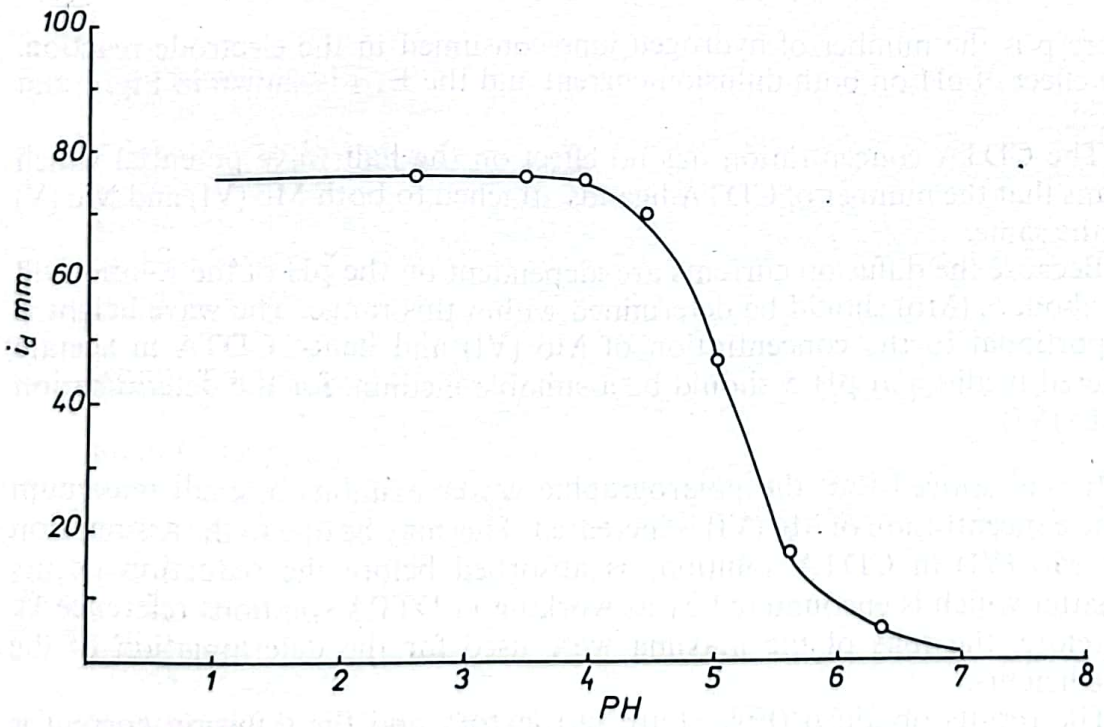

Fig. 1: Effect of pH on the wave height of Mo (VI) in the presence of CDTA.

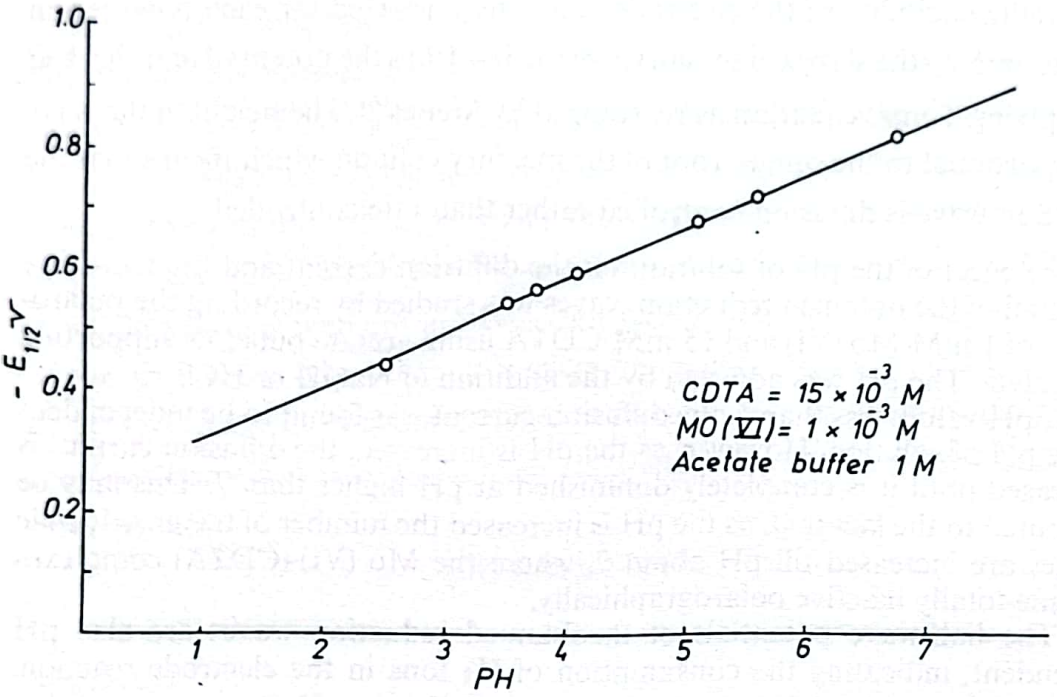

Fig. 2: Variation of $E_{1/2}$ with pH.

$$\frac{\Delta E_{1/2}}{\Delta pH} = \frac{0.05915}{\alpha n} p$$

where p is the number of hydrogen ions consumed in the electrode reaction. The effect of pH on both diffusion current and the $E_{1/2}$ is shown in Fig. 1 and Fig. 2.

The CDTA concentration has no effect on the half wave potential which means that the number of CDTA ligands attached to both Mo (VI) and Mo (V) are the same.

Because the diffusion currents are idependent on the pH of the solution till pH about 5, (Mo) should be determined within this range. The wave height is proportional to the concentration of Mo (VI) and hence CDTA in acetate buffered medium at pH 5 should be a suitable medium for the determination of Mo (VI).

It was noticed that the polarographic waves exihibits a small maximum as the concentration of Mo (VI) is increased. This may be due to the assumption that Mo (VI) in CDTA solutions is absorbed before the reduction occurs (a matter which is encountered by as working in DTPA solutions reference 1). Therefore, the tops of the maxima were used for the determination of the wave heights.

The results obtained (Fig. 3) are satisfactory and the diffusion current is proportional to Mo (VI) concentration from 0.2 mM up to 1.3 mM.

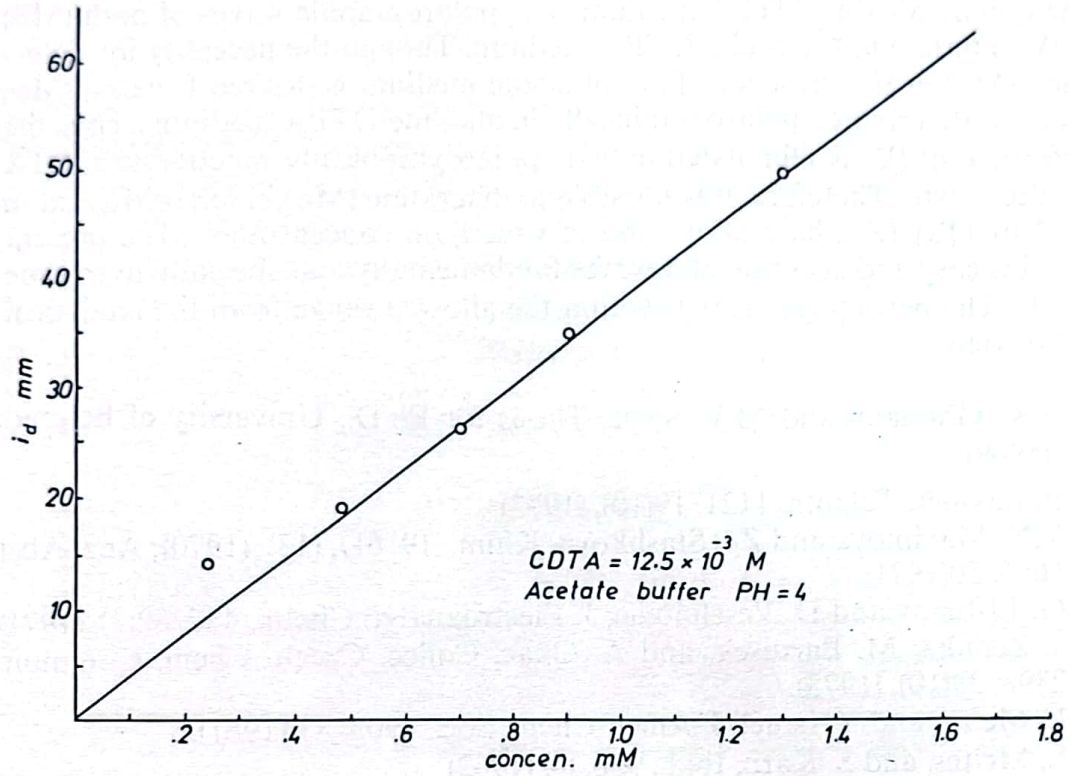

Fig. 3: Effect of Mo(VI) concentration on the diffusion current.

Interfering Elements:

Our experiments show that Te, Cr, Co, W, Ta, Nb, Zr and V are inactive polarographically all over the investigated pH range in the CDTA medium up to 10 fold excess. Al and Fe if present as in the case of ferro-molybdenum alloys can be separated by means of precipitation as hydroxides and filtration before the determination of molybdenum by the following recommended procedure:

Recommended procedure:

10 ml of the sample solution is transfered to the polarographic cell. Add 5 ml of 1 M acetate buffer of pH 4-5, and 10 ml of 0.05 M CDTA solution. Remove the dissolved air with oxygen-free nitrogen and record the polarogram from -0.2 to - 1.0 v vs S.C.E. Determine the concentration of Mo (VI) from a calibration curve.

Disussion:

The recommended procedures for the polarographic determination of molybdenum as indicated in the literature (8,9,10) are not sufficient. Our previous investigation[1] offers only a method for the determination of (Mo) alone in acidic DTPA solutions and for (V) in the presence of 10 fold excess

of (Mo) in an alkaline DTPA medium. The polarographic waves of both (Mo) and (V) interfere in the acidic DTPA medium. Though the necessity for determining (Mo) in the presence of (V) in acidic medium is desired because (Mo) can not be determined polarographically in alkaline DTPA medium . Thus the interference of (V) is eliminated as it is polarographically inactive in CDTA base electrolyte. Therefore, it is possible to determine (Mo) in ferro-Mo and in (W), (Nb), (Ta), (Zr), base alloys and in vanadium concentrates . The present method is easy and accurate and serves fundamentally and specially in routine analysis. The percentage error is within the allowed range from the analytical point of view.

(1) A.K. Ghonaim and M.V. Susic, Thesis for Ph.D., University of Belgrade (1969).
(2) E. Lassner, Talanta, 1121, 19(10), (1972).
(3) V.N. Maximova and Zh. Stashkova, Khim., 19 6D, (13), (1970); Anal.Abst. 1646, 20(1971).
(4) G. El-Inany and D. Veselinovic, J. Electroanalyt. Chem., 437, 32(3), (1971).
(5) J. Zelinka, M. Bartusek, and A. Okac, Collec. Czech. Chem. Commun., 2898, 38(10), (1973).
(6) L. Meites and Y. Israel, J. Amer. Chem. Soc., 4903, 83 (1961).
(7) L. Meites, and S. Karp, Ibid., 906, 84 (1962).
(8) R.S. Saxena and M.L. Mittal, J. Indian Chem., Soc., 1014,44(12), (1967).
(9) C.B. Riolo, T.F. Soldi and C.Occhipinti, Annali Chim., 1344, 57 (11), (1967).
(10) A. Hiroshi, Japan Analyst, 1073, 15 (1966).

الخلاصـــــــــة

درست الخواص البولاروجرافية للموليبدينوم في وجود CDTA وكذلك تأثير تركيز آيون الهيدروجين على كل من تيار الانتشار وجهد نصف الموجة . ولقد وجد أن تركيز CDTA ليس له أي تأثير على جهد نصف الموجة . أما تيار الانتشار فانه دالة لتركيز العنصر . وعلى ذلك اقترحت طريقة بولاروجرافية لتعيين تركيز الموليبدينوم .

PETROGRAPHY AND ORIENTATION STUDY OF PEBBLES IN TOBRA FORMATION, PUNJAB SALT RANGE, PAKISTAN

Samir A. Hussein and Issa M. Makhlouf
Geology Dept. Al-Mustansiriyah University.
Baghdad-Iraq

Received, 15 March 1976

ABSTRACT

The Tobra formation exposed in Punjab Salt Range was studied from stratigraphic and petrographic points of view. The boulder bed met at the base of this formation is composed of boulders, cobbles and pebbles of granite, quartzite, rhyolite, quartz, breccia, porphyries, jaspar, dolomite and conglomerate. Pebbles are studied as to their petrography, surface feature, size, shape, sphericity, roundness and orientation. Remarks to environment of deposition and source area are also given.

INTRODUCTION

Deposits of glacial origin are found over widely separated parts of India and Pakistan. They have been traced in Khashmir, Hazara (Tannaki Boulder Bed), Simla, Sikkim, Bhutan (Blani Boulder Bed), Salt Range (Tobra formation), Garhwai (Mandhali Beds) and in Rajputana, Bihar and Orisa (Talchir Boulder Bed).

The presence of boulder beds over large area of the subcontinent with pebbles and boulders often showing facets and striae of glacial origin along with a variety of other glacial and glaciofluvial deposits as positive indication of extensive glacial activity in this region during the Permo-Carboniferous time.

It is believed that the belt of the glacial deposits marks the northern limits of Gondwanaland of that time and necessarycorollary to that most of the boulder beds of India-Pakistan were laid down by glaciers into the sea,[1].

The Tobra formation which was earlier known as Talchir Boulder Bed[2] is known to the geologists of this region as consisting of the boulder bed of glacial origin, which resemble those found in Talchir area in India. The first published report on Tobra formation is by Stratigraphic Committee of Pakistan,

(G.S.P.)[3]. This report provided many intersting details about lithology, age fossils and facies change within Tobra Formation. Wadia[4] considered that the possible source area of the glacier deposits of Pakistan may have been radiated from the Aravalli outliers (South Punjab) which was quite high at that time.

The present work is an attempt to study the boulders of glacial origin exposed in Punjab Salt Range (Tobra Formation) and to deduce their nature and origin. The main work is done on stratigraphy, petrography, direction of transport and ultimately the location of the source area from where the glaciers may have moved.

LOCATION

The Punjab Salt Range lies in the western part of the Punjab, Pakistan, between longitudes 73° 35′-71° 30′N and latitudes 32° 24′-32° 56′ E., (Fig. 1),

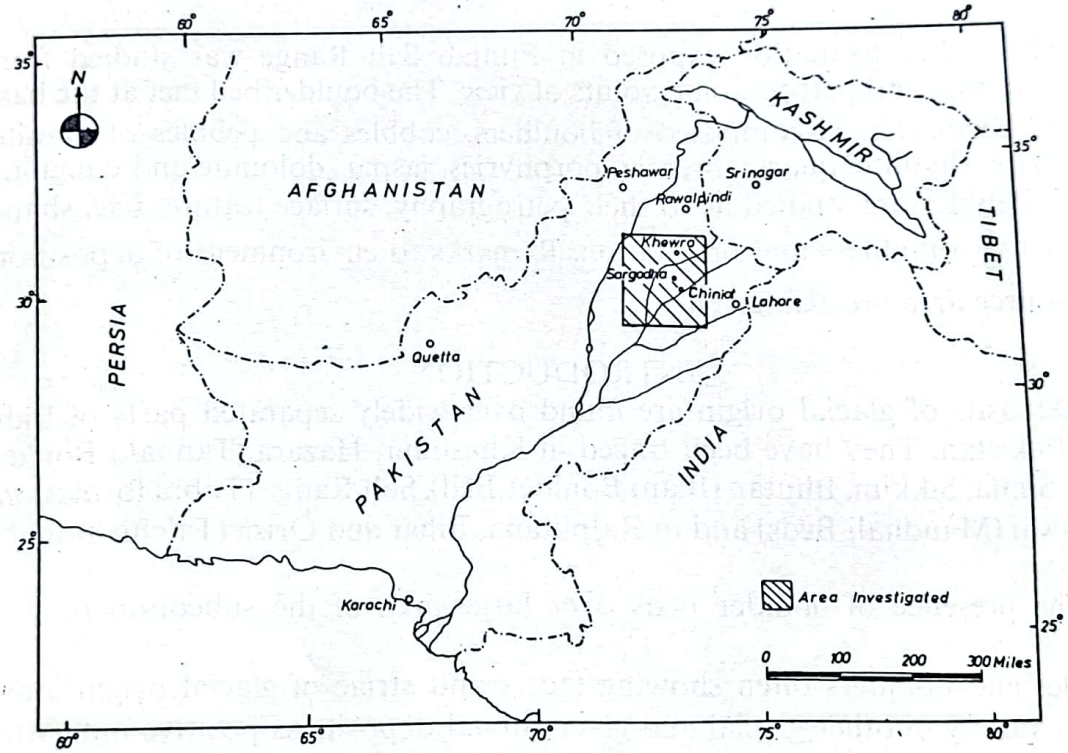

FIG. 1. LOCATION MAP.

eight sections have been studied*, where Tobra Formation is well exposed, these areas: Khewra Gorge, Tobra-Khewra, Tobra, Dondot, SE Pidh, Pidh, Nilawahan Ravine and Warcha Gorge.

---

* The sections were studied and sampled by the second author during his post-graduate fellowship (1974). The analyses and interpretations were carried out by the two authors Mustansiriyah University (1975-1976).

STRATIGRAPHY

The term Tobra Formation was assigned by G.S.P.[3] to over whelmingly petromict boulder bed, formerly called the Talchir Boulder bed. Formerly the age of the Tobra Formation was considered to be late Carboniferous on the basis of spores, leaf impressions and other remains of lower Gondwana Plants[1]. However, recent studies based on spores and pollens indicate that the age of the Tobra Formation is early Permian[3]. The boulder beds of similar age and nature are present in widely separated parts of Indo-Pakistan sub-continent. On Global scale the deposits of Permo-Carboniferous age and of glacial origin, are present in Australia (RisdunFormation), South Africa (Dywk series), East Africa (Lutoe series), South America (Tubarao series) and in many other areas lying in the southern hemisphere.

The following is a brief description of the different rock units of Tobra Formation, (from base to top).

1. Boulder Bed: It forms the basal part of Tobra Formation and maintains a thickness ranging between 10 to 15 feet. It consists of an unsorted assemblage of pebbles, cobbles and boulders ranging in size from few inches to a maximum of 4 feet across. The pebbles are composed of a variety of granitic rocks, quartizite, rhyolite, volcanic porphyries, quartz and small percentage of some dark coloured rocks embedded in fine clayey matrix. It can be called a petromiet boulder bed. There are some lenses and bands of clay intercalated within the boulder bed, which show pinch and swell structures.
2. Yellowish-Green Sandstone: It is very coarse grained sandstone, yellowish-green to yellowish-brown in colour and has a thickness ranging between 10 to 70 feet. Thick bands of gritty and pebbly material are interbedded at various stratigraphic levels. This sandstone bed is missing from the sections between Tobra-Khewra Gorge, Tobra and Warcha Gorge.
3. Carbonaceous Shale: It is a black coloured shale with nodular appearance, with a thickness ranging between 15 to 20 feet. Medium to large pebbles are embedded in the shale towards the top. The unit becomes more arenaceous towards the top in Khewra Gorge and near Pidh.
4. Coarse Grained Sandstone: It is exposed only in Khewra Gorge and near Pidh. It is yellowish-green, coarse grained sandstone, with a thickness varying between 40 to 60 feet. At many levels, angular fragments, pebbly bands and patches of boulder clay or the channel sand of finer material are interbedded.
5. Medium Grained Sandstone: It is a cream coloured, medium grained sandstone and finer in texture as compared with the underlying sandstonebed. It's thickness ranges between 20 to 70 feet. Intercalations of clayey and carbonaceous material are present.
6. Rusty-Brown Sandstone: It forms the upper most part of Tobra Formation. It's thickness ranges between 10 to 40 feet. This sandstone is very coarse grained and can be easily distinguished from the other units due to striking difference in colour and texture. Bed of grit and pebbles are frequent.

Fig. (2) shows the succession of Tobra Formation as exposed in the different studied sections.

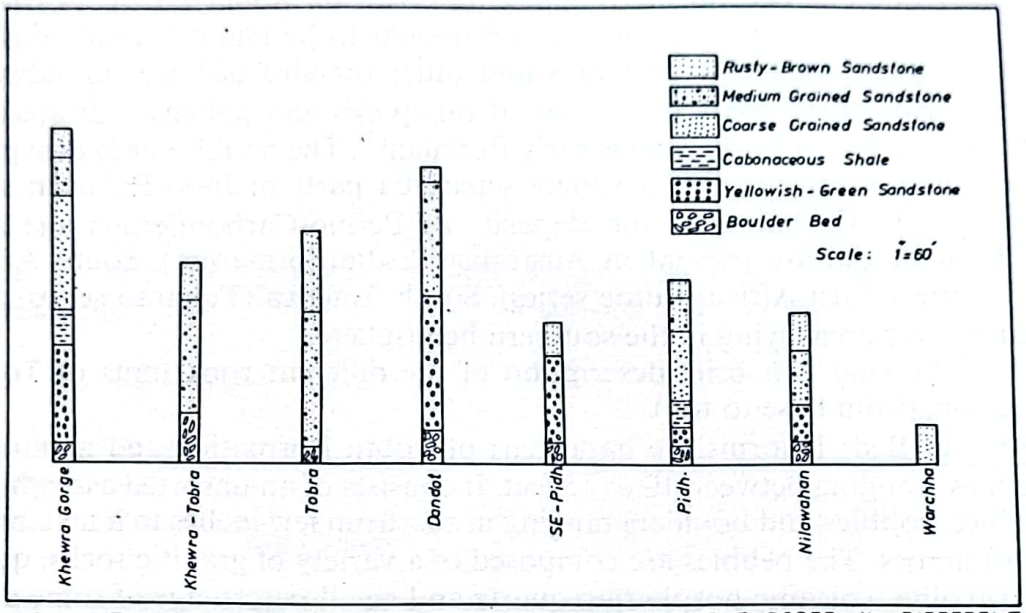

FIG. 2. LITHOLOGICAL COLUMNS OF THE TOBRA FORMATION AS EXPOSED IN DIFFERENT LOCALITIES.

PETROGRAPHY OF THE BOULDERS

The Tobra Formation included boulders, cobbles and pebbles of igneous, sedimentary and metamorphic rocks, e.g. granite, quartzite, rhyolite, prophyries, breccia, quartz, jaspar, dolomite, schist and conglomerate. Fig. (3) shows the percentage of different rock types which are counted in these pebbles.

Granites: Various coloured granite-boulders are included in the Tobra Formation, colour varies from pink, light pink, dirty white, light grey to almost dark grey in some cases. Most of the studied samples are fairly fresh, although completely weathered samples are observed. Texturally all the granites are coarse grained, hypidomorphic and inequigranular. Mineralogically, the granite pebbles are composed of feldspars (up to 55°/₀), quartz (10-25°/₀), biotite (12°/₀), muscovite (3-5°/₀) and chlorite. The feldspar grains are considerably altered, but fresh crystals of alkali feldspars and plagioclase are not uncommon. Quartz is present as discrete grains as well as an intersticial material. Some grains are fractured and free of any kind of inclusions. Biotite is fairly found as fresh grains, but has been usually altered to chlorite. The alteration has been started along the cleavage planes in biotite flakes, as can be seen in some crystals with alternate bands of green and brown colour. Muscovite is present as an accessory mineral , in the form of thin tabular crystals. Chlorite is found as alteration product of biotite. It is present mostly in the form of

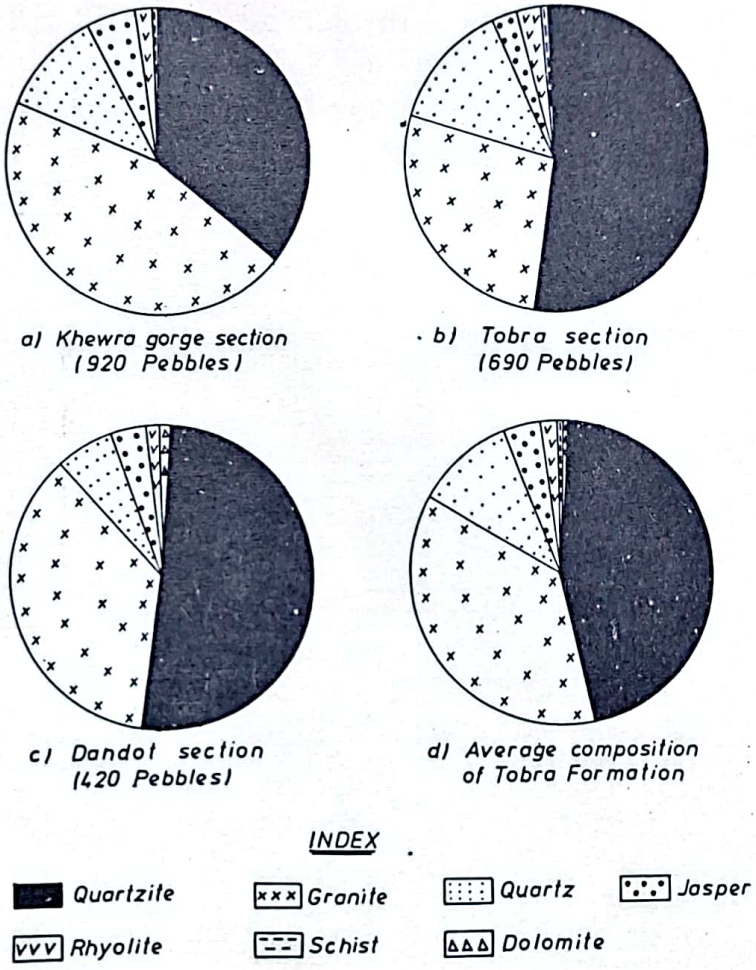

Fig. (3) Pie diagrams showing the average composition of Tobra pebbles in different localities.

irregualr elongated grains. However, some aggregate of spindle shaped of chlorite crystals are recognized (Fig. 4).

Volcanic porphyries; Fresh boulders of volcanic porphyries are present in light grey and dark brown colour. The colour is slightly darker on the fresh surface. Phenocrysts of quarkz and feldspars have been observed (Fig. 5) Greasy appearance on the weathered surface is a prominent feature. The microscopic study shows that chlorite, biotite and feldspars are the abundant constituent minerals alongwith iron and volcanic glass. Chlorite is present in the form of small anhedral crystals in the groundmass, or it is found as alteration product of biotite. Feldspar is present in the form of anhedral to subhedral crystals. Most of the feldspar crystals are altered, while few are comparatively fresh and show twinning. Biotite is present as elongated tabular flakes of dark brown colour. Margins of these flakes show alteration of chlorite at places. Quartz is present as euhedral crystals, some of the grains are fractured and filled with iron oxides (Fig . 6).

Rhyolite: Dark grey boulders of rhyolite are recognized in Tobra Formation. These boulders are very fine grained texture and consist of quartz (12%), potash feldspars, few crystals of plagioclase (andesine), with glassy and felsitic groundmass.

Fig. (4) Photomicrograph of granite showing aggregation of chlorite. Plane polarized light, X 50.

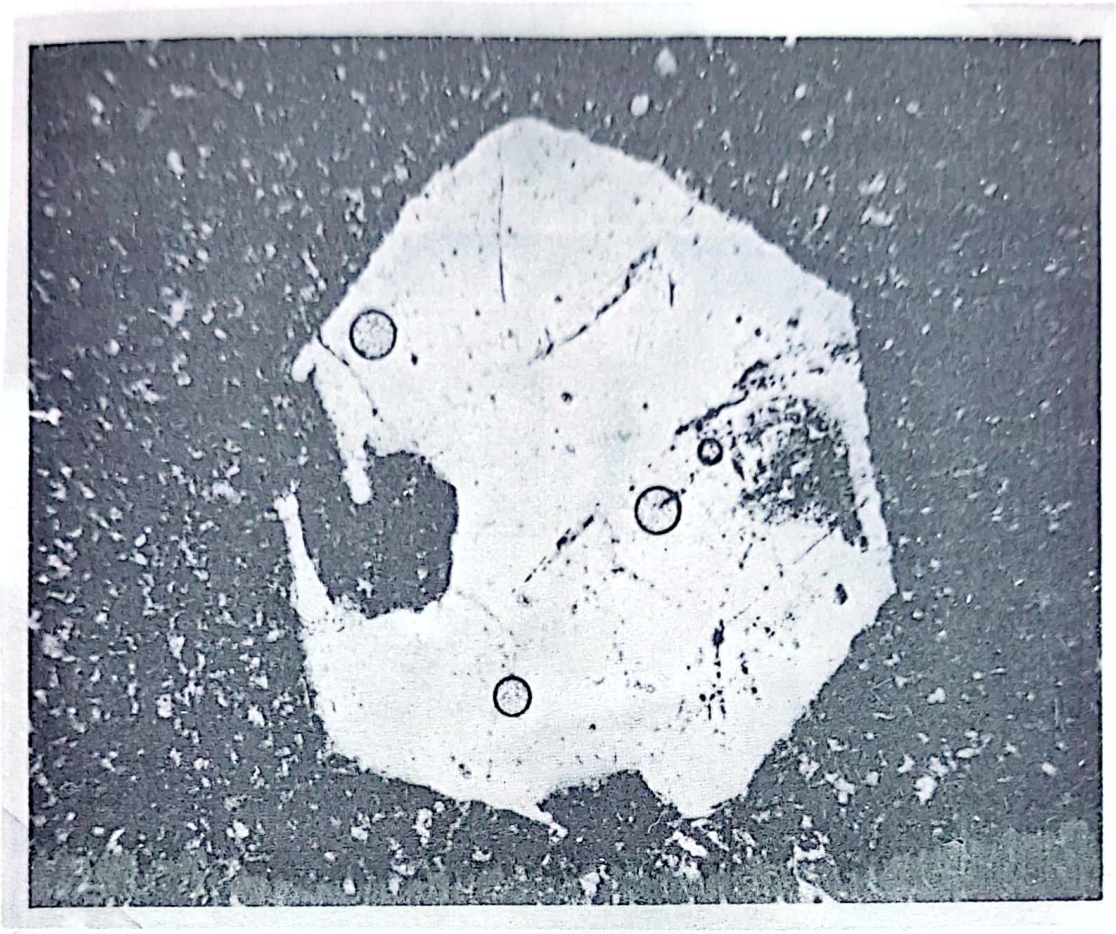

Fig. (5) Photomicrograph of porphyry showing an euhedral crystal of quartz which is surrounded by very fine grained material. Plane polarized light X 50

Volcanic breccias: These are brown coloured boulders and composed of angular rock fragments, main constituent of which is quartz. These angular fragments are embedded in volcanic glass and iron oxide matrix.

Quartzite: It is found as brown, dark grey and cream coloured pebbles. Mineralogically quartzite is composed of quartz, iron oxides, biotite, chlorite, muscovite, feldspars and opaque minerals. Quartz ranges between60-87% in frequency, and occurs as subangular to subrounded grains. Fractured quartz grains are not uncommon and the fractures are filled with iron oxides. Iron oxides are intersticial minerals and appear as rustybrown opaque minerals. Biotite is a common mineral of these quartzites which shows alteration to chlorite. Feldspar is present in the form of anhedral crystals. Most of the crystals of feldspar are altered.

Fig. (6) Photomicrograph of porphyry showing rounded fractured grain of quartz surrounded by very fine grained materials. The fractures are filled with iron oxides. Plane polarized light, X 50.

Conglomerate: Conglomerate is found as greenish grey and badly weathered boubоulders. They are composed of well rounded pebbles of rocks which are mainly composed of quartz and feldspars. The pebbles are embedded in an argillaceous matrix, (Fig. 7).

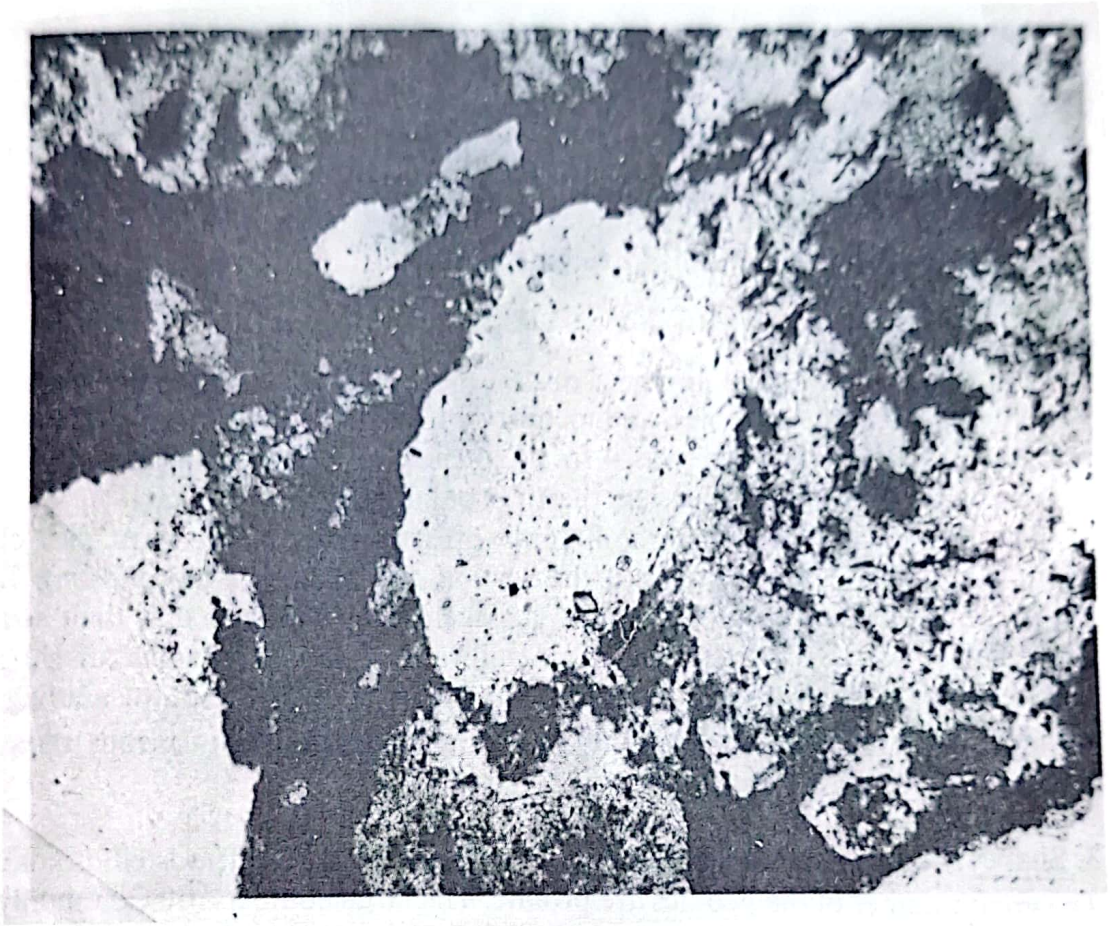

Fig. (7) Photomicrograph of conglomerate showing pebbles which are surrounded by iron oxides and argillaceous terials. Plane polarized light, X 50.

Dolomite: Light grey boulders of dolomite which are fairly fresh, are present in Tobra Formation. These boulders are very fine grained texture.

THE PEBBLE STUDY

The study of the general features of the pebbles and their orientation in Tobra Formation, is carried out to determine the nature of deposition. Attempt has been made to determine whether this formation is entirely of glacial origin or it is partly glacial and partly fluvial, lacustrine or marine.

1. Surface Features: Features like striations, scratches and faceting are characteristic of glacial marine are uncommon in this area. Only very few pebbles and boulders show glacial facet and striations which again are so insignificantly present that it is hard to say whether these features are realy of glacial origin.

There are no edges or corners on the surface of pebbles and they show an extreme degree of smoothness. Most of the pebbles have developed polished surfaces. This feature may be attributed to the later action of streams which have beenflowed there in the past. It was, however, interesting to note that steep excarpments which expose freshly weathered surfaces and the road cut sections also show the same characters of the pebbles and boulders. It is thus very evident that uniformly smooth and polished surfaces may have been developed by the original transporting agencies.

2.Size:

The fragments present in the Tobra Formation are of different grades. There are boulders, cobbles and pebbles of all sizes. The largest boulder measured in Khewra Gorge was 4 feet, 2 inches long (the maximum length). The least size of pebble is even less than 1/4 of an inch.

The big boulders are more commonly present in the lower most part of the boulder bed. Though some of the sections do not show any grading in the size of boulders from base to top, it is generally observed that their size decreases upwards. The decrease in size upward is, however, not systematic and often layers of large sized boulder at the upper levels interrupt the grading. Besides, the boulder sized fragments are present in the carbonaceous shale, especially in the upper part.

3. Shape:The most dominant shape of the pebbles and boulders is ellipsoidal. The great number of the pebbles are prolate. The large boulders are Commonly spherical in shape, especially in the lower part of the boulder bed. Rod-shaped pebbles are present in the pebble beds in sandstone at different levels. Discoidal shaped are rare.

4. Sphericity and Roundness: According to visual estimate, it has been infered that majority of pebbles and boulders are well rounded and their sphericity is between 0.7 and 0.8.

5. Pebble Orientation: The pebble orientation study is of great assistance in determining the direction of paleocurrent and nature of deposition. The random orientation of the pebbles would indicate entirely glacial origin, while preferred orientation of long axes of pebbles, having a definite inclination direction would point towards fluvial or glacio-fluvial origin, [5]. The orientation of the long axes of the ellipsoidal and rod-shaped pebbles almost normal to the bedding would indicate the direct deposition from the glacial mass.

The pebble orientation study was carried out in three different sections (Dandot, Khewra Gorge and Tobra) and more than 900 readings are obtained, from the boulder bed of Tobra Formation. The other pebble horizons have generally small sized pebbles in which the possibility of error could be greater.

The following readings were taken; the dip and strike of the bed, and the direction and inclination of the long axis of the pebbles. These readings were later plotted on Wulf's Stereonet and necessary correction were made in order to determine the pre-deformational attitudes of the pebbles [6]. The data obtained are represented in the form of circular diagram [7,8]. Using 10° class interval for each locality (Fig. 8), and for Tobra Formation as a whole

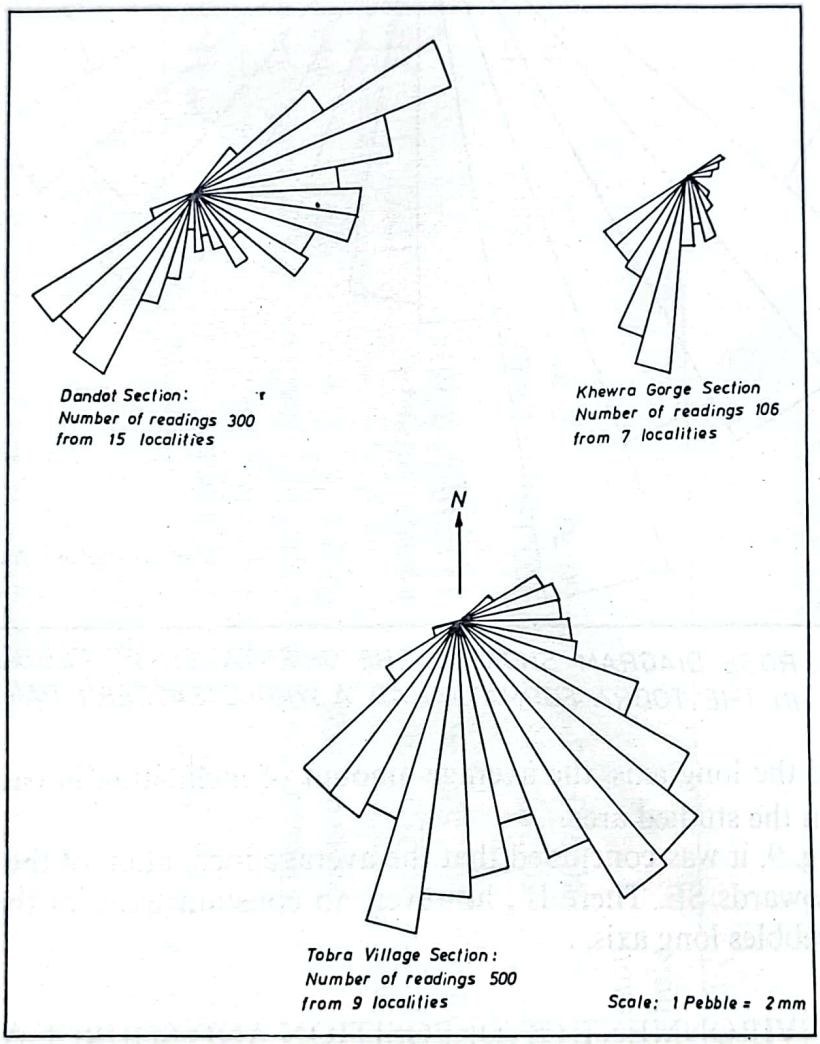

FIG. 8. ROSE DIAGRAMS SHOWING THE ORIENTATION OF PEBBLES IN THE TOBRA FORMATION (EASTREN PART).

(Fig. 9). The same data are also tabulated in Table 1, giving the dominant

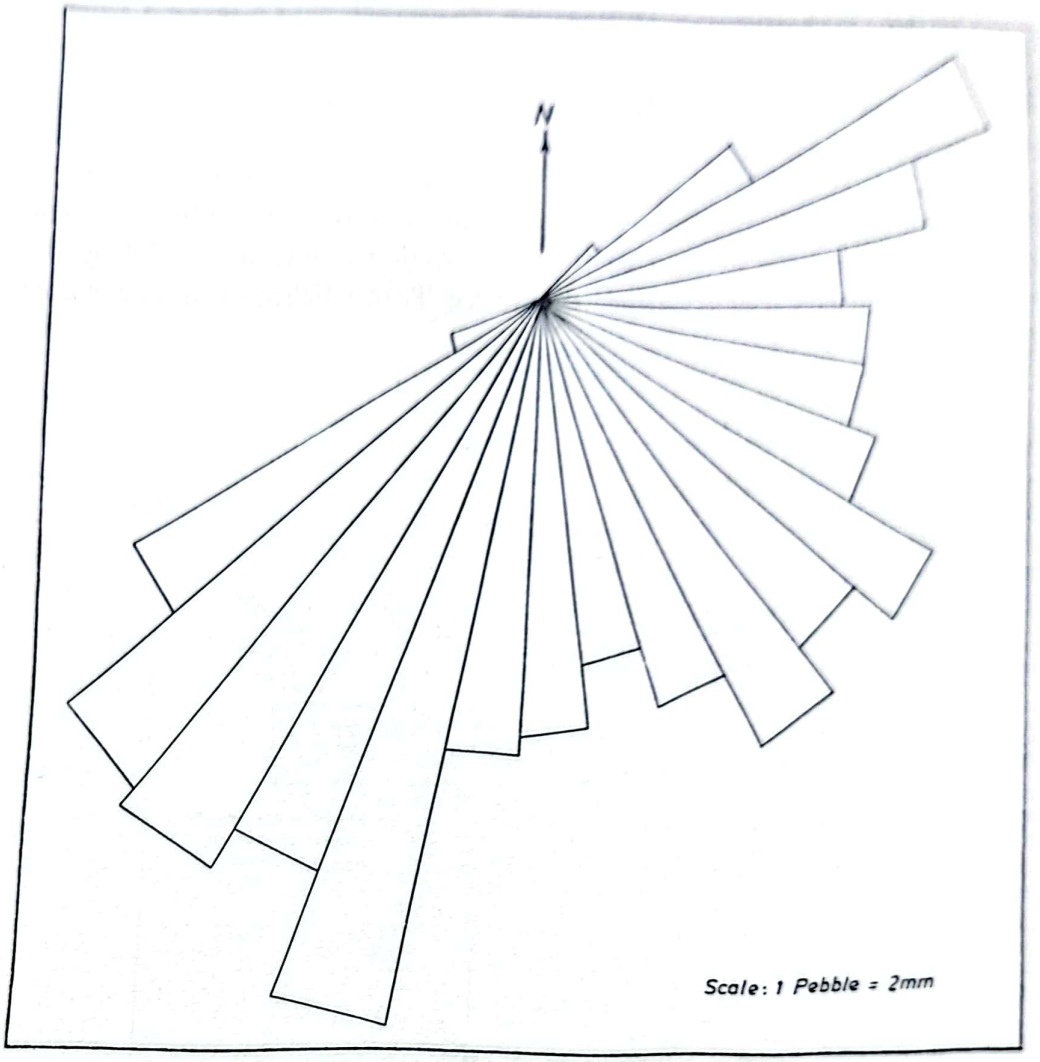

FIG. 9. ROSE DIAGRAM SHOWING THE ORIENTATION OF PEBBLES IN THE TOBRA FORMATION AS A WHOLE (EASTERN PART).

directions of the long axis, the average amount of inclination in each section and finally in the studied area.

From Fig. 9, it was concluded that the average inclination of the long axis of pebbles towards SE. There is , however, no constant trend of the orientation of the pebbles long axis.

ENVIRONMENT OF DEPOSITION AND SOURCE AREA

The study of the pebbles shows that few pebbles and boulders show glacial facet, striations and scratches. Most of the grains are smooth and with no edges or corners. This feature is attributed to the later action of streams.

Table (1): The analysis of the pebble orientation data

Section	General Spread	1st Maximum			2nd Maximum			Mos trend distinct
		°/₀ of readings	Trend of long axis	Inclination	°/₀ of readings	Trend of long axis	Inclination	
1. Dandot	40-250°	20°/₀	60-80°	0-24°	17°/₀	210-240°	1-18°	None
2. Khewra Gorge	60-240°	40°/₀	190-210°	3-16°	– –	– – – –	– – – –	190-210°
3. Tobra	50-250°	18°/₀	120-150°	12-30°	16.6°/₀	170-200°	11-24°	None
4. Tobra Formation as a whole	40-250°	5°/₀	60-70°	0-20°	7°/₀	190-200°	0-28°	None

The overlying sandstone beds have occasional pebbly and gritty beds with distinct cross-bedding. Carved sediments are also observed. All these features are indication of changing conditions of deposition from glacial to glacio-fluvial (at places glacio-lacustrine) and finally to shallow marine. While the lateral facies change is very much there, they are not as systematic as described by Teichert (In G.S.P.) [3]. True tillitic facies are not observed at all during the course of the present work. In fact lateral variations are of local nature and depend on the position of land and sea. The glacier may have moved in valleys and on gently sloping surfaces towards the sea.

The petrographic study of Aravalli outliers (southern parts of Punjab) shows that they consist of sandstone, siltstone, breccias, volcanic tuffs, quartzite and pebbly carbonaceous rock. There is no match in lithology between Tobra Formation in Salt Range and Aravalli outliers. Besides, Aravalli outliers reveal that within the outliers there are deposits of glacial origin near Chenab and Rabwah which prove that the great masses of ice may have radiated from Rajastan region further south.

CONCLUSION

The Tobra Formation exposed in Punjab Salt Range was studied from stratigraphic and petrographic points of view. Six units were recognized in this formation, these are from top to base: Rustybrown sandstone, medium grained sandstone, carbonaceous shale, yellowish green sandstone and boulder bed. The boulder bed is composed of granite, quartzite, rhyolite, quartz, breccia, porphyries, jaspar, dolomite and conglomerate. Most of pebbles are well rounded, polished and only a small percentage of the pebbles has striations and facets. Besides, the pebble orientation study shows general inclination of the long axis of pebbles towards SE. There is however, no constant trend of the orientation of the pebbles long axis. All features are attributed to the later action of streams. Vertical succession of Tobra Formation reveals the change of conditions of deposition from glacial to glacio- fluvial (at places glacio-lacustrine) and finally to shallow marine. Aravalli outliers in Punjab are not the source area because there is no match in lithology of the two .

REFERENCES

(1) M.S. Krishnan, Geology of India and Burma (4th eddition): Higginbothams (P) Ltd., Madras (1968).

(2) A.N. Fatmi, Lithostratigraphic units of Kohat-Potwar Province: Stratigraphic Committee of Pakistan, (1964).

(3) Memoirs of the G.S.P., 1964, vol. 10, Lithostratigraphic units of Kohat-Potwar Province, Indus Basin, Pakistan: Stratigraphic Committee of Pakistan.

(4) D.N. Wadia, Geology of India: The E.L.B.S. and Macmillan Co. Ltd., London. (1966).

(5) F.J. Pettijohn, Sedimentary rocks: Harper and Row, New York. (1957).

(6) J.C. Haff, Preparation of Petrofabric Diagrams: Am. Min., Vol. 23, 543-574 (1938).

(7) B.R. Pelletier, Pacono Paleocurrents in Pennsylvania and Maryland: Bull. of the Geol. Soc. of America, vol. 69, 1033-1064, (1958).

(8) F.P. Williams, and R. Rast, The Sedimentation of a River: Jour. Sed. Pet., 39 (1969).

الخلاصـــــــــــة

تمت دراسة تكوين طوبرا الذي يظهر في سلسلة بنجاب من الناحيتين الاستراتيجية والبتروجرافية . وتتكون طبقة الحصى التي تقع اسفل هذا التكوين من حبيبات من الجرانيت الكوارتزيت ، الريوليت ، الكوارتز ، البريشيا ، البوفيرى ، الجاسبر ، الدولوميت والكونجلوميرات . وقد تم وصف هذه الحبيبات من النواحي البتروجرافية ومعالم السطح والحجم والشكل والتكور والتدور والترتيب ومن ناحية اخرى تمت مناقشة بيئة الترسيب والمصدر الصخري لهذه الحبيبات .

PETROLOGY AND MINERALOGY OF SOME EGYPTIAN BLACK SHALES

Samir Ahmed Awad Hussein
Geology Department, Al-Mustansiriyah University
Baghdad, Iraq .

Received, 19th Feb. 1976

ABSTRACT

The black shale intercalations within the so-called "variegated shale" have been analyzed to determine their stratigraphic, petrographic, mineralogical, chemical and physical properties . Petrographic studies including grain size and thin section analyses were made and interpreted. X-ray diffraction and differential thermal analyses data are discussed to identify the mineralogy of these balckshales. A general discussion of their environment of deposition is also given.

INTRODUCTION

Much has been published concerning clay and shale deposits in Egypt. The majority of these papers discusses the paleontology, biostratigraphy or the petrography of some selected formations. "Black" or "steel" shales have widespread occurrence within the different encountered formations in Egypt, e.g. Variegated shale (Lower Maestrichtian), Dakhla Shale (Maestrichtian-Danian) and Esna Shale (Paleocene).

The aim of the present work is to study some occurrence of black shales intercalated within the variegated shale member. Four samples are chosen from four localities for this study, where best sections of these shales are attained. This study was pursued to give in detail the mineralogical, chemical, physical and petrographic properties of the black shales. A general discussion of the environment of deposition and origin of black shales are also given.

Geologic setting and Lithostratigraphic Characters of the Black Shales:

The stydied shale samples are collected from four localities, (Fig. 1): Gebel Abu Tartur (Kharga Oasis), Gebel Teneida (Dakhla Oasis), Aswan and Quseir. The black shale laminations are found as thin bands with in the so-called variegated shale member. which consists mainly of bedded shale and siltstone

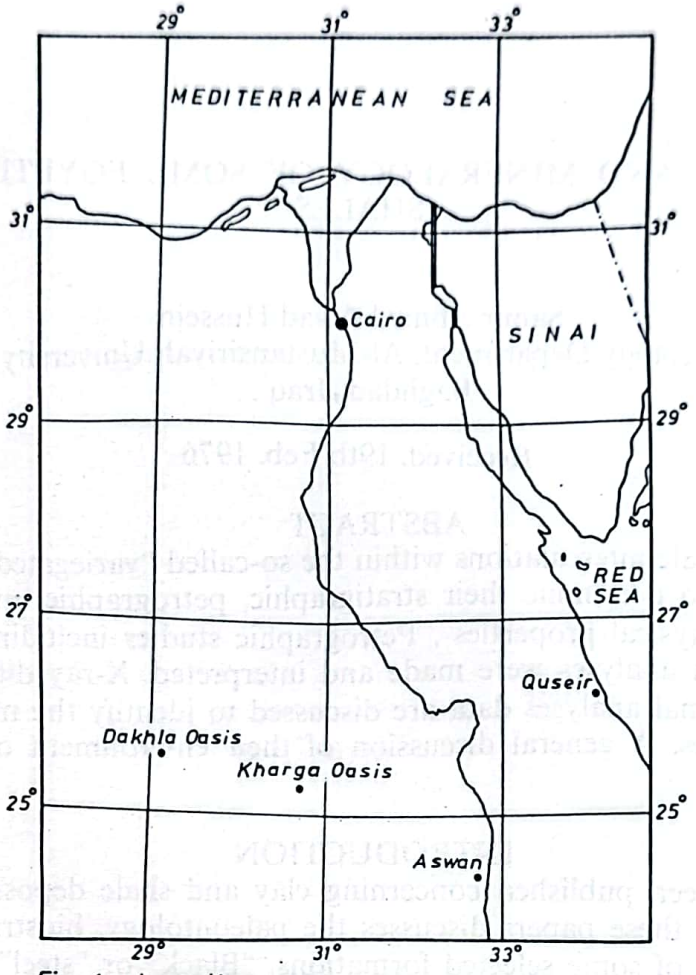

Fig. 1. Location map.

strata exhibiting a wide variation in colours. The variegated shale beds constitute the upper part of the "Nubia" formation (Pre-Maestrichtian) and range in thickness from few meters up to 70 meters.

The variegated shales are encountered in different localities in Egypt, e.g. Kharga Oasis, Dakhla Oasis, Nile Valley, Quseir, Safaga and Central Sinai. Beadnell[1] was the first to describe a section of 116 m thick shale below the phosphate beds in the Nile Valley. Ghorab[2] gave the name "Quseir Formation" to the variegated shale which overlies the Nubia Sandstone and underlies the phosphate beds in Egypt. Youssef[3] was the first author who suggested the name "Quseir variegated shale" for this unit. Hermina[4] considered the variegated shales as formation constituting the upper part of the "Nubia group".

Many authors described the faunal and floral content of the variegated shales, e.g. Newton[5], Edwards[6], Seward[7], Cox[8] and Faris and Hassan[9].

The black shales are found as intercalated bands within the variegated shales, ranging from thin limited beds to moderatly thick extensive sheets

or lenses. The shales are generally nonfossiliferous, although visible fragments or structures of plant remains have been recorded. Most of the black shales are thinly laminated, moderately hard and have abundant pyrite and /or marcasite nodules[10]. Large clayironstone concretions are characteristic of some layers. Most of the black shale bands are black or steel-grey in colour and contain flatty, waxy, resinous, carbonaceous or bituminous materials.

Fig. (2) illustrates the general succession in the studied areas. From this

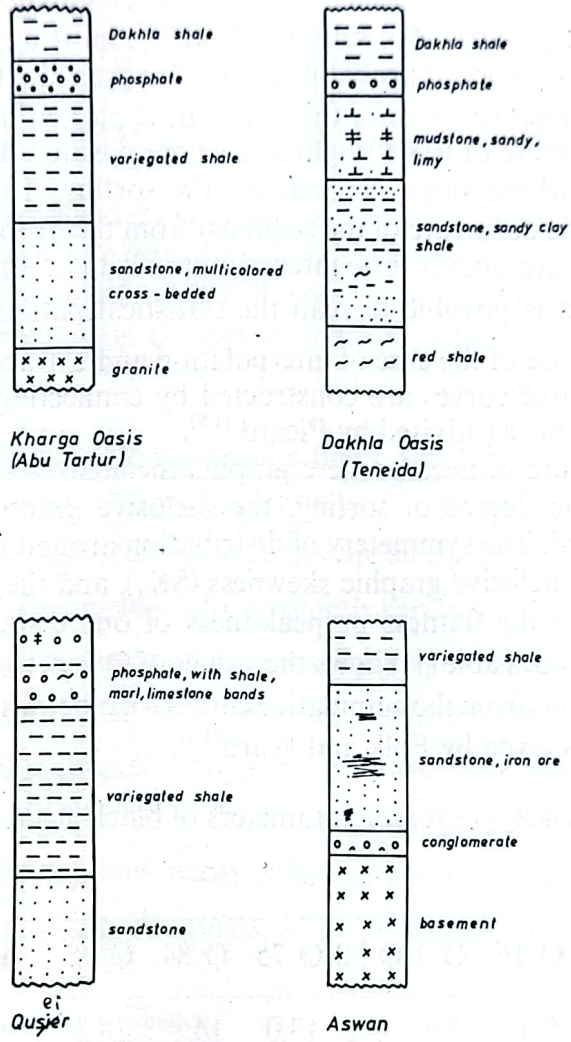

Fig. 2: Vertical sections showing the general successions in the studied areas.

figure it appears that the variegated shale (including black shale bands) rest conformably upon the Nubian Sandstone series. The later may reach more than 120 m in thickness. Above the variegated shale, there is a series of phosphatic beds (including coprolites) with some bands of shales, marls and limestone, referred to as the Duwiformation. The thickness of the Duwiformation may may reach up to 66 m in its type locality (Quseir area).

Grain Size Analysis:

The grain size analysis method (disaggregation and dispersal) was carried out according to the procedure recommended by Ingram[11]. The sand fraction was separated by wet sieving on 0.063 mm sieve (4μ) and analyzed by screening. The silt-clay fraction was collected and analyzed by the well known pipette method Galehouse[12].

From the results of grain size analyses, cumulative curves were plotted on a probability paper. According to Folk[14], most unimodel sediments tend to approach the "normal probability curve" in their size frequency distribution, i.e., if the cumulative curve of the sediment is plotted on a probability paper, the result is a more or less straight line whose position depends on the average particle size, whose slope depends on the sorting. Therefore, it is valuable for studying the departure of the sediment from the probability law. Moreover, since the tails are oftenly straightened out and the sample tends to plot as a straight line, it is possible to read the statistical parameters with greater accuracy because of the ease of interpolation and extrapolation. In the present work, cumulative curves are constructed by connecting the data points with straight segments as advised by Picard [15].

As a measure of average size; graphic mean size (M_z) was used and as a measure of the degree of sorting, the inclusive graphic standard deviation (σ_I) was applied. The symmetery of distribution around the mean was determined using the inclusive graphic skewness (SK_I), and the graphic kurtosis (K_G) which refers to the flatness or peakdness of one distribution in relation to another was used. Table (1) shows the values of ϕ 5, ϕ 16, ϕ 25, ϕ 50, ϕ 75, ϕ 84, and ϕ 95 readings from the cumulative curves together with the calculated grain-size parameters given by Folk and Ward[13].

Table (1): Statisical grain-size parameters of black shale

Sample	ϕ 5	ϕ 16	ϕ 25	ϕ 50	ϕ 75	ϕ 84	ϕ 95	M_z	σ_I	SK_I	K_G
Kharga	3.5	5.0	5.9	9.2	13.0	14.8	18.3	9.70	4.65	0.18	0.84
Dakhla	5.3	6.0	6.9	8.5	10.2	11.0	12.7	8.50	3.06	0.12	0.88
Aswan	2.2	3.0	3.5	6.0	9.5	11.5	15.0	6.91	4.06	0.04	0.86
Quseir	5.8	8.7	9.9	12.0	14.3	15.2	17.3	12.01	3.37	0.02	1.06

The calculated mean size (M_z) reveals that the black shale sample of Aswan is coarser than those encountered in the other sections, it has a mean size value of 6.91 ϕ (i.e. fine silt). On the other hand the samples of Kharga, Dakhla and Quseir sections are the finest samples encountered; they have mean size ranging between 8.5 - 12.01 ϕ (i.e. clay).

The calculated inclusive graphic standard deviation (σ_1) shows that these shlaes are poorly sorted (3.37-4.65 Ø) in character. In a statistical sense, this means that the scatter of fraction sizes around the "mean size" is relatively large.

The inclusive graphic skewness (SK_1) values indicate that the curves of distribution of Aswan and Quseir samples are mainly nearsymmetrical, while those of Kharga and Dakhla samples are generally fine-skewed and strongly fine-skewed.

The graphic Kurtosis (K_G) values point out that the black shale samples of Aswan and Quseir sections have mesokurtic curves of distribution, i.e. normal distribution, on the other hand, Kharga and Dakhla samples have platykurtic curves.

Besides the above mentioned characters of the black shale samples, grain size analysis indicates a marginal shallow water environment of deposition. Mason and Folk[16] pointed out that the poorly sorted, the nearly symmetrical skewed and the mesokurtic characters indicate a beach environment (or a marginal one).

Petrography and Organic Content of the Black Shales:

The black shales have carbonaceous matter content ranging between 12% and 30% . In thin section, the black shales are steelgrey and rarely laminated. The groundmass is argillaceous, silty or slightly sandy in places. They are rich in carbonaceous materials and plant remains. Pyrite grains and iron oxides occur as scattered small spots. Filling fissures are scattered within the groundmass, some fibrous and fine-grained anhydrite and carbonate minerals (calcite and dolomite) are detected. Scattered fine to medium grained, subangular to sub-rounded detrital quartz grains, occasionally with undulose extinction, are embedded in the argillaceous groundmass. Some pelletes of glauconite are recorded.

X-ray analysis of the Black Shales:

X-ray diffraction analysis are carried out to study the composition of both clay and non-clay minerals. X-ray diffraction patterns (Table 2) determined for the minus 74 micron fraction reveals the predominance of quartz with lesser amounts of kaolinite, illite, carbonates, anhydrite and pyrite.

The Action of Heat:

The action of heat on the black shales has been studied from their differential thermal analysis, using the apparatus and technique devised by Grimshow, Heston and Roberts[17]. The black shales show a behaviour characterized in Fig. (3) and may be summarized as follows:

Table (2): X-ray diffraction data of black shale*

Kharga		Dakhla		Aswan		Quseir	
dA°	I/I°	dA°	I/I°	dA°	I/I°	dA°	I/I°
13.19	6	13.60	5	13.20	7	13.62	8
12.42	10	10.05	5	12.40	8	10.00	8
7.14	10	7.14	4	7.14	10	7.14	8
4.25	40	4.96	4	4.25	40	4.99	4
3.58	10	3.95	6	3.56	8	3.95	6
3.50	8	3.56	40	3.52	10	3.55	4
3.34	100	3.35	100	3.34	100	3.35	100
2.90	15	2.92	25	2.89	20	2.90	20
2.56	5	2.45	5	2.50	5	2.48	5
2.46	10	2.28	4	2.28	8	2.28	5
2.28	8	2.24	4	2.24	4	2.24	4
2.23	5	2.13	6	2.12	5	2.12	6
1.99	8	1.98	4	1.99	8	1.99	5
1.82	15	1.82	7	1.80	12	1.82	8

* Indentified minerals:

Quartz : Using lines at d = 3.34,4.26, 1.82 A° (ASTM card 5-0490)
Kaolinite : Using lines at d= 7.15,3.57,2.30 A° (ASTM card 5-0143)
Illite : Using lines at d = 4.29,3.36,2.86, 2.57 A° (ASTM card 9-334)
Dolomite : Using lines at d = 2.89, 2.19, 1.79 A° (ASTM card 11-78)
Anhydrite : Using lines at d = 3.50, 2.85, 2.33 A° (ASTM card 6 0226

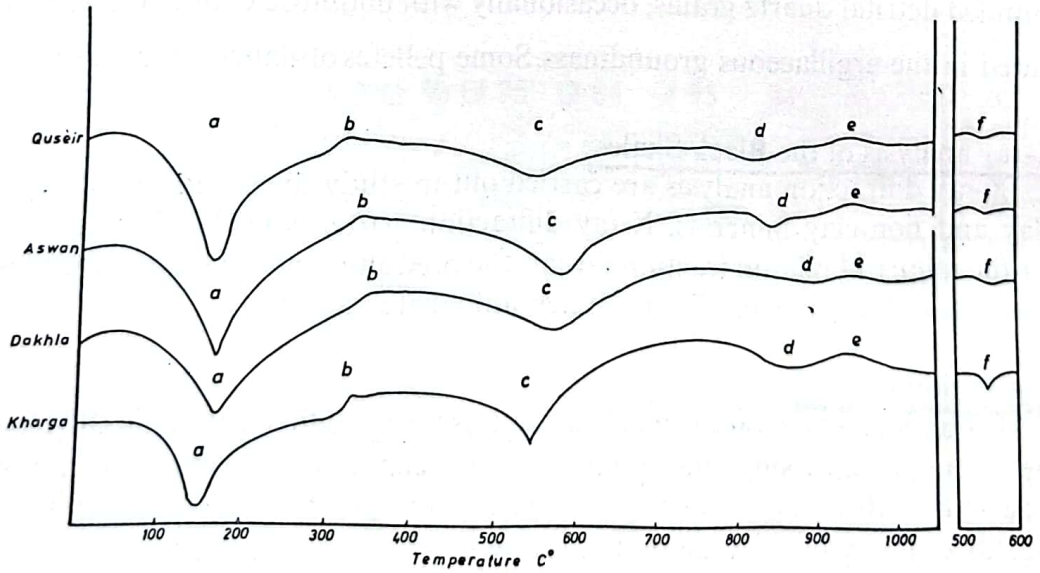

Fig. 4. Thermal behaviour of the black shales.

1. An endothermic reaction (a) taking place between 80-220°C and reaching a maximum at 150°C. This loop indicates that the energy is absorbed to drive off the moisture content. Kaolinite does not show this low-temperature reaction, while illite exhibits this reaction.
2. A slight exothermic reaction (b) taking place in gradual stages between 300-400°C. This exothermic reaction indicates the presence of organic matter which is not easily volatilized in one stage.
3. An endothermic reaction (c) taking place between 400-600°C, reaching a maximum at about 550 and represents that the energy is absorbed to remove water of crystallization. Kaolinite and illite minerals loose their hydroxyls within this range.
4. A slight endothermic reaction (d) taking place between 850-900°C. Most of the three layer lattice clay minerals undergo this reaction associated with the final break-down of the clay lattice[18].
5. A broad small exothermic reaction (e) between 900-100°C, with a peak at 940°C, due to the re-crystallization of alumina. According to Grim and Bradley[18], this peak is characteristic of either illite and /or montomorillonite.
5. A broad small exothermic reaction (e) between 900-1000°C, with a peak
6. The re-heating curve at 500-600°C indicates the presence of quartz detected by the peak (f).

The thermal behaviour of the black shales suggests the type of clay mineral which is different from illite group, but in the same time approaching the characteristic thermal behaviour of kaolinite. Thermal analysis shows also the presence of quartz and organic matters. These results agree with those obtained from X-ray analysis.

Environment of Deposition:

Based on the fore-going observations, the following conclusions can be achieved about the environment of deposition of the black shales:

The black shales consist mainly of detritus rich in carbonaceous and organic materials (12-30%). These are inherited from the weathering of source rocks and soils and transported by fresh water (as indicated from plant remains) to the basin of deposition. The environmental conditions of deposition are mainly marine as reflected by the assemblage of clay minerals present (kaolinite and illite). Keller[19] indicated that passing from a non- marine to marine environment, the clay suites changed from kaolinite to a largely illite suites. Millot[20] found kaolinite to be dominant in fluviolacustrine deposits.

Stratigraphically, the black shale lamination within the variegated shale conformably overlies the sandstone of Nubia formation. The latter had been deposited in a shallow water environment [10]. These shales are overlain by phosphatic beds with much detritus. This indicates the deposition of black shales in a near-shore environment.

The characters of grain size parameters indicate a shallow marginal environment of deposition.

Twenhofel [21] favours environments with poor circulation, with little or no oxygen and with concurrent toxic conditions as responsible for most black shales. So, the black shales may be deposited in lakes, ponds, lagoons or in shallow nearly tideless epicontinental seas. The marine environment of deposition has mainly alkaline chemical characters as indicated by the presence of carbonates. The presence of chlorides and sulphates indicates a more saline environment.

CONCLUSION

The Egyptian black shales have been studied in detail from mineralogical, chemical, physical and petrographic points of view. The shales range from fine siltstone to claystone. The identified clay minerals are kaolinite and illite, the non-clay minerals are quartz, anhydrite and carbonates. The environment of deposition was mainly marine, near shore, alkaline and saline.

REFERENCES

(1). H.J.L. Beadnell, The relations of the Eocene and Cretacous systems in the Esna-Aswan reach of the Nile Valley. Quart. J. Geol. Soc. London, 61, 244, 667-678 (1905).

(2) M.A. Ghorab, A summary of a proposed rock stratigraphic classification of the Upper Cretaceous rocks in Egypt. Geol. Soc. of Egypt (1956).

(3) M.I. Youssef, Upper Cretaceous rocks in Qusseir area. Bull. Inst. Desert Egypt, 7, 2, 35-54 (1957).

(4) M.H. Hermina, Geology of the Northwestern approaches of Kharga. Geol. Surv. and Min. Res. Dept., Cairo, Egypt (1967).

(5) R.E. Newton, In some fossil from the Nubian sandstone series of Egypt. Micropleontology, New York, 4-5, 453-472 (1909).

(6) W.N. Edwards, Fossil plants from the Nubian Sandstone of Darfur Quart. J. Geol. Soc. London, 82, 94-100 (1926).

(7) A.C. Seward, Leaves of Dicotyledons from the Nubian Sandstone o Egypt. Egypt Geol. Surv., 21 (1935).

(8) L.R. Cox, Lamellibranchia from the Nubian Sandstone Series of Egypt Bull. Inst. Egypt, 37, 465-480 (1956).

(9) M.I. Faris, and M.Y. Hassan, Report on the Stratigraphy and fauna o the Upper Cretaceous - Paleocene Rocks of Umm ElHuetat, Safaga area. Ain Shams Sci. Bull. Cairo, 4, 191-207 (1959).

(10) S.A.A. Hussein, Studies on the mineralization in Wadi El-Gedid area. Ph.D. Thesis, Fac. Sci., Ain Shams University (1971).

(11) R.L. Ingram, Sieve analysis: In procedures in Sedimentary Petrology, by R.E. Carver-Wiley Interscience (1971).
(12) J.S. Galehouse, Sedimentation analysis: In "Procedures in Sedimentary Petrology" by Carver. R.E. Wiley interscience (1971).
(13)R. L. Folk, and W.C. Ward, Brazos River bar, a study in the significance of grain size parameters. J. Sed. Petrology, 27, 3-27 (1957).
(14) R.L. Folk, Petrology of Sedimentary Rocks- Hemphills, Austin, Texas, pp. 170 (1968).
(15) M.D. Picard, Classification of fine grained sedimentary rocks. J. Sed. Petrology, 41, 1, 179-195 (1971).
(16) C.C Mason, and R.L. Folk, Differentiation of beach, dune and aeolian flat environments by size analysis. J. Sed. Pet. 28 (1958).
(17) W. Grimshow, E. Heston and A.L. Roberts, The constitution of refractory clays. Trans. Brit. Ceram. Soc., 51, 327(1952).
(18) R.E. Grim and W.F. Bradley, Re-hydration and de-hydration of the clay minerals, Amer. Miner., 33, 50-59 (1948).
(19) W.D. Keller, Clay minerals as influenced by environments of their formation. Bull. Amer. Assoc. Petro. Geol., 40, 11 (1956).
(20) G. Millot, "Geology of clays". Springer-verlog, New York (1970).
(21) W.H. Twenhofel, Environments of origin of black shales. Amer. Assoc. Pet. Geol., 23, 1178-1198 (1939).

الخلاصـــــــــــة

درست عينات من الطين المصري الاسود في عدة قطاعات مختلفة وذلك لمعرفة خواصها المعدنية ، الكيمياوية ، الطبيعية والبتروجرافية . وقد وجد أن هذا الطين يتراوح في قطر حبيباته بين الطمى الدقيق والطفل . وقد اظهرت التحاليل بواسطة حيود الاشعة السينية والتحليل الحراري ، أن معادن هذا الطين هي :
كاولينيت ، ايليت ، كوارتز ، انهيدريت وكربونات ، وقد تعرض البحث لبيئة ترسيب الطين الاسود ، التي دلت الدراسة على أن هذه البيئة بحرية وقرب الشاطيء قلوية ومالحة .

PENETRATION FACTORS IN WIDE APERTURE TAPERED COLLIMATORS

Bishara A.Bishara* and Mohamed S. El-Nagdy

Department of Physics, Faculty of Science

University of Cairo, Giza, Egypt.

Received, 4th April 1976.

ABSTRACT

A method for calculating the penetration factors in wide aperture tapered square collimators for axial point sources has been given. The formulae obtained are especially suitable for numerical computation by the digital computer.

The penetration factors have been measured experimentally in the case of focusing conical collimators for axial point sources. Satisfactory agreement is found between the experimental values and the calculated curves .

INTRODUCTION

The tapered collimators are used either as "focusing" collimators in radiological scanning, or as "inverted" wide-angle collimators in uptake measurements for studying the functions of body organs by radioisotopes[1].

This paper presents a theoretical study of the penetration factors in the case of wide aperture square tapered collimators from axial point sources. The penetration factors are measured experimentally for the conical collimators to test the validity of the calculated values which have been given in a previous work [2].

---

* Now at the Faculty of Science,
Al-Mustansiriyah University, Baghdad, Iraq.

THE SQUARE TAPERED COLLIMATOR

The square tapered collimator's hole geometry is that of a truncated right pyramid (Fig. la). The penetration factor, f, is defined as,

$$f = I/C \qquad (1)$$

where, I is the rate of monoenergetic gamma photons penetrating through the walls of the collimator and C is the rate of photons, of the same energy, passing through the geometrical aperture of the collimator.

The calculation of the penetration factors depends in the location of the axial point source with respect to the vertex of the pyramid, i.e., whether the height of the source, h, is greater or smaller than the "focal length", F, of the collimator. In the following sections, each case is treated separately.

(a) Case of $h < F$:

The detector's responce, C, to the axial point source is proportional to the square solid angle. It has been shown[3] that

$$C = (N/4\pi)\, 4 \arctan \left[a^2 / \{ H (2a^2 + H^2)^{1/2} \} \right] \qquad (2)$$

where N is the rate of emission of the photons, a is the half of the length of the pyramid base, and H is the height of the source from the base center.

To calculate the number of photons penetrating through the walls of the collimator, it is essential to find the distance QR (Fig. la) travelled through the collimator's material. This is obtained by finding the point of intersection of the ray PQR with the inclined plane of the collimator's wall. It is found that the height, z, of the intersection point is given by

$$z = HL (a - x) / (aH - Lx) \qquad (3)$$

The number of photons striking the walls at an angle θ in the element solid angle $d\Omega$ is $N (d\Omega/4\pi)$. These photons suffer attenuation by passing through the distance QR in the collimator's material, the attenuation factor equals $\exp(-\mu.z/\cos\theta)$. Using that, the element solid angle is given by

$$d\Omega = dx\, dy \left[H/(x^2 + y^2 + H^2)^{3/2} \right] \qquad (4)$$

The rate of gamma photons penetrating through the walls of the collimator, I, could be shown to be given by

$$I = (N/4\pi)\, 8H \int_{y=0}^{m} \int_{x=a,y}^{m} (x^2 + y^2 + H^2)^{-3/2} \exp(-\mu z/\cos\theta)\, dx\, dy \ldots (5)$$

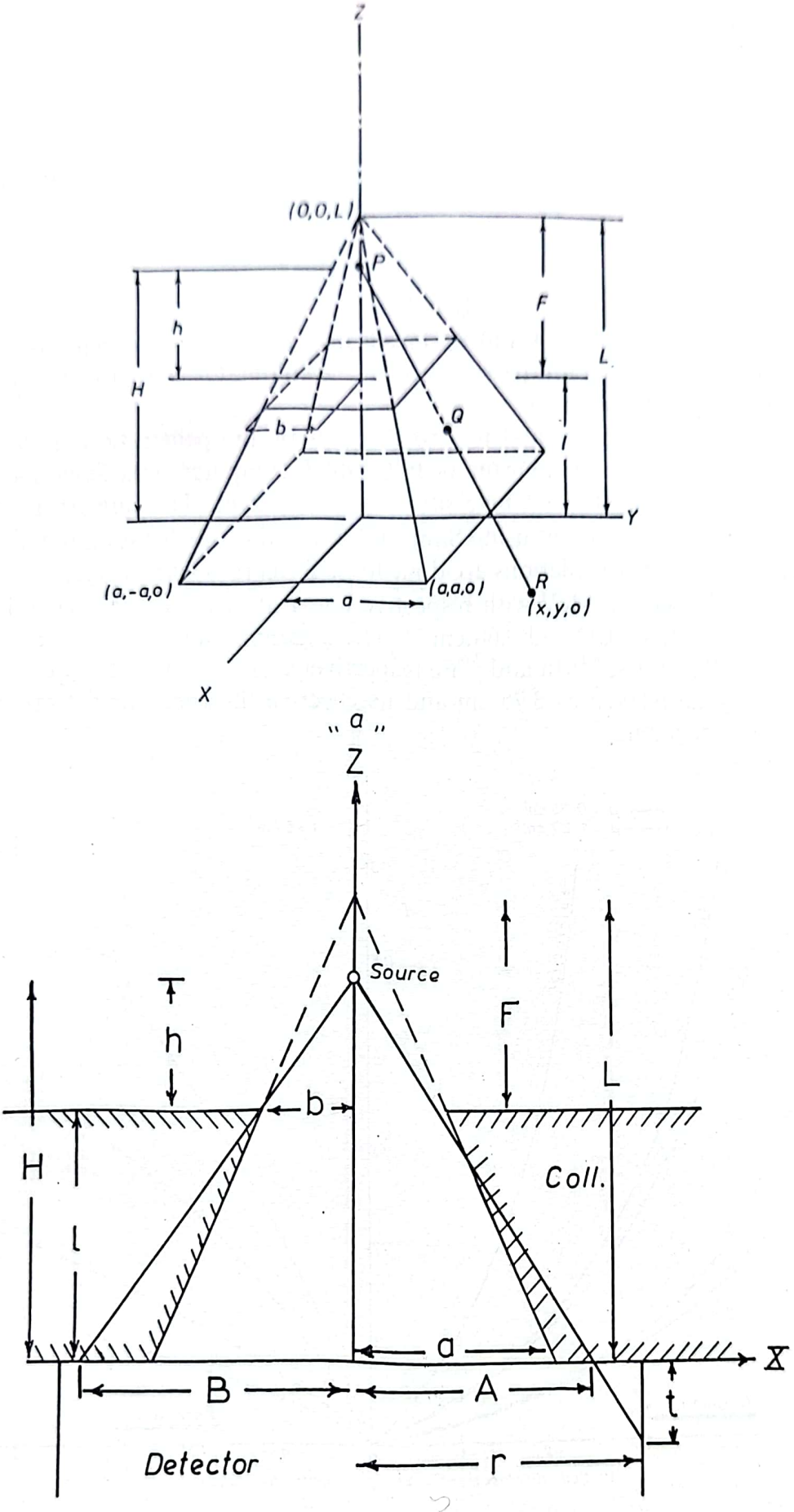

(Fig. 1) The geometry of tapered square collimator.

The upper limit m can be defined in terms of two constants A and B (Fig. 1b) which are related to the radius of the detector, r, and its effective thickness t[4]. The constants are given as:

$$A = rH / (H + t) \qquad (6)$$
$$B = bH / h$$

m equals the smaller of A and B, since if $A < m < B$, the gamma photon will not be detected even if it passes through the collimator walls, due to the finite dimensions of the detector.

The ray tracing method is used to calculate the penetration factors. The calculations have been done on the ICL 1905 E computer of the Scientific Computation Centre of the University of Cairo, Egypt. The numerical double integration is carried out using Simpson's one-third rule for several collimator dimensions. The calculations are done for gamma rays with energies 0.28, 0.48, 0.66, 0.84 and 1.20 MeV with respective linear absorption coefficients in lead of 5.2, 1.84, 1.20, 0.92 and 0.68 cm^{-1}. These gamma rays follow the decays of ^{203}Hg, ^{7}Be, ^{137}Cs, ^{54}Mn and ^{59}Fe respectively. The radius of the viewing NaI (T1) crystal istaken as 3.75 cm and its effective thickness for detection, t, is taken to be 8 mm.

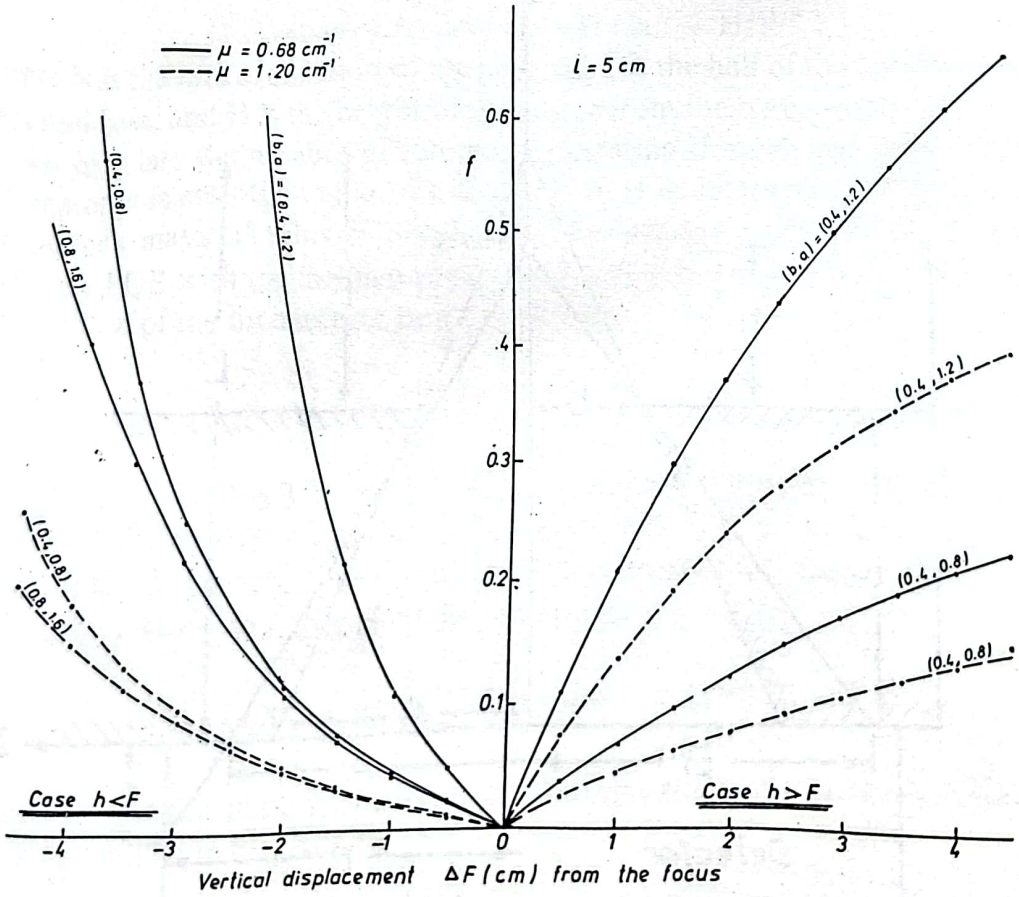

(Fig. 2) The penetration factor f as a function of the displacement from the vertex of the tapered square collimator in case of different b/a values.

Some of the results obtained are plotted in left side of Figure 2 to demonstrate the main features of the penetration factors. The penetration factor increases as the displacement from the vertex AF increases and it is greater for narrower collimators of the same a/b ratio. The main features of f are similar to the corresponding features in the case of conical collimators which are given in a previous work[2]. The differences in the values of the two types do not usually exceed 20°/₀ in the case of a collimator with dimensions 0.4 and 0.8 cm.

(b) Case of h > F:

When the axial point source is higher than the vertex of the pyramid, the response of the detector is given by

$$C = (N/4\pi)4 \arctan [\, b^2/\{ h(2b^2 + h^2)^{1/2} \}\,] \qquad (7)$$

The distance travelled by the gamma ray through the collimator's material in this case is $(L - z)/\cos\theta$. The number of photons penetrating the walls of the collimator is calculated in a similar way as in eqn (5), now

$$I = (N/4\pi)\, 8H \int_{y=0}^{a} \int_{x=n,y}^{a} (x^2 + y^2 + H^2)^{-3/2} \exp\{ -\mu (L - z)/\cos\theta \}\, dx\, dy \qquad (8)$$

$$\text{where, } n = bH/h \qquad (9)$$

The values of the penetration factors, calculated under the same conditions described in section (a), are plotted in the right side of figure 2. The rate of increase of f in this case is smaller than the rate in case (a) because the source is moving at relatively large values of h. For the same reason, the sensitivity of the penetration factor to the width of the collimator is smaller. The value of f increases as the ratio a/b increases due to the decrease of the distance travelled in lead. The values obtained in this case are very close to the corresponding values of f for conical collimators; the differences do not exceed 5°/₀ in the case of the collimator with dimensions 0.4 and 0.8 cm.

EXPERIMENTAL DETERMINATION OF F

It is interesting to study the general trends of the penetration factors experimentally and to test how they would agree with the calculated values. The lead conical collimators are chosen for the experimental work because they are relatively easy to be cast and machined in the college workshop , and also because the differences in the values of penetration factors for the conical and tapered square collimators are small[2].

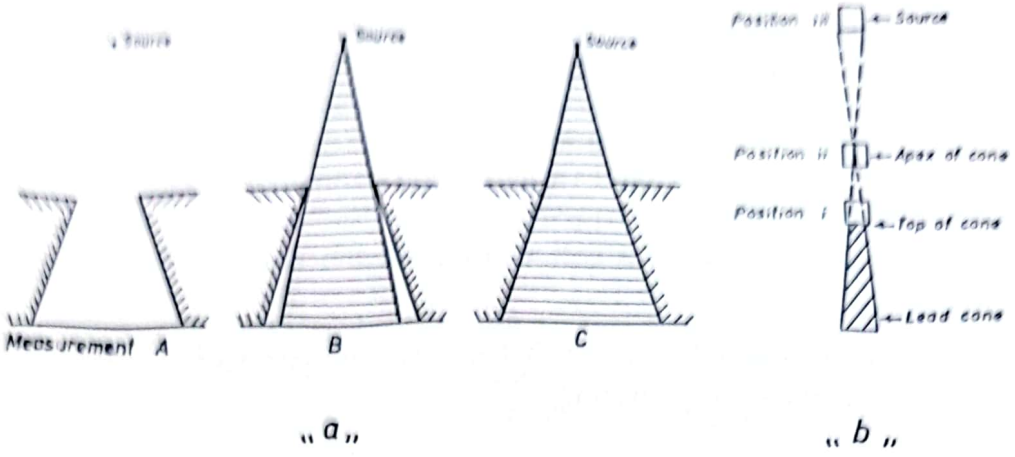

(Fig. 3) a – The counting arrangement.
b – The screening effects due to flat top of a lead cone.

The method used has been described in the literature [4,5]. Three measurements of the count rates are made with a "point" source placed on the axis of the lead collimator in front of a scintillation counter; the three situations are shown in Figure 3a. Measurement A records the rate of radiations passing through the geometrical aperture plus the radiations penetrating through the collimator's walls. Measurement B records the rate of radiations penetrating through the walls, while measurement C records the rate of radiations penetrating through the whole thickness of the collimator's block. The background is measured separately in each case and is subtracted from the corresponding total counting. From the measurements A, B and C the penetration factor is given by:

$$f = \frac{(B-s+e)-C}{A-(B-s+e)} \qquad (10$$

where, s is the loss in counting rate due to screening of the source by the truncated lead cone (position i, Fig. 3b) and e is the rate of radiations penetrating through the edges of the cone. It has been shown[4] that at position (iii) the values s and e are almost equal and eqn. (10) is reduced to

$$f = (B - C) / (A - B) \qquad (11)$$

To measure the penetration factors, the source is placed at position (iii) to eliminate any screening. The window of the pulse-height analyser is set to select the pulses in a narrow energy band around the photopeak to eliminate scattered radiations. The three measurements A, B and C are performed using ^{137}Cs and ^{59}Fe sources at different heights. The counting is continued for

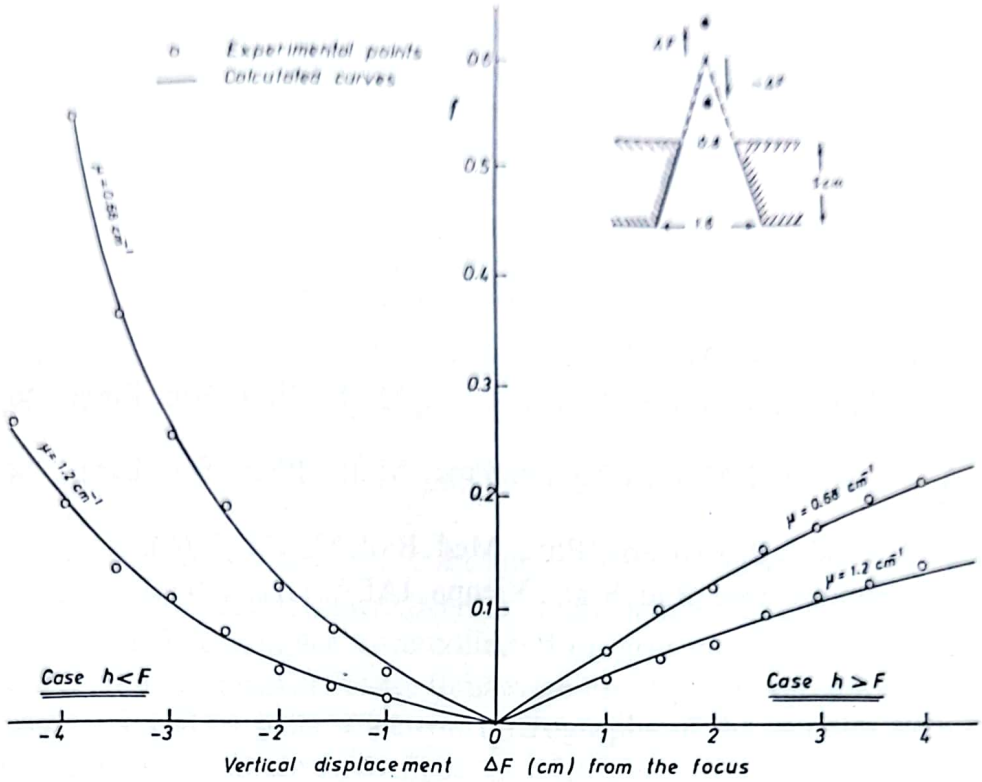

(Fig. 4) Experimental values of penetration factors for the focusing conical collimator.

periods of time long enough to give good statistics. The collimators used are of length equal to 5 cm, their smaller and larger radii are 0.4 - 0.8, 0.4 - 1.2, 0.8 - 1.6 and 0.8 - 2.4 cm.

Figure (4) gives a sample of the measured values of the penetration factors for focusing collimators, the experimental values are compared with the previously[2] calculated curves. The results show satisfactory agreement between theory and experiment. The deviations of the measured f values are found to be within 5°/₀ of the corresponding calculated values.

CONCLUSIONS

The ray tracing method is used for calculating the penetration factors in the tapered square collimators for axial point sources and the results are compared to those of the conical collimators. The penetration factors are particularly large for high energies, large a/b ratios, narrow collimators and when the source is close to the collimator.

The penetration factors are measured experimentally in the case of conical collimators and the resuls have shown satisfactory agreement with the theoretical values even when the source is relatively close to the collimator's face.

A thorough knowledge of the penetration factors is quite important both in the design and the execution of a careful experiment.

REFERENCES

(1) J.R. Mallard, Phys. Med. Biol., 10,309 (1965).
(2) B.A. Bishara and M.S. El-Nagdy, Proc. Math. Phys. Soc. Egypt, 39, 69 (1975).
(3) B.A. Bishara and M.S. El-Nagdy, Proc. Math. Phys. Soc. Egypt, 38, 29 (1974).
(4) T.K. Bell and A.R. Johnston, Phys. Med. Biol, 13, 401 (1968).
(5) H.A.B. Simons, Med. Rad. Scan., Vienna, IAEA, 1,115 (1964).

الخلاصة

درست طريقة حساب معاملات النفاذ خلال جدران المجمعات الهرمية المربعة المتسعة لمصادر نقطية محورية ، وامكن الحصول على علاقات عامة في طبيعتها وملائمة للحساب الالكتروني بوجه خاص .

كذلك تم قياس معاملات النفاذ عمليا في حالات المجمعات المخروطية البؤرية لمصادر نقطية محورية ، وقد كان التطابق كافيا بين النتائج العملية والمنحنيات المحسوبة نظريا .

SIZE DISTRIBUTION OF PARTICLES IN BAGHDAD ATMOSPHERE

Mohie A.Abbas
Physics Department, Al-Mustansiriyah University,
Baghdad, Iraq

Received, 21 April 1976

ABSTRACT

Measurements of the size distribution of particles in Baghdad atmosphere due to petroleum products have been undertaken and the results are presented in this article. The samples were collected on grid meshes covered with thin films of carbon or formvar. These films were produced by vaccum evaporation of carbon on a glass plate. Electron micrographs of the samples were taken by means of an electron microscope.

Statistical information concerning the amount of consumption of different types of petroleum products since 1948 have been analysed and presented in graphical forms. It was seen that the combustion of an amount of about 1400 millions of litres of petroleum are being injected into Baghdad atmosphere in the current year. The estimated amount of consumption up to 1987 has been taken into consideration also.

INTRODUCTION

The problems of environment and air pollution have become a matter of international concern and all governments and health organizations are now well aware of the hazards to human health and property arising from atmospheric pollution[1].

On global basis, the trend of world temperatures in this century appears to be directly related to the trends of atmospheric carbon dioxide content and atmospheric turbidity[2]. Both are believed to be related to human activies. Since 1940, the effect of the rapid rise in atmospheric turbidity appears to have exceeded the effect of rising carbon dioxide, resulting in a downward trend of world temperature[3]. There is no indications what so ever, that these trends will be reversed and therefore there is some reason to believe that man made pollution will have an increasing effect in future.

Al-Mustansiriyah Journal of Science, Vol. 1 (1976).

However the global effects of air pollution is a very long range problem. Relatively the local effects of the pollution is a matter of immediate concern. The pollution of the atmosphere by various irritating or toxic materials is increasing rapidly with the industrial growth and unprecedented increase in world population. The current economic trends indicate that air pollution due to hydrocarbons, petrochemical products and engine exhausts will become increasingly evident in most cities[4,5]. Over a city, the smoke pall from industry and other sources change the character of the radiation falling on the city[6], specially reducing the ultraviolet penetration, rearranging the long wave radiation balance, and providing condensation nuclei which contribute greater precipitation over a city and a higher frequency of fog[7].

STATISTICAL INFORMATION

In Baghdad atmosphere, contribution to air pollution comes mostly from automobile engine exhaust gas, smoke from house chimneys and brickfactories which are spreading all over the city. However, beside the above sources, the Oil refinery and the cement factory are adding different amounts of air contaminants continuously and regularly. Informations concerning the amount of consumption of different types of Oil products in the whole country could be obtained from the Ministry of Oil. These informations are analysed and then plotted as a function of time as shown in figure(1) .It can be seen

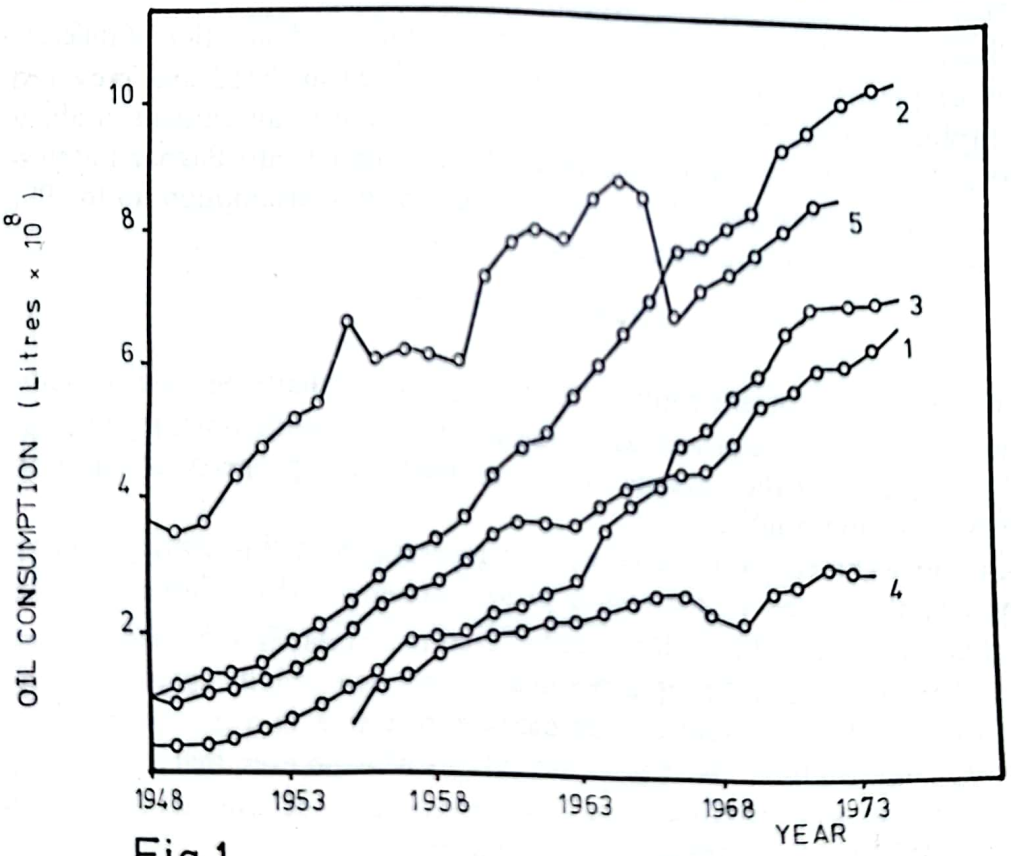

Fig.1

Curve 1 car petrol.
Curve 2 kerosine oil.
Curve 3 gas oil.
Curve 4 diesel oil.
Curve 5 crude oil.

Fig. 1 : The consumption of different types of Oil in Iraq.

from this figure that the consumption of all types of Oil products increases rapidly with time. Figure(2) shows the amount of consumption of Oil in future up to 1987, as estimated by the Ministry of Oil[11].

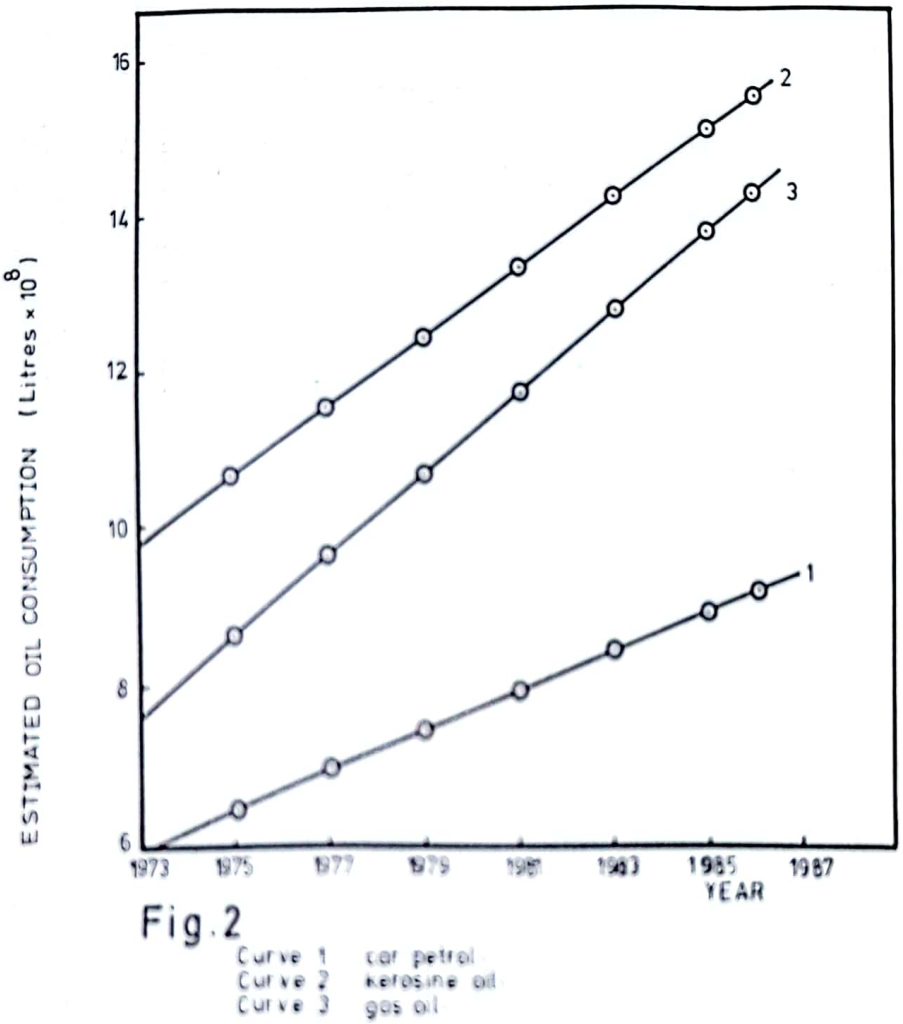

Fig. 2 : The estimated increase in Oil consumption.

For the city of Baghdad, informations concerning the consumption of car petrol and gas Oil are obtained. These informations are plotted as a function of time as shown in Figure(3). It can be concluded from these figures that the total consumption of all types of Oil products is about 3500 million litre per year in 1975 in the whole country and this amount is expected to increase to about 7000 million litre per year by 1987. For the city of Baghdad alone, the present consumption of all types of Oil products is estimated to be around 1400 million litre in 1975 and by the year 1987 this figure will increase to

about 2300 million litre. This means combustion product of about 1500 million litre of Oil products are being injected into Baghdad atmosphere during the current year. Thus present trend indicates that contribution to

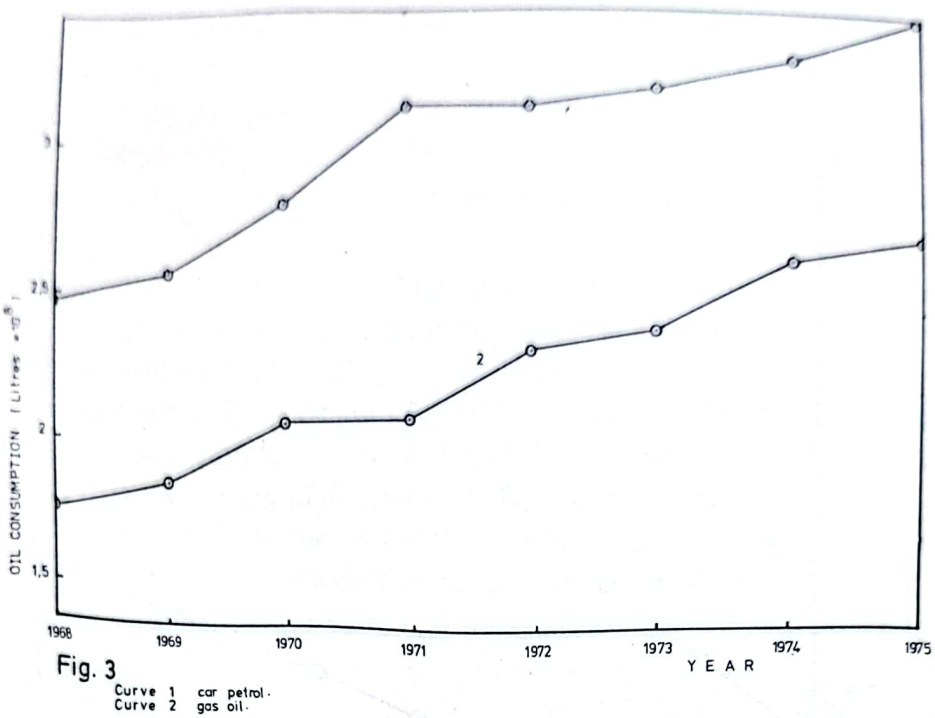

Fig. 3 : The consumption of car petrol and gas Oil in Baghdad.

the air pollution will rapidly increase when various industrial projects in and around Baghdad are completed and come into full operation .

We are faced with the problem of protecting our air supplies against contamination by gasoline vapours, exhaust gas, smokes and dust particulates. A study of air pollution, therefore seems very desirable at present and as a first step in this direction an investigation of the particulates in automobile engine exhausts, in smokes from burning bitumen and cigarettes and in dust fall has been undertaken. The small particulate pollutants can remain floating in air for considerably long period and behave in many ways very similar to gases. Particles smaller than 2 to 3 microns are inhaled readily and they can stick to the walls of the lungs; larger particles are excluded for the most part by being trapped in the nasal passages but they helped in making chemical reactions in the atmosphere between gaseous pollutants possible by adsorbing them on their surfaces so that the reactive molecules could remain near each other for sufficient time to take part in the reaction. Thus some toxic gases are produced in the atmosphere.

EXPERIMENTAL

Collection of samples:

Different workers have followed different procedures in sample collection depending on the type of studies and the nature of sources. The procedure used in the present work consists of collecting the samples on grid meshes by means of which electron micrograph of the particles could be taken using the electron microscope. For collecting particulate sample, grid meshes covered with thin film of carbon or formvar film were used. The grid mesh is a small disc, 2mm in diameter, of fine wire mesh containing large number of very small rectangular or square open spaces. The film was produced by vacuum evaporation of carbon on a glass plate. It is then removed from the glass plate by the action of water and transferred to the grid mesh by the fishing method. The same method was used to transfer the formvar films . The grid meshes covered with films were dried in desiccator for one day. The grid meshes become then ready for use.

In samples collection, there grid meshes were arranged on the middle part of a clean glass slide. The slide then placed flat inside a large container which was covered tightly to prevent undesirable particles entering it.

Exposure to diesel engine exhausts:

The cover of the container was removed and the sample was exposed to the plume of exhaust gas from a diesel truck to allow the smoke to pass into the container. The sample was exposed for five minutes at the end of which the container was covered again and the smoke was allowed to settle down on the film covered grid meshes. Many such samples were collected.

The grid meshes exposed to the diesel engine exhausts were examined in the beam of the electron microscope at the institute of Biological Research Center, Baghdad and the electron micrograph of the smoke particles deposited on the grid meshes were taken. Plate - 1 shows one of the electron micrographs of the smoke particles from the diesel engine exhausts (magnification = 12750 x).

Cigarette smoke:

To collect the cigarette smoke sample, a very tightly covered containcer, having a long glass tube connected with it, was used. After the grid meshes, resting on a glass slide, were placed inside the container, the latter was closed tightly and then Al-Jamhuriyah cigarette was smoked and the smoke was allowed to pass through the glass tube. This process was repeated many times till the container looked cloudy. Then the glass tube was closed and the smoke was allowed to settle down on the grid meshes lying in the bottom of the container.

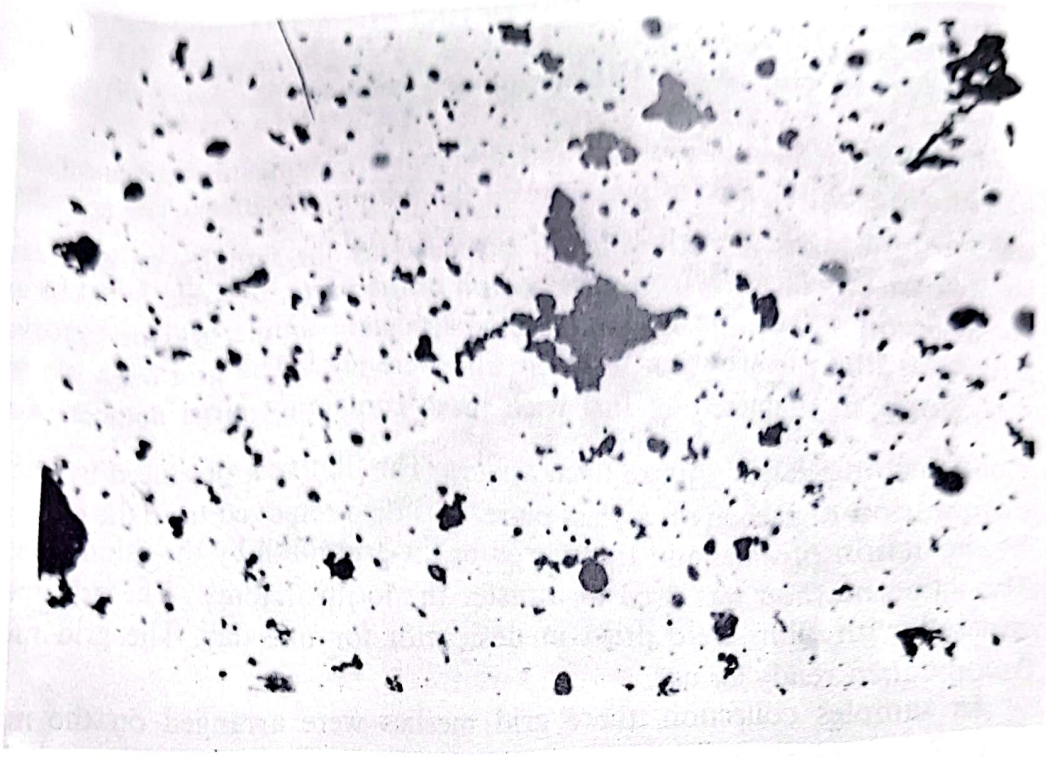

Plate 1: An electron micrograph of smoke particles from a diesel engine exhaust (magn. 12750 x).

The grid meshes exposed to the cigarette smoke were examined by the electron microscope and several electron micrographs were taken. Plate - 2 shows one of the electron micrographs of the cigarette smoke (magnification = 16830 x).

Dust sample:

Samples of dusts from the atmosphere were collected in a large glass plates placed on the roofs of several houses lying in different districts in Baghdad area for 5 days. The dust so collected were dispersed dusts were placed on the grid meshes covered with formvar film and then examined under the electron microscope beam. Plate - 3 shows one of the electron micrograph of the dust sample (magnification = 10030 x).

Bitumen smoke:

The container containing the grid meshes was exposed to the plume of smoke from the burning bitumen for about 5 minutes. The container was then covered tightly and the smoke was allowed to settle down on the grid meshes covered with carbon films. The smoke particles deposited on the grid meshes were finally examined under the electron microscope and plat - 4 shows one of the electron micrographs (magnification = 12750 x).

Plate 2: An electron micrograph of cigarette smoke (magn. 16830 x).

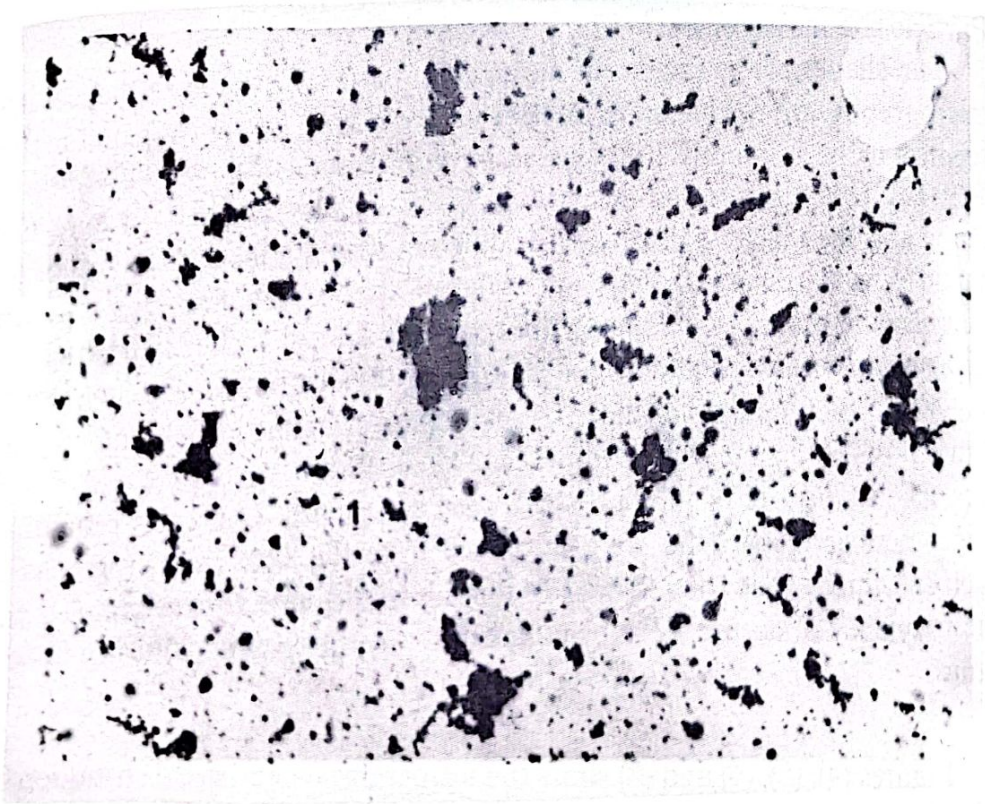

Plate 3: An electron micrograph of dust particles (magn. 10030 x).

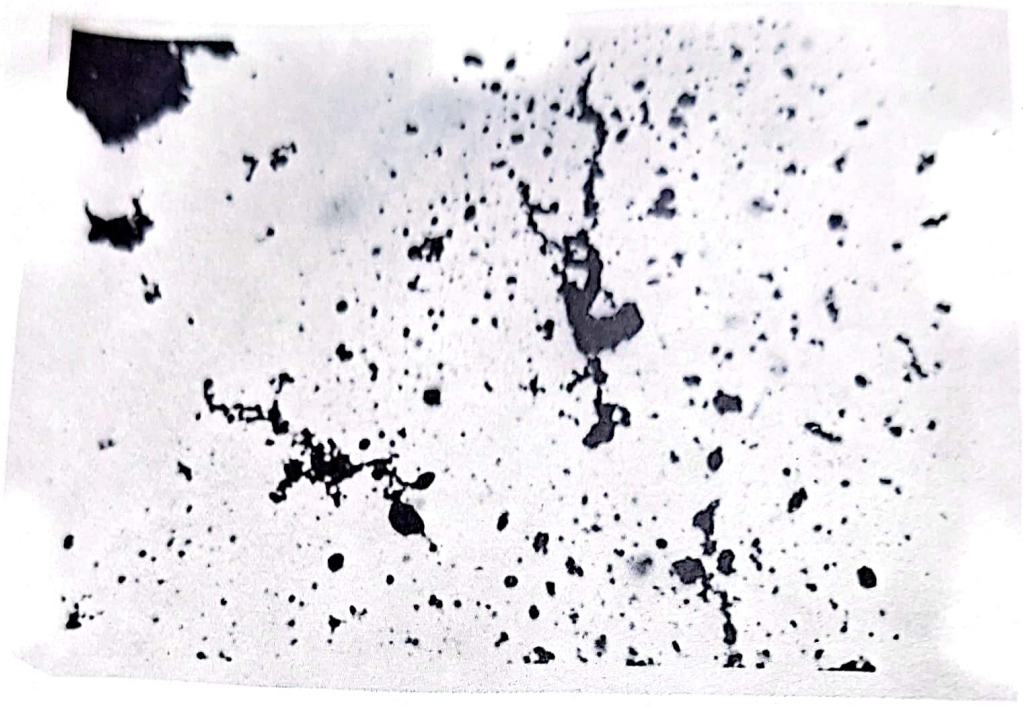

Plate 4: An electron micrograph of smoke burning bitumen (magn. 12750 x).

MEASUREMENTS AND RESULTS

Particle size measurement:

The shapes of the images of most of the particles, as seen in the electron micrographs, are neither spherical nor of any other geometrical pattern; they seemed to be randomly irregular as have been shown by previous workers (8, 9, 10). This suggests that the particles in the samples studied have no regular shape and the images will have quite different shapes if the orientations of the particles with respect to the electron beam are changed. Only for spherical particles the shapes of the image will remain unaltered whatever the direction of the beam with respect to the particle orientation. Under these circumstances, the size of each image was determined by measuring the longest and shortest dimensions of the image. Knowing the magnifications at which the micrograph was taken "the size of the particles" were determined. Using this procedure, large number of particles were measured from the electron micrographs of each specimen. Then the readings of the size measurements were sampled and the frequency of occurence of each size of the particles were plotted in histograms.

Figures (4), (5), (6) and (7) show the histograms for the size distributions of diesel exhaust particles, Al-Jamhuriyah cigarette smoke particles, dust particles and bitumen smoke particles respectively. The average size of the particles was

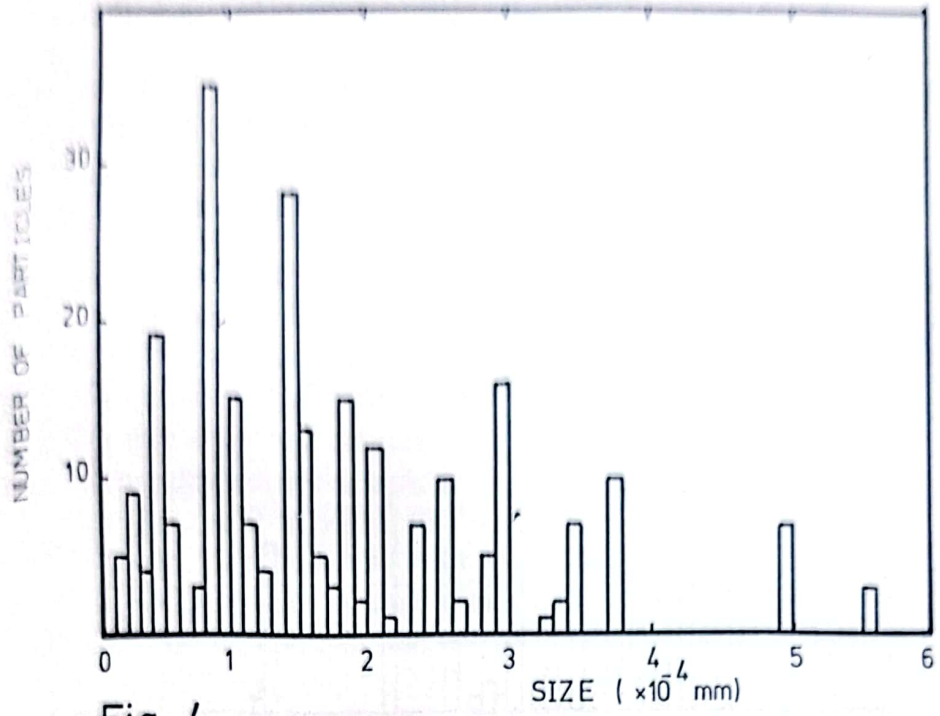

Fig. 4

Automuble engine exhaust

Fig. 4 : The size distribution of particles from a diesel engine exhaust.

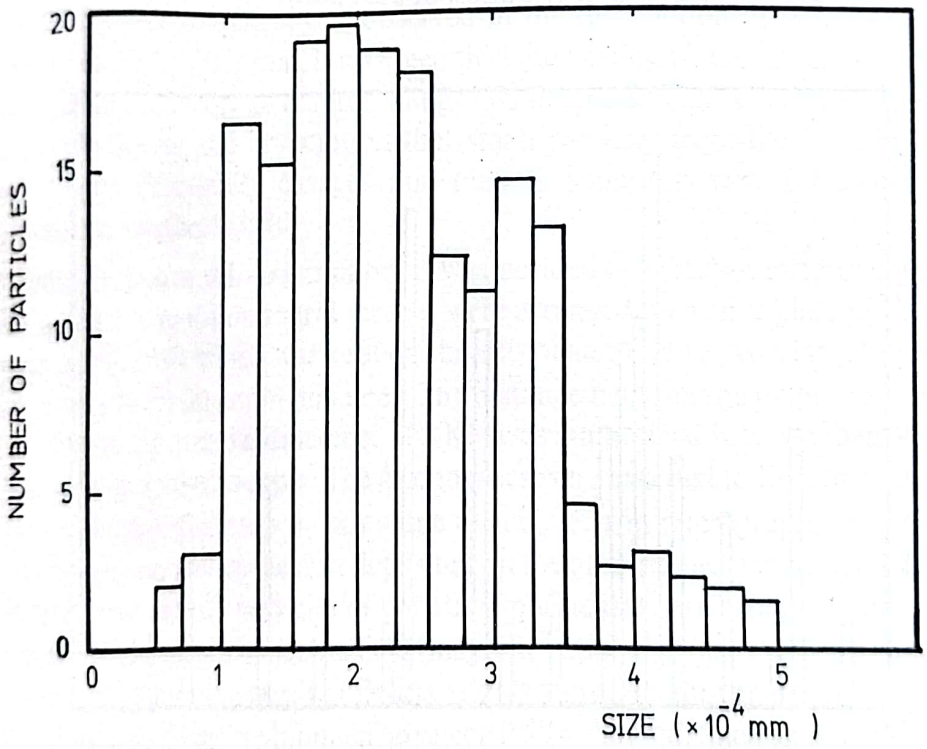

Fig. 5

Cigarette smoke

Fig. 5 : The size distribution of particles from cigarette smoke.

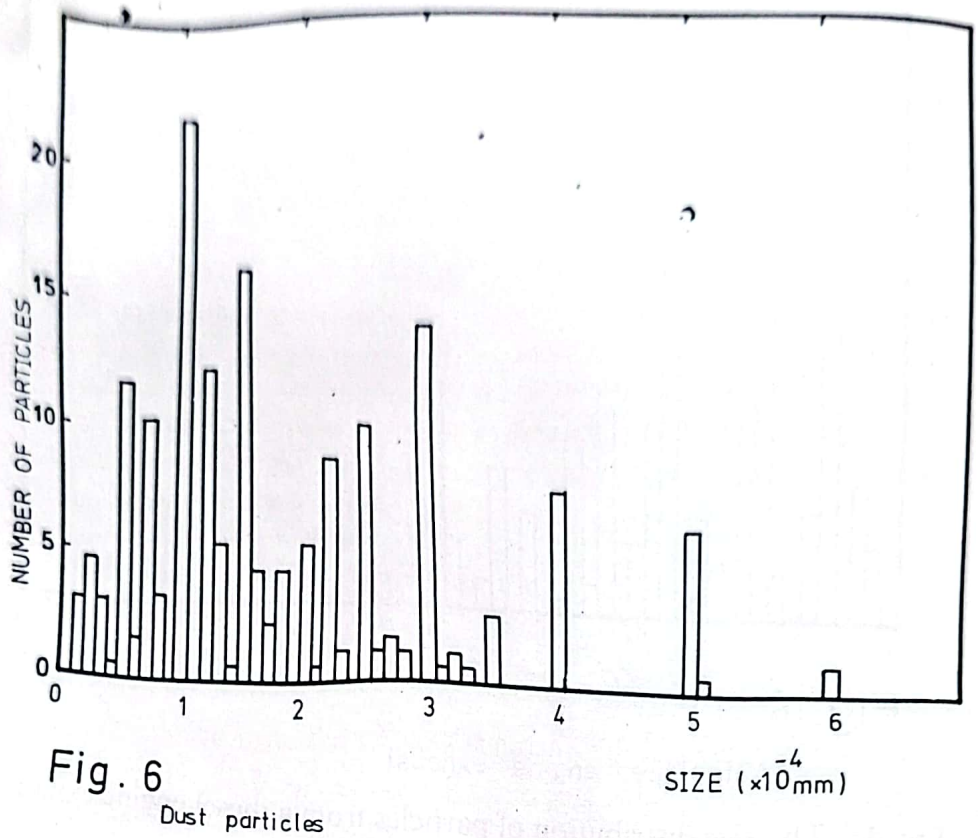

Fig. 6 : The size distribution of dust particles.

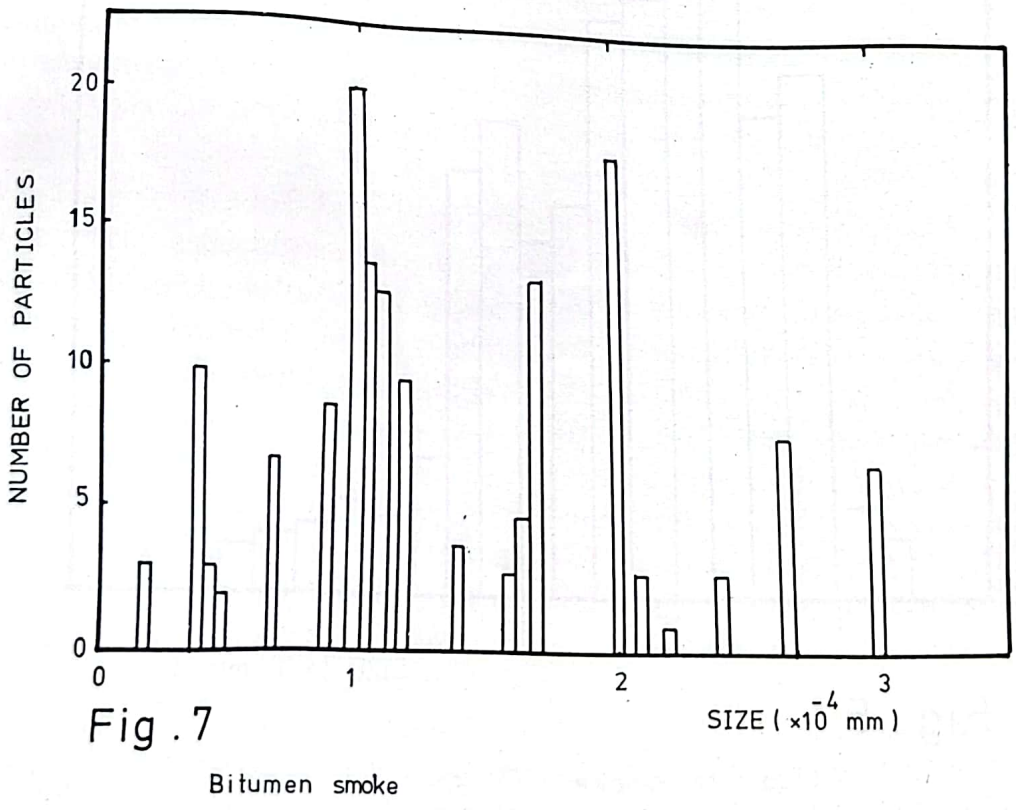

Fig. 7 : The size distribution of particles from bitumen skoke.

found to be 1.2 x 10^{-4}mm. for engines exhaust gas and many of these particles seen to aggregate in a line of thin filaments on which the individual particles presented a granular structure. In some cases these particles aggregated to form an irregular flat surfaces. On the other hand it was observed, for cigarette smoke that there were large number of small particles with average size of 1 x 10^{-4}mm. These particles are seen to have rounded shape with edges not so familiar as for particles in the engine exhaust smoke. Besides these small particles, many cloudy vortex or rings were also observed. These cloudy rings do not show any granular structure, and smoke sourced other than cigarette did not show such pattern. However,dust particle images are well defined and the average size of these particles was found to be 7 x 10^{-4}mm. Since the electron micrographs were taken by dispersing the sample with water, many of the particles may be an aggregate of smaller ones. A large number of "very small particles" were also observed in the micrographs, the size of these particles was estimated to be less than 1 x 10^{-4} mm.

The smoke from burning bitumen was observed to consist of three distinguished sizes of particles. Firstly, particles which are few in number that have a very large size with an average size of 3 x 10^{-3}mm. Secondly, a large number of particles with an average size of 1 x 10^{-3} mm, and thirdly a vast majority of small particles with an average size of 1.2 x 10^{-4}mm.

A very intersting effect was observed in the distribution of the third kind of mean size 1.2 x 10^{-4}mm, it was seen that the particles lie on a definite curve in much the same way as the iron filings in a magnetic field. This phenomenon was explained on the assumption that small particles from the hot bitumen smoke were electrically charged and their distributions were influenced by the local atmospheric field.

In order to ensure this assumption, it was decided to vertify it experimentally. This was done as follows: grid meshes were arranged on a slide glass placed in an open petri dish which was kept on the axis of and midway two large aluminium plates about 30 cm in diameter. The distance between the plates were kept at 15 cm and a potential difference of 5 KV was maintained between them using a high voltage power supply. The grid meshes were exposed to the atmospheric dust for 96 hours. Plate - 5 shows one of the electron micrographs. From the electron micrograph of the dust deposited on the grid meshes it is clearly evident that the "very small" particles of the atmospheric dust are arranged along the direction of the applied electric field (magnification = 10030 x).

This experimental result supports the assumption that many particles in hot smoke from burning bitumen are electrically charged. Such smoke particles are potentially more responsible for providing nuclei for fog formation in suitable weather condition. However, much more research is required, involving both field studies and laboratory investigation of the polution phenomena in this country, before can be established definitively whether it is of significance in our atmosphere.

Plate 5: An electron micrograph for dust particles subjected to an electric field (magn. 10030 x).

ACKNOWLEDGEMENTS

The auther wishes to express his gratitude to the director and the staff of the Biological Research Institute, Baghdad: for providing the facilities to use the electron microscope.

REFERENCES

(1) Health Hazards of the Human Health, WHO pp 22-31, Geneva 1972.
(2) Mitchell Jr. J. M. ann N. Y. Acad 95, 235-50, 1961.
(3) Reid A. Bryson and Wayne M. Wendland global effects of Atmospheric pollution Edtd. S. Fre singer, D.Reidel publishing company, Dordrecht Holland 1970.
(4) Gates R.W. Standford Res Inst Report No.2 Men. Park California 1955.
(5) Glover I.J. Inst Petrol 52, No 509, 157-160, 1966.
(6) Letau H and Lettau K. Tellus 21, 208, 1969.
(7) Landsberg, H.E. symposium-Air over cities, Sanitary Eng Center Tech Report A62-65 Cincinnati Ohio 1962.

(8) Davies C.N. Nature 195, 769,1962
(9) Wadel H. J Franklin Inst 217, 469 (1934)
(10)Cartwright J. Ann Occupational Hygn 5, 163 (1962)
(11)The Iraqi Ministry of Oil, Private Communication

الخلاصة

لقد تم قياس التوزيع الحجمي للجسميات المنتشرة في جو بغداد الناتجة عن التلوث الجوي بسبب حرق المنتجات النفطية المختلفة وعرضت النتائج على شكل رسوم بيانية .

لقد جمعت الملوثات المختلفة باستخدام احواض صغيرة مشبكة مغطاة باغشية دقيقة من الكاربون او من مادة الفورمفار ، حيث تم انتاج هذه الاغشية الرقيقة عن طريق تبخير الكاربون في الفراغ على شرائح زجاجية . وقد تم تصوير العينات باستخدام جهاز المجهر الالكتروني .

كما تم تعزيز هذه الدراسة بمعلومات احصائية تتضمن الكميات المستهلكة لمختلف المنتجات النفطية منذ عام ١٩٤٨ ، حيث تم تحليلها وعرضها بشكل رسوم بيانية يستدل منها على تزايد الاستهلاك بمرور الزمن . ويتضح من الرسوم البيانية ان كمية مايحرق ويترك مختلف الملوثات في جو بغداد يقدر بحوالي ١٤٠٠ مليون لتر من مختلف المنتجات النفطية في العام الحالي . كما تم ايضا دراسة ما يتوقع ان يحترق من المنتجات النفطية لغاية عام ١٩٨٧ .

TECHNIQUE FOR THE CALIBRATION OF HIGH-PRESSURE MERCURY VAPOUR LAMPS AND LOW-PRESSURE FLUORESCENT LAMPS

Elaine G.T. Wassef*, Mohamed M. Khodair** & Mostafa M. El-Sherif**

Received,21 April, 1976

ABSTRACT

A technique for measureing the spectral power distribution of high pressure mercury vapour lamps and low pressure fluorescent lamps developed at the National Institute for standards of Cairo is described. Assessment of the accuracy and precision of the technique is carried out by the statistiscal analysis of the data and comparison with measurements previously obtained for the same group of lamps at the National Physical laboratory of England and the Mendeleeve Institute at the USSR. The analysis gives reliable indices of the precision attainable and leads to suggestions for improving the technique.

INTRODUCTION

Photometric measurements concerning light sources are based on comparison with the standard source agreed upon in 1931 by the Commission Internationale de l 'Eclairage (CIE) to be a black-body radiator of colour temperature 2854° K having a continuous spectrum of known spectral power distribution (s.p.d.)

The calibration of incandescent lamps possessing continuous spectra has since been carried out simply and to a high degree of precision. On the other hand the heterochromatic comparisons involved in the calibration of mercury vapour and fluorescent lamps which have line spectra in addition to continuous spectra imposed serious limitations on calibration accuracy. The international comparisons carried out in 1962 on flourescent lamps[1] and in 1966 on high-pressure mercury-vapour lamps[2] did not turn out satisfactory results[3]. Considering the discordances, the photometry committee of the CIE emphasized the need for further studies of the sources of error[4].

* Presently at Physics Department, Faculty of Science, Al-Mustansiriyah University, Baghdad, IRAQ.

** National Institute for Standards-Cairo, EGYPT..

The present paper is the outcome of a study designed to explore the sources of error in the calibration technique developed in the Photometry Laboratory of the National Institute for standards (NIS) in Cairo. The paper sets out with a brief description of the calibration of the instruments. This is followed by a presentation of the measurements carried out at the NIS on lamps previously measured in England at the National Physical Laboratory (NPL) and in the USSR at the Mendeleeve Institute (VNIIM). A statistical treatment of the data leads to an evaluation of the accuracy and indicates the possibilities of improvement.

CALIBRATION OF EQUIPMENTS

A subtractive double monochromator of the Terrien-Desvignes type was used for dispersing the radiation emitted by the sources and the light flux in very narrow wave bands coming out from the monochromator was measured by means of an EMI photomultiplier receiver.

A wavelength calibration curve in the visible spectrum was made for the monochromator giving the wavelength in terms of scale readings. The estimated uncertainty in the wavelength setting varied from $\pm .3$ A° in the blue region to $\pm$ .2 A° in the red region of spectrum. The slit widths: . 1 mm, .3 mm and 1·5 mm were found suitable for the entrance, middle and exit slits respectively.

The EMI photomultiplier receiver used is sensitive in the region . 16 μ to .65 μ. Tests carried out to study linearity of response of the receiver-galvanometer combination was found to be $\pm$ .7°/$_o$ for a 240:1 variation in illumination level. The fatigue effect of the receiver was minimised by using a shutter in front of the receiver.

The monochromator receiver combination was calibrated for s.p.d. measurements using a secondary standard tungsten filament lamp of colour temperature 2854° K. The calibration constant C_λ was calculated for each wavelength where

$$C_\lambda \frac{P_{s\lambda}}{R_{s\lambda}}$$

$P_{s\lambda}$ = radiant flux emitted by the standard lamp at wavelength (as given in Table (1)

& $R_{s\lambda}$ = output of the monochromator receiver combination at wavelength.

C_λ is sometimes referred to as the spectro-radiometric response factor.

To assess the accuracy of this calibration the spectral power distribution of a secondary standard lamp of colour temperature 2353° K was measured using the full technique. Comparision of the obtained results with those

computed from Plank's formula[4] for the same colour temperature showed agreement up to ± .7 %, except at the two ends of the measured range where the differences were larger[10].

METHOD OF MEASUREMENT

For measurement of s.p.d. of a flourescent lamp, the lamp was mounted horizontally in front of the entrance slit of the monochromator supported from its current pins. The lamp was manually shorted after cathode preheating for 10 secs. The two electrodes were short-circuited to avoid any possible changes in power dissipation in the electrodes if the lamp is replaced for another measurement with reversed electrode connections. The lamp was operated with its suitable ballast from an A.C. stabilizer. The temperature of the laboratory was controlled to within ± 2° C. The lamp was first run at the rated electrical values for 20 minutes for stabilization.

The readings of the galvanometer deflections R_x every 10 nm interval of wavelength for the continuous spectrum were recorded. The relative power R_x was calculated from the equation

$$P_{x\lambda} = C_\lambda \cdot R_{x\lambda}$$

The power of the lines was evaluated by the peak response method[7] and by the integration method[8]. Comparison of results obtained by these two methods showed agreement within ± 1.2 % at the spectral line 435.8 nm and ± .8% at 546.1 nm. for lamp of the colour matching type.

ASSESSMENT OF THE TECHNIQUE

Precision and accuracy of the technique were studied by resort to statistical analysis of the results.

Precision of measurement: The s.p. d. of each of the fluorescent lamps was calculated from a mean of five readings while that of high pressure mercury vapour lamps was taken from a mean of eight readings. These readings were taken from separate runs made on each lamp. The precision of determination of the s.p.d. of the lamps was estimated by calculating the coefficient of variation V for one 20 W fluorescent lamp and for one 400 W HPMV lamp as well as for the calibration constant C . The coefficient of variation V was calculated from the equation[9]:

$$V_\lambda = \frac{\sigma_\lambda}{P_\lambda} \times 100$$

computed from Plank's formula[5] for the same colour temperature showed agreement up to ± .7% except at the two ends of the measured range where the differences were larger[6].

METHOD OF MEASUREMENT

For measurement of s.p.d. of a flourescent lamp, the lamp was mounted horizontally in front of the entrance slit of the monochromator supported from its current pins. The lamp was manually shorted after cathode preheating for 10 secs. The two electrodes were short-circuited to avoid any possible changes in power dissipation in the electrodes if the lamp is replaced for another measurement with reversed electrode connections. The lamp was operated with its suitable ballast from an A.C. stabilizer. The temperature of the laboratory was controlled to within ± 2° C. The lamp was first run at the rated electrical values for 20 minutes for stabilization.

The readings of the galvanometer deflections R_x every 10 nm interval of wavelength for the continuous spectrum were recorded. The relative power R_x was calculated from the equation

$$P_{x\lambda} = C_\lambda \cdot R_{x\lambda}$$

The power of the lines was evaluated by the peak response method[7] and by the integration method[8]. Comparison of results obtained by these two methods showed agreement within ± 1.2 % at the spectral line 435.8 nm and ± .8% at 546.1 nm. for lamp of the colour matching type.

ASSESSMENT OF THE TECHNIQUE

Precision and accuracy of the technique were studied by resort to statistical analysis of the results.

Precision of measurement: The s.p. d. of each of the fluorescent lamps was calculated from a mean of five readings while that of high pressure mercury vapour lamps was taken from a mean of eight readings. These readings were taken from separate runs made on each lamp. The precision of determination of the s.p.d. of the lamps was estimated by calculating the coefficient of variation V for one 20 W fluorescent lamp and for one 400 W HPMV lamp as well as for the calibration constant C . The coefficient of variation V was calculated from the equation[9]:

$$V_\lambda = \frac{\sigma_\lambda}{P_\lambda} \times 100$$

where σ_λ is the standard deviation given by:

$$\sigma_\lambda = \sqrt{\frac{\Sigma (p_{\lambda i} - p_\lambda)^2}{n - 1}}$$

$P_{\lambda i}$ being the individual values of the relative power at wavelength λ, calculated from n repeated readings. The results are given in Table (1). The table shows that the precision of C_λ is high in the middle part of the spectrum (from 400–600 nm) and is lower at both ends of the spectrum. Lower precision in the s.p.d. measurements for both lamps in these regions should therefore be expected.

Comparisons with results obtained in other laboratories:

The results of calibration of nine 20 W fluorescent lamps provided by the NPL England (1970), were compared with the measurements made at the NIS Cairo using the described technique. These same lamps had been measured at NPL England and at the VNIIM USSR, in the intercomparison of the CIE in 1962. The s.p.d. measurements of one of these lamps (6.1.1.) are given in table (2). The percentage differences (VNIIM - means NPL "1962") and (NIS – NPL "1970") are also given in Table (2). The table shows that the s.p.d. values obtained by both VNIIM and NIS laboratories tend to be higher than those obtained by the NPL in the blue-green and in the far red regions of the spectrum. Fig. (1) shows the percentage differences from NPL measurements against wavelength for one of the calibrated lamps. The sequence of the three measurements at the NPL laboratory shows the trend of variations in the s.p.d. of the continuous spectrum with age.

Accuracy of results:

To assess the accuracy of the adopted spectroradiometric method, the s.p.d. results of one 20 W fluorescent lamp (6.3.1) were subjected to statistical analysis as follows:

To test the hypothesis that the standard deviation of measurements at NIS does not differ from the standard deviation of measurements at NPL at the significance level .05, the F-significance test was applied to the ratio of the variances[9] calculated at every wavelength in the measured range. The results are given in Table (3). It appears that in the blue and the blue-green regions of the spectrum the variances did not differ significantly. In the green to red regions the variances of the measurements at the NIS exceeded the variances of the NPL measurements significantly. This indicates that the sensitivity of the NPL receiver surpassed that of the NIS receiver in these regions

The significance of the differences between the values of the s.p.d. was tested using the t- significance test:

$$t = (X - Y)\left[\left((1/n_x) - (1/n_y) \right) \left\{ \Sigma n_x (X_1 - X)^2 + \Sigma n_y (Y_1 - Y)^2 \right\} / (n_x + n_y - 2) \right]^{-1/2}$$

Table (1): Precision of dtermination of the calibration constant of the system and the s.p.d. of the lamps 6.3.1. and HA.

Wave-length	Calibration constant		fl. lamp 6.3.1.		HPMV-400W.HA	
(nm)	C	V_c	P_x	V_p	P_x*	V_p
380	1.209	± 0.8	3.48	± 3.7	18.47	± 2.7
90	0.960	±	5.35	± 2.2	8.45	± 2.1
400	0.770	± 1.4	7.08	± 1.9	10.78	± 4.2
10	0.610	± 0.5	9.26	± 0.9	11.28	± 2.9
20	0.499	± 0.6	11.33	± 0.3	11.65	± 1.9
30	0.405	± 0.0	13.77	± 0.3	12.63	± 3.4
40	0.335	± 0.2	16.04	± 0.4	12.87	± 2.5
50	0.281	± 0.3	17.77	± 0.2	12.54	± 0.2
60	0.245	± 0.2	19.42	± 1.3	10.24	± 0.2
70	0.217	± 0.4	20.58	± 0.6	11.72	± 0.2
80	0.194	± 0.3	21.04	± 0.6	11.74	± 0.2
90	0.176	± 0.0	21.54	± 0.3	10.95	± 0.2
500	0.162	± 0.3	21.24	± 0.5	10.41	± 0.2
10	0.152	± 0.3	22.67	± 0.4	10.87	± 0.2
20	0.146	± 0.0	26.33	± 0.3	10.18	± 1.7
30	0.145	± 0.5	32.82	± 0.4	9.46	± 1.4
40	0.150	± 0.5	50.12	± 3.2	9.30	± 2.3
50	0.161	± 0.6	67.46	± 1.4	9.51	± 1.1
60	0.177	± 0.4	100.00	—	10.00	— —
70	0.197	± 1.2	125.73	± 0.1	10.68	± 1.0
80	0.228	± 0.6	144.70	± 2.8	12.04	± 1.1
90	0.300	± 0.9	140.32	± 2.5	15.02	± 1.5
600	0.428	± 0.8	125.67	± 3.7	20.98	± 1.8
10	0.639	± 0·9	107.52	± 3.8	39.19	± 1.8
20	0.890	± 1.0	87.33	± 4.5	79.08	± 2.3
30	1.289	± 0.9	68.55	± 4.8	115.77	± 1.5
40	1.826	± 0.7	54.17	± 5.7	102.94	± 1.5
50	2.378	± 1.2	40.27	± 4.2	152.63	± 2.0
60	3.245	± 1.3	30.94	± 4.8	211.21	± 1.7
70	4.425	± 0.9	24.21	± 3.7	114.11	± 4.2
80	6.181	± 1.4	19.23	± 2.1	52.11	± 1.9
90	11.943	± 2.4	13.28	± 4.7	28.59	± 5.3
390.6	— — —	— — —	— — —	— — —	10.66	± 1.7
405	0.670	± 0.6	44.01	± 1.1	333.13	± 1.1
435.8	0.364	± 0.2	120.22	± 1.8	502.11	± 2.4
491.6			— — —	— — —	12.14	± 1.5
546.1	0.157	± 0.5	50.14	± 1.3	799.88	± 2.7
578	0.222	± 0.8	58.71	± 1.3	998.90	± 1.7

* The values of the relative s.p.d. of the HPMV lamp HA given here were adjusted so that the value at 560 nm is equal to 10.00.

Table (2): Comparison of spectral power distribution results for the lamp 6.1.1.

Wavelenght	Relative power					% differences	
	1962 intercomparison			1970	VNIIM –		
(nm)	NPL	VNIIM	NPL 2nd	NPL	mean of the NIS NPL.(1962)		NPL (1970)
380	7.8	——	8.0	8.0	7.6	– –	– 5.0
90	12.0	——	12.0	12.5	12.8	——	+ 2.4
400	16.0	16.3	16.3	16.9	16.8	+ 0.6	– 0.6
10	21.0	20.2	21.1	22.0	22.3	– 3.9	+ 1.4
20	26.7	27.2	27.0	27.7	27.7	+ 1.4	0.0
30	32.3	33.1	32.8	33.1	33.7	+ 1.5	+ 1.8
40	38.2	40.1	38.5	39.0	39.2	+ 4.4	+ 0.5
50	43.3	45.2	43.6	44.0	44.5	+ 4.1	+ 1.1
60	47.5	48.7	47.7	47.9	49.0	+ 2.3	+ 2.3
70	50.6	51.8	50.5	50.5	51.9	+ 2.3	+ 2.8
80	51.7	53.5	51.8	51.9	53.1	+ 3.2	+ 2.3
90	51.8	52.6	51.6	52.0	53.0	+ 1.7	+ 1.9
500	50.7	51.1	50.7	51.0	51.2	+ 0.7	+ 0.4
10	49.2	49.1	49.2	49.7	49.6	– 0.2	– 0.2
20	49.6	48.2	49.5	50.1	49.8	– 2.9	– 0.6
30	54.3	55.0	54.3	54.5	54.1	+ 1.2	– 0.7
40	65.2	65.4	65.3	65.3	66.3	+ 0.3	+ 1.5
50	81.8	80.3	81.8	82.3	82.2	– 1.8	– 0.1
60	100.0	100.0	100.0	100.0	100.0	——	——
70	113.9	113.3	113.9	114.0	112.6	– 0.5	– 1.2
80	119.3	117.5	119.2	118.9	122.3	– 1.4	+ 2.9
90	114.3	117.0	114.0	113.3	106.1	+ 2.4	– 6.8
600	102.8	108.3	102.6	101.2	94.0	+ 5.4	– 7.1
10	87.2	87.4	86.6	85.3	77.5	+ 0.5	– 9.1
20	70.3	73.0	69.8	68.8	63.6	+ 4.2	– 7.6
30	54.8	59.4	54.7	53.5	47.1	+ 8.3	–12.0
40	41.3	44.1	41.0	40.6	39.1	+ 7.0	– 3.7
50	31.4	30.7	31.0	30.6	29.1	– 1.6	– 4.9
60	23.7	23.3	23.4	22.9	23.6	– 1.2	+ 3.1
70	17.7	18.7	17.6	17.3	16.5	+ 6.2	– 4.6
80	13.3	17.0	13.4	13.2	15.0	+26.8	+13.6
90	10.5	14.8	10.4	10.5	12.5	+42.3	+19.0
700	8.1	13.2	8.4	8.1	11.6	+60.9	+43.2
404.7	44.2	39.2	43.5	37.7	42.9	– 5.7	+13.8
407.8	2.2	2.2					
435.8	117.2	116.8	116.5	102.8	113.0	0.0	+ 9.9
546.1	55.3	55.7	53.2	50.5	52.5	+ 2.7	+ 4.0
578	15.7	15.3	15.0	15.9	14.2	– 0.6	–10.7

Table (3) : Significance of variances and the differnces between the N.I.S.and N.P.L. 1970 results.

(nm)	NIS mean x	NPL mean y	Variance NIS_2 x	Variance NPL_2 y	F value NIS	F value NPL	t value NIS	t value NPL
380	3.5	3.6	0.0169	0.0225		1.33		1.21
90	5.6	5.7	0.0169	0.0025	6.76			1.61
400	7.1	7.3	0.0169	0.0000	——			3.33*
10	9.3	9.3	0.0049	0.0100		2.04	——	——
20	11.3	11.5	0.0010	0.0100		6.25		4.29*
30	13.8	13.7	0.0016	0.0196		12.25*	1.21*	
40	16.0	15.9	0.0064	0.0025	2.56		3.04*	
50	17.8	17.8	0.0016	0.0400		25.00*		
60	19.4	19.3	0.0081	0.0196		2.42	1.82	
70	20.6	20.4	0.0225	0.0196	1.15		2.26	
80	21.0	20.9	0.0121	0.0100	1.21		1.24	
90	21.6	21.2	0.0081	0.0100		1.23	6.23*	
500	21.2	21.5	0.0121	0.0025	4.84			4.61*
10	22.7	22.9	0.0121	0.0169		1.40		3.58*
20	26.3	26.6	0.0016	0.0169		10.56*		5.40*
30	32.8	33.6	0.0121	0.0576		4.76		6.44*
40	50.1	47.0	4.1209	0.0196	(210.25)*		3.02	
50	67.4	70.5	0.8649	0.0841	10.28*			6.22*
60	100.0	100.0						
70	125.8	128.3	0.0225	0.4624		20.55*		8.10*
80	144.7	146.3	16.24	0.6084	26.69*			0.75*
90	140.3	148.8	12.18	1.04	11.71*			4.63*
600	125.7	138.4	29.05	1.5129	19.20*			4.55*
10	107.5	119.8	16.65	0.2916	57.01*			5.93*
20	87.3	98.2	15.60	0.9409	16.58*			5.30*
30	68.5	76.9	11.02	0.2268	27.97*			4.92*
40	54.2	58.4	9.67	0.1600	60.44*			2.64*
50	40.2	43.4	2.89	0.1089	26.54*			3.58*
60	30.9	31.9	2.10	0.0484	43.39*			1.26
70	24.2	23.2	0.7921	0.0484	16.37*		2.20	
80	19.2	17.1	0.1600	0.0841	1.90		8.71*	
90	15.0	12.7	0.3136	0.0100	31.36*		8.07*	
700	13.3	9.0	0.3844	0.0441	8.72		13.14*	
405	44.0	35.8	0.2601	1.2769		4.91	14.50*	
436	120.2	99.3	4.7089	3.9601	1.19		14.88*	
546	50.2	46.9	0.4489	3.7249		8.30*	3.50*	
578	15.6	16.0	0.1156	0.0289	4.00		3.21*	

* indicates the significant values.

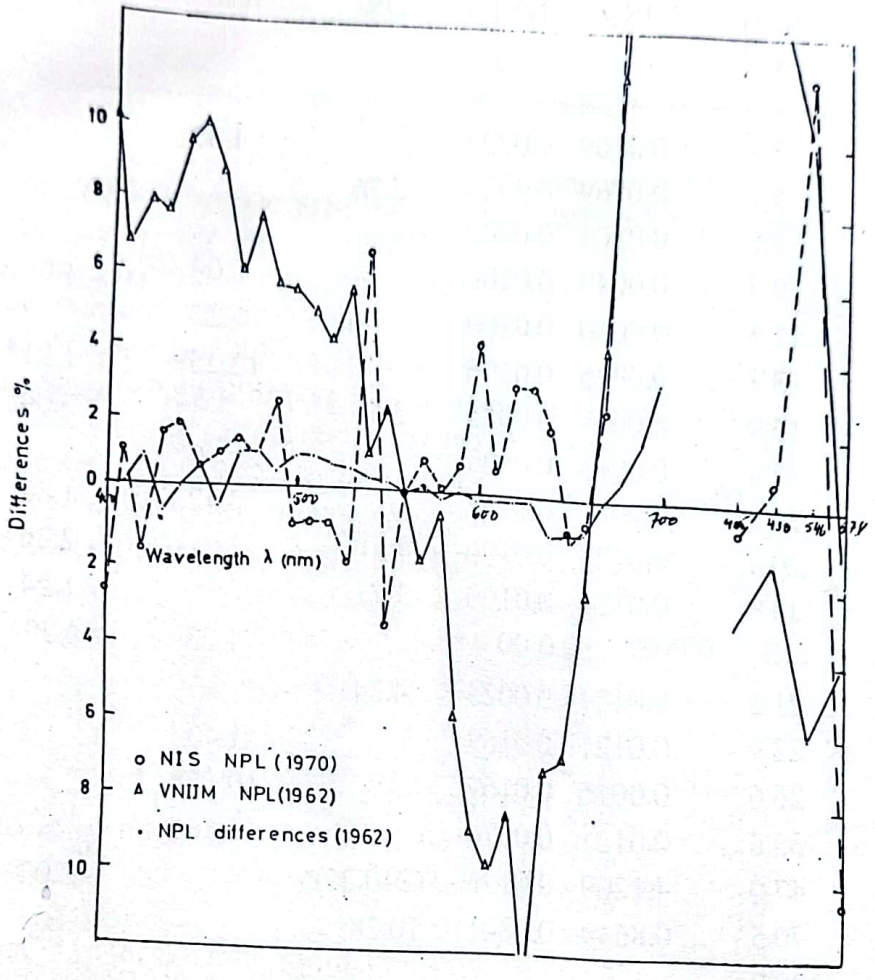

Fig.(1): Percentage differences in determination of the s.p.d. of the lamp No. 6.3.1.

where:

$\overline{X}$ and $\overline{Y}$ are the means of the NIS and NPL respectively. X_1 & Y_1 are the individual values of n_x measurements at NIS and n_y measurements at NPL. The calculated values of t (table 3) were compared with t = 2.36 corresponding to the significance level. 025 with seven degrees of freedom. The results show that the differences within the region 380-480 nm are not statistically significant while most of the differences are highly significant at other wavelengths .

CONCLUSION

The results of the calibration at the NIS, Cairo of the 20 W fluorescent lamps already calibrated at the NPL, England at 1962 & 1970 and at VNIIM, USSR offered a chance for assessing the technique employed at NIS. The statistical analysis of the differences in spectral power distribution measurements and the comparison of their variances give reliable indices of the precision attainable at each laboratory and provides the possibility of testing the significance of the apparant discordances between the results.

The analysis given in this paper shows that the precision of measurements at NPL England is higher in the blue-green regions than in the red regions. The lower precision of the measurements at NIS can be improved by using another receiver in the red region.

REFERENCES

(1) L.O. Sayce, Report on the international intercomparison of photometric and colorimetric measurements on fluorescent lamps, N.P.L., Teddington, Middlessex (1962).

(2) K. Yoshie, Report on the international intercomparison of photometric measurements on high-pressure mercury vapour lamps, E. T. L., Japan (1966).

(3) F. Lindgren, Report on the meetings of the C.I.E., E.1.2. photometry, in Paris 1965.

(4) Recommendations on the photometric measurements of gas discharge lamps, C.I.E. Proceedings (1970).

(5) G.W. Wyszecki & W.S. Stiles, Colour Science, John Wiley & Sons, Inc., N.Y., (1967).

(6) Mostafa M. El-Sherif; M.Sc. Thesis, Ain Shams University, Cairo (1971).

(7) M.P. Lord, Proc. Phys Soc., 58, 477 (1946).

(8) L. Foitzik and H. Zschack, Feingeratetechnik 7, 105 (1958).

(9) A.H. Bowker, G.J. Lieberman, Engineering Statistics, Prentice-Hall, Inc. N.Y., 6th printing, (1964).

الخلاصة

في هذا البحث وصف للطريقة التي تستخدم في المعهد القومي للقياس والمعايرة بالقاهرة لمعايرة مصابيح الزئبق ذات الضغط العالي والمصابيح الفلورنسية ذات الضغط المنخفض وبمقارنة نتائج المعايرة مع نتائج اخذت على نفس المصابيح في المعامل الاهلية الأخرى بانكلترا والاتحاد السوفيتي وباستخدام التحليل الاحصائي امكن تقييم الطريقة المستخدمة من ناحية الدقة كما امكن اقتراح التطوير اللازم للحصول على دقة اعـــلى .

ON THE DISTRIBUTION OF DIFFERENCES OF A MATRIX

S. R. Al-Ani

Al-MustansiriyahUniversity

Faculty of Science, Baghdad - Iraq.

Received, 17th May 1976

INTRODUCTION

Many distributional problems in multivariate analysis involve certain Polynomials, namely, Zonal Polynomials, which are expressible in terms of elementary symmetric functions (esf) of the latent roots of a matrix.

Al-Ani[1,2] and Pillai[5] have studied the individual roots and the ratios of some matrices in multivariate analysis . In this paper we study the distribution of differences of latent roots which follow the Fisher-Hsu-Girshick-Roy distribution, the study has been carried out up to (including) the four roots case.

ZONAL POLYNOMIALS

Let V_k be the vector space of homogeneous polynomials Ψ (S) of degree k in the n = (1/2)m (m+1) different elements of the m x m symmetric matrix S. The dimension N of V_k is the number

$N = (n + k - 1) ! / (n - 1) ! K !$ of nomials

$\prod_{i<j}^{m} k_{ij}^{s_{ij}}$ of degree $k = \sum_{i \leqslant j}^{m} kij$

Corresponding to any congruence transformation

$$S \longrightarrow LSL' \qquad (2.1)$$

by a non-singular m x m matrix L, we can define a linear transformation of the vector space V_k of polynomials Ψ (S), namely

$$\Psi \longrightarrow L\Psi : (L\Psi)(S) = \Psi(L^{-1}SL^{-1}) \qquad (2.2)$$

A subspace $V' \subset V_k$ is called invariant if $LV' \subset V'$ for all non-singular matrix L. V' is called irreducible invariant subspace if it has no proper invariant subspace.

Now V_k (see Thrall [7]) decomposes into a direct sum of irreducible subspaces V_p. Corresponding to each partition P of K into not more than m parts . .

$$V_k = + V_p \qquad (2.3)$$

where $P = (K_1, K_2, \ldots, K_m), \sum_1^m Ki = P,$

$K_1 \geqslant K_2 \geqslant \ldots \geqslant K_m \geqslant 0$

Since $(tr' S)^k \varepsilon V_k$, then has a unique decomposition

... $(trS)^k = \Sigma\ C_p(S)$
p

into polynomials, $C_p(S) \varepsilon V_p$, belonging to the respective invariant subspace.

Hence the Zonal polynomial $C_p(S)$ is defined as the component of $(trS)^k$ in the subspace V_p. It is a symmetric homogeneous polynomials of degree K in the latent roots of S, (See Al-Ani [3]).

THE DISTRIBUTION OF THE DIFFERENCES

In this section we find the joint and the marginal distributions of the differences $\theta i - \theta j$, i> j when P = 2,3,4. The joint density of a P non-null roots of a matrix derived from sample observations under certain null hypotheses can be expressed in the form:

$$C \prod_{i=1}^{p} \theta^m{}_i\ (1-\theta_i)^n \prod_{i>j} (\theta_i - \theta_j) \qquad (3.1)$$

where, $O < \theta_1 \leqslant \theta_2 \leqslant \ldots \leqslant \theta_p \leqslant 1$, parameters c, m, and n are differently for various situations described in [5].

Transform $q_i = \theta_i/\theta_p$, i = 1,2, ... , P -1, then the distribution of $q_1, q_2, \ldots, q_{p-1}, \theta_p$ can be written as

$$C\,\theta_p^{mp} + (p\ 1)(1 + p/2)(1 - \theta_p)^n \prod_{i=1}^{p-1} \left\{ q_i (1 - q\,\theta_p)^n (1 - q_i) \right\}$$

$$\prod_{i>j} (q_i - q_j),\ O \leqslant q_1 \leqslant \ldots \leqslant q_{p-1} \qquad (3.2)$$

Now consider the transformation $d_i = \theta_p (1 - q_i)$

$i = 1, \ldots, p-1$. Then $d_1, \ldots, d_{p-1}, \theta_p$ will be distributed as:

$$C \left| D \right| \prod_{i<j} (d_i - d_j) \sum_{d=o}^{\infty} \sum_{a} (-m)a/d! \sum_{k=o}^{\infty} \sum_{b}$$

$$\frac{(-1)^k (-n)_b C_a (D) \theta_p^{mp-d} (1-\theta_p)^{p-k}}{K!} \qquad (3.3)$$

where a and b are the partitions of d and k, and

$$(A)_b = \prod_{i=1}^{m} (A - 1/2 (i-1))_{bi} \text{ where } (A)_{b1} = A(A+1). \; D = \text{diag}$$

$(d_1, d_2, \ldots, d_{p-1})$. Now integrate equation (3.3) with respect to θ_p, then d_1, d_2, $- . d_{p-1}$ are distributed in the form,

$$C \left| D \right| \prod_{i<j} (d_i - d_j) \sum_{d=o}^{\infty} \sum_{a} \frac{(-m)\, a}{d!} \sum_{k=0}^{\infty} \sum_{b} \frac{(-1)^k (-n)\, b}{K!}$$

$$C_a (D) C_b (D) \, I (d_1, 1; m(1/2) - d, np - k), \qquad (3.4)$$

$o < d_{p-1} \leqslant d_{p-1} \ldots \leqslant d_1 \; 1$

where $I (a, b; c, d) = \int_a^b x^c (1 - x)^d \, dx$

for $p = 2$, equation (3.4 reduces to:

$$f(d_1) = C \sum_{j=o}^{m} \binom{m}{j} (-1)^j \sum_{i=o}^{n} \binom{n}{i} d_1^{\, m+n+1-(i+j)}$$

$$L (d_1, 1; m + j, n + i) \qquad (3.5)$$

For $p = 3$, the joint density of d_1, d_2 can be written in the form:

$$C \sum_{d=o}^{\infty} \sum \frac{(-m)\, a}{dl} \sum_{k=o}^{\infty} \sum_{b} \frac{(-1)^k (-n)\, b}{k!} \sum_{c} g(a,b) \sum_{i+j=t}$$

$$hij \left\{ d_1^{\, i+2} d_2^{\, j+1} - d_1^{\, i+1} d_2^{\, j+2}) \, I (d_1, 1; 3m\text{-}d, 3n - k) \right\} \qquad (3.6)$$

we notice that g- coefficients come from

$$C_a(D)\, C_b(D) = \sum_c g_{a,b}\, C_c(D)$$

tabulated up to the 7^{th} degree in Khati and Pillai[4].

hij are such that $C_c\begin{pmatrix} d_1 & 0 \\ o & d_2 \end{pmatrix} = \sum_{i+j=t} \text{hij}\, d^i{}_1\, d^j{}_2$; c is the partition of t and $t = k + d$.

Integrate equation (3.6) with respect to d_2, then the density of d_1 is of the form,

$$C \sum_{d=o}^{\infty} \sum_a \frac{(-m)a}{d\,!} \sum_{k=o}^{\infty} \sum_b \frac{(-1)^k (-n)\, b}{K!} \sum_T g\,(a,b)$$

$$\sum_{i+j=t} \left\{ \text{hij}\, \frac{di^{t+4}}{(j+2)_2} I\,(d_1, I\,;\, 3m-d, 3n-k) \right\} \qquad (3.7)$$

Again, integrate equation (3.6) with respect to d_1 (by parts) then the density of d_2 is given by:

$$C \sum_{d=o}^{\infty} \sum_a \frac{(-m)a}{d!} \sum_{k=o}^{\infty} \sum_b \frac{(-1)^k (-n)b}{k!} \sum_T g(a, b)$$

$$\sum_{i+j=t} \text{hij}\, \frac{1}{(i+2)_2} \{\, d^t{}_2{}^{+4} I(d_2, 1\,;\, 3m-d, 3n-k) +$$

$$d^j{}_2{}^{+1}\, (i+2)\, I\,(d_2, 1; 3m-d\, +\, i+3, 3n\, -\, k)\, -\, (i+3)$$

$$d^j{}_2{}^{+2}\, I(d_2, 1; 3m-d+i+2, 3n-k)\} \qquad (3.8)$$

Now let $a_1 = d_1{}^{-d2} = \theta_2 - \theta_1$, then find the density of a_1 and d_1, then integrate again with respect to d_1, we get the density of a_1 in the form,

$$C \left[\sum_{d=o}^{\infty} \sum_a \frac{(-m)a}{d!} \sum_{k=o}^{\infty} \sum_b \frac{(-1)^k (-n)b}{k!} \sum_T g(a, b) \right.$$

$$\left. \sum_{i+j=t} \text{hij} \sum_{r=o}^{j+1} (-1)^r \binom{j+1}{r} / t+r-3 \right] (-a_1\, I\,(a_1, 1; 3m-d,\ 3n-k)$$

$$+\, a_1{}^r + 1\, I\,(a_1, 1;\ 3m-d\, +\, t+3-r,\ 3n-k) \qquad \ldots \qquad (3.9)$$

For P = 4, let P = 4 in equation (3.4) and integrate with respect to d_1 and further with respect to d_2 we get the density of d_3 in the form,

$$C \sum_{d=o}^{\infty} \sum_{a} \frac{(-m)a}{d!} \sum_{k=o}^{\infty} \sum_{b} \frac{(-1)^k(-n)b}{K!} \sum_{T} g(a,b)$$

$$\sum_{hi1,\, i_2,\, i_3} d_3^{\,i_3+1} \Bigg[- \frac{2d_3^{\,i_1+i_2+7}}{(i_1+2)_3(i_1+i_2+5)_3} I(d_3, 1; a', b')$$

$$+ \frac{I(d_3, 1; c' + 3, 'b)}{(i_2+3)_2(i_1+i_2+7)} - \frac{2d_3\, I(d_3, 1, e+2, b')}{(i_2+2)(i_2+4)(i_1+i_2+6)}$$

$$+ \frac{d_3^2\, I(d_3, 1; c' + 1, b')}{(i_2+2)_2(i_1+i_2+5)} - \frac{d_2^{\,i_2+3}\, I(d_3, 1; e_{1+2}, b')}{(i_2+2)_2\,(i_1 + 4)} \qquad (3.10)$$

where $a = 4m - d$, $b = 4n - k$, $c = d_1^{\,i_1+1}\, d_2^{\,i_2+1}\, d_3^{\,i_3+1}$

$e = i_1 + i_2 + 4 + a$, $e_1 = a + i_1 + 2$

Similarly one can obtain the density of d_1 as:

$$C \sum_{d=o} \sum_{a} \frac{(-m)a}{d!} \sum_{k=o}^{\infty} \sum_{b} \frac{(-1)^k\,(-n)b}{k} \sum_{T} (g(a,b)$$

$$i_1 + i_2 + i_3 = t \; hi_1, i_2, i_3$$

$$\frac{2(i_2 + 2i_3 + 9)}{(i_3+2)_3(i_2+i_3+5)_3} I(d_1, 1; a', b') \qquad \ldots\ldots\ldots\ldots \qquad (3.11)$$

and the density of d_2

$$C \sum_{d=o}^{\infty} \sum_{a} \frac{(-m)a}{d} \sum_{k=o}^{\infty} \sum_{b} \frac{(-1)^k(-n)b}{k} \sum_{T} g(a,b)$$

$$i_1 + i_2 + i_3 = t$$

$$hi_1, i_2, i_3\, d_2^{\,i_2+i_3+4} \left[2(i_1 - i_2) d_2^{\,i_1+4} / (i_1+2)_3(i_3+2)_3 \right] I(d_2, 1; a', b')$$

$$+ \frac{I(d_2, 1\, e_1 + 2, b')}{(i_1+4)(i_3+2)_2} - \frac{2d_2\, I(d_2, 1; e_1+1, b')}{(i_1+3)(i_3+2)(i_3+4)} + \frac{d_2^2\, I(d_2, 1; e_1, b')}{(i_1+2)(i_3+3)_2} \quad \ldots\ldots \quad (3.12)$$

Now make the transformation
$d_1 = r_1 + r_2 + r_3$, $d_2 = r_2 + r_3$, $d_3 = r_3$, $r_{13} = \theta_3 - \theta_1$
Then one can find the joint distribution of r_1, d_2 further, integrate d_2 over $o < d_2 < 1 - r_1$ then the distribution of r_1 can be written in the form;

$$C \sum_{d=o}^{\infty} \sum_{a} \frac{(-m)a}{d} \sum_{k=o}^{\infty} \sum_{b} \frac{(-1)^k (-n)\, b}{K} \sum_{T} g(a,b)$$

$$i_1 + i_2 + i_3 = t^{hi_1,\ i_2.,\ i_3}$$

$$\left[\frac{r_1}{(i_3 + 2)_2} \int_o^{1-a} \left\{ \sum_{r=o}^{i_1+1} r^{(i+1)}\, {r_1}^{r+1}\, {d_2}^{t+6-r}\, (d_2 + r_1)^a (1 - d_2 - r_1)^b \right.\right.$$

$$\left.\left. (r_1/t+6-r) + + \left(2/(i_3+4)(t+7-r) \right) /(t+6-r) \right\} dd_2 \right] \qquad (3.13)$$

Similarly one can find the density of r_2 and of r_{12}.

REFERENCES

1. S. Al-Ani, "On-the noncentral distribution of the second largest roots of three matrices in multivariate analysis", Canadian Math. Bull., 13 (3), pp. 299 - 304 (1970).
2. S. Al-Ani, "On the i^{th} latent roots of a complex matrix", Canadian Math. Bull., 15 (3), (1972).
3. S. Al-Ani, "On the moments of elementary symmetric functions of the roots of a matrix", Al-Mustansiriyah University Review, Vol. 4, pp. 151 - 158 (1974)
4. C.G. Khati, and K.C.S. Pillai, "On the non-centraldistribution of two tests criteria in multivariate analysis", Ann. Math. Statist., Vol. 39, pp. 215-226 (1968).
5. K.C.S. Pillai, "On the distribution of the largest root of a matrix in multivariate analysis", Ann. Math. statist, 38, pp. 616-617 (1967).
6. K.C.S. Pillai, and S. Al-Ani, "Power comparisons of tests of equality of two covariance matrices Based on Individual characteristic roots", J. Amer. Stat. Assoc., Vol. 65, pp. 438-446 (1970).
7. R.M. Thrall, "On symmetrized Kronecker Powers and the structure of the free liering", Amer. J. of Math., 64, pp. 371-388 (1942).

PREDICTION OF STATIONARY STOCHASTIC PROCESSES Lag h, h > 1, WITH ASYMPTOTIC BEHAVIOR OF ERRORS THE Lag h PREDICTION OF A STATIONRY STOCHASTIC PROCESS, h > 1.

Magdy G. Riskalla

Mathematics Department, Al-Mustansiriyah University,
Baghdad-Iraq.

Received, 17th Feb. 1976

ABSTRACT

The finite predictor is expressed in terms of Szego polynomials on the unit circle, and the infinite predictor is introduced in terms of the spectral density function of the process. Then, the error of prediction with asymptotic relationship to the spectral density function are introduced. Finally , the additional error introduced by using a finite section of the infinite predictor instead of the finite predictor is shown to be related to both the error of prediction and the spectral density function.

INTRODUCTION

Baxter [1-5], and Hirschman, Jr., [10] have obtained some extremely, interesting results in the problem of Linear prediction of a regular stationary stochastic process lag 1. The purpose of this paper is to present general results for the class of prediction problems lag h, h $\geqslant$ 1.

AMS 1970 *subject classification.*

Primary 60G25; Secondary 42A08

Key phrases: Stationary stochastic process, Lag h, finite predictor, infinite predictor, Szego polynomials.

2. The finite predictor lag h, h $\geq$ 1

Let $\{x_n\}_{-\infty}^{+\infty}$ be a stationary stochastic process which is linearly regular, i.e., it has an a.e. positive spectral density function $C(\theta)$ such that $\int \log C(\theta) > -\infty$.

Suppose that $x_{-n}, x_{-n+1}, \ldots x_0$ are given, and we are to predict x_h; $h > 1$ (in the least square sense). This is equivalent to minimizing

$$\| x_h - \sum_{m=0}^{n} a(n,m)\, x_{-m} \|_2^2 = \int | g_n(z) |^2 C(\theta)\, d\theta \qquad (1)$$

$$\text{where } z = e^{2\pi i\theta}, \text{ and } g_n(z) = z^h \sum_{m=0}^{n} a(n,m)\, z^{-m} \qquad (2)$$

Theorem 1:

Among all functions of the form (2), there exists one which minimizes (1). Such function has the form

$$g_n^*(z) = \sum_{j=1}^{h} b_j^{(n)} e^{2\pi i j\theta} v(n+j, \theta) \qquad (3)$$

where the $b_j^{(n)}$,s are the unique solution of the system

$$\sum_{j=0}^{m} b^{(n)}_{h-j}\, v(n + h - j, m - j) = \delta_{m,0} \qquad (4)$$

$$m = 0, 1, \ldots, h - 1.$$

Also,

$$a(n,m) = -\sum_{j=1}^{h} b_j^{(n)}\, v(n + j,\ m + j). \qquad (5)$$

First of all, such a predictor exists. If we consider the closed linear hull $L_2(X)$ defined by the process $\{X_n\}_{-\infty}^{+\infty}$, then $L_2(X)$ is a complex Hilbert space (8; 10.2) with the scalar product $(f,g) = Efg$. Moreover, let $L = (X_{-n}, \ldots, X_0)$ be the linear manifold generated by $X_{-n}, X_{-n+1}, \ldots, X_0$. Since $\int \log C(\theta) > -\infty$ then (9; 3.1) X_h does not lie completely in L. Then

$$L_2(X) = L + (L_2(x) - L).$$

So, $X_h = \hat{X}_h + X_h'$, where $\hat{X}_h \varepsilon L$ and $X'_h = X_h - \hat{X}_h \varepsilon L_2(X) - L$

and $\hat{X}_h \perp X_h'$. Finally, $\| \hat{X}_h - X_h \| = \min_{x \varepsilon 1} \| X_h - X \|$.

Secondly, we show that corresponding to X_h the function $g_n^*(z)$ has the form (3). We consider

$\int \left| g_n(z) \right|^2 C(\theta)\, d\theta$. Let $\{\Phi(n,\theta)\}$ and $\{\Psi(n,\theta)\}$ be Szego polynomials

defined by $C(\theta)$. Then, $z^n g_n(z) = \sum_{j=0}^{n+h} a_j \Phi(j,\Phi)$, and, $\int \left| g_n(z) \right|^2 C(\theta)\, d\theta =$

$\sum_{j=0}^{n+h} |a_j|^2 > \sum_{j=n+1}^{n+j} |a_j|^2$.

Consequently, the function

$$g_n^*(z) = z^{-n} \sum_{j-n+1}^{n+h} a_j \Phi(j,\theta)$$

$$= z^h - \sum_{m=0}^{n} a(n,m)\, z^{-m}$$

attains the minimum.

By comparing coefficients we get

$$g_n^*(z) = \sum_{j=1}^{h} b_j^{(n)}\, e^{2\pi i i\theta}\, v(n+j,\theta), \tag{6}$$

where the $b_j^{(n)}$'s are the unique solution of the system

$$\sum_{j=0}^{m} b_{h-j}^{(n)}\, V(n+j,\ m-j) = \delta_{m,0} \tag{7}$$

$m = 0, 1, 2, \ldots, h-1$.

Therefore, the finite predictor is

$$\hat{X}_h = -\sum_{m=0}^{n} \sum_{j=1}^{h} b_j^{(n)}\, V(n+j,\ m+j)\, X_{-m}. \tag{8}$$

3. The infinite predictor

It is easy to see that prediction of X_n based on an infinite section of the past $\{X_0, X_{-1}, X_{-2}, \ldots\}$ can be done in the same manner as in 2, or simply by taking limits as $n \to \infty$.
So,

$$\hat{X}_h = \sum_{m=0}^{\infty} a(m)\, X_{-m},$$

where

$$a(m) = \sum_{j=1}^{h} b_j^{(\infty)}\, V(m+j),$$

and the $b_j^{(\infty)}$'s are the unique solution of

$$\sum_{j=0}^{m} b_h^{(\infty)}{}_j\, V(m-j) = \delta_{m,0} \tag{9}$$

$m = 0, 1, 2, \ldots, h-1.$

We proceed now to formulate the infinte predictor in terms of V (θ). If we write the system of equations (9) in a determinant form, we get

$$\begin{vmatrix} V(0) & 0 & \cdots & 0 \\ V(1) & V(0) & \cdots & 0 \\ \vdots & \vdots & & \vdots \\ V(h-1) & V(h-2) & \cdots & V(0) \end{vmatrix} \begin{vmatrix} b_h \\ b_{h-1} \\ \vdots \\ b_1 \end{vmatrix} = \begin{vmatrix} 1 \\ 0 \\ \vdots \\ 0 \end{vmatrix}$$

which is equivalent to

$$\begin{vmatrix} 1 & 0 & 0 & \cdots & 0 \\ \frac{V(1)}{V(0)} & 1 & 0 & \cdots & 0 \\ \frac{V(2)}{V(0)} & \frac{V(1)}{V(0)} & 1 & \cdots & 0 \\ \vdots & \vdots & \vdots & & \vdots \\ \frac{V(h-1)}{V(0)} & \frac{V(h-2)}{V(0)} & \frac{V(h-3)}{V(0)} & \cdots & 1 \end{vmatrix} \begin{vmatrix} b_h \\ b_{h-1} \\ b_{h-2} \\ \vdots \\ b_1 \end{vmatrix} = \begin{vmatrix} \frac{1}{V(0)} \\ 0 \\ 0 \\ \vdots \\ 0 \end{vmatrix}$$

Let $D_h = |a_{ij}|$ denote the h X h determinant on the left side of the past equality. Then,

$b_{h-j} = 1/V(0) \cdot (-1)^j$. (co-factor of a_{ij} in D_h).

Let $B_h(z) = \sum_{j=1}^{h} b_j z^{j-1}$ so that consequently $B_1(z) = \frac{1}{V(0)}$.

then,

$$B_h(z) = \begin{vmatrix} z^{h-1} & -z^{h-2} & z^{h-3} & \cdots & (-1)^h \\ \frac{V(1)}{V(0)} & 1 & 0 & \cdots & 0 \\ \frac{V(2)}{V(0)} & \frac{V(1)}{V(0)} & 1 & \cdots & 0 \\ \vdots & & & & \\ \frac{V(h-1)}{V(0)} & \frac{V(h-2)}{V(0)} & \frac{V(h-3)}{V(0)} & \cdots & 1 \end{vmatrix}.$$

Now let

$$E_j = \begin{vmatrix} \frac{V(1)}{V(0)} & 1 & 0 & \cdots & 0 \\ \frac{V(2)}{V(0)} & \frac{V(1)}{V(0)} & 1 & \cdots & 0 \\ \vdots & & & & \\ \frac{V(j-1)}{V(0)} & \frac{V(j-2)}{V(0)} & \frac{V(j-3)}{V(0)} & \cdots & 1 \\ \frac{V(j)}{V(0)} & \frac{V(j-1)}{V(0)} & \frac{V(j-2)}{V(0)} & \cdots & \frac{V(1)}{V(0)} \end{vmatrix}$$

for $j \geq 1$ and let $E_o \equiv 1$.
Then,

$$B_h(Z) = Z\, B_{h-1}(z) + \frac{1}{V(0)} E_{h-1}$$

$$= Z\,[Z\, B_{h-2}(Z) + (1/V(0)E_{h-2}\,] + 1/V(0)\; E_{h-1}$$

$$= Z^2\, B_{h-2}(Z) + 1/V(0)\,[\,Z\, E_{h-2} + E_{h-1}]$$

$$= Z^{h-1}\, B_1 + 1/V(0)\,[\,Z^{h-2}\, E_1 + Z^{h-3}\, E_2 + \ldots + E_{h-1}].$$

Therefore,

$$B_h(Z) = \frac{1}{V(0)} \sum_{j=0}^{h-1} E_j Z^{h-j-1}.$$

Next, let $A_r = V(r)/V(0)$, so that

$$(-1)^j E_j = \begin{vmatrix} A_1 & A_2 & \cdots & A_j \\ 1 & A_1 & \cdots & A_{j-1} \\ 0 & 1 & \cdots & A_{j-2} \\ & & \cdots & \\ 0 & 0 & \cdots & A_1 \end{vmatrix} = (-1)^{j+1} \sum_{r=1}^{j} A_r E_{j-r}$$

Thus, we have the system of equations

$$\sum_{k=0}^{j} A_k E_{j-k} = \delta_{j,0,j} \geqslant 0,$$

which can be written in the form

$$\left(\sum_{j=0}^{\infty} E_j Z^j \right) \left(\sum_{j=0}^{\infty} A_j Z^j \right) \equiv 1,$$

so that

$$\sum_{j=0}^{\infty} E_j Z^j = V(0)/V(\theta).$$

Consequently, $B_h(Z) = \dfrac{Z^{h-1}}{V(0)} \sum_{j=0}^{h-1} E_j Z^j$

$$\therefore Z^{h-1} E^+(-h+1) \left(1/V(0)\right), \tag{10}$$

where $E^+(n) \sum_{k=-\infty}^{\infty} a_k Z^k = \sum_{k \geqslant n} a_k Z^k$.

Therefore, the minimizing function is

$$g_\infty^*(Z) = \left(\sum_{j=1}^{h} b_j Z^j \right) . V(\theta)$$

$$= Z^h . V(\theta) . E^+(-h+1) 1/V(\theta).$$

If we now let $1/V(\theta) = g(\theta) = \sum_{k=0}^{\infty} g(k) Z^{-k}$, then

$$g_\infty^*(Z) = \left(\sum_{k=1}^{h} g(h-k) Z^k \right) V(\theta) \tag{11}$$

Also,

$$a(m) = -\sum_{k=1}^{h} b_k V(m+k), \text{ and}$$

$$X_h = -\sum_{m=0}^{\infty} \sum_{k=1}^{h} g(h-k) V(k+m) X_{-m}. \tag{12}$$

3. The error of prediction based upon a finite section of the past

$$\text{Let } \mu_n = \left\| X_h - X_h \right\|^2 = \int \left| g_n^*(Z) \right|^2 C(\theta)\, d\theta$$

$$= \int \left| \sum_{j=1}^{h} b_j^{(n)} d_{n+j} \varphi(n+j,\theta) \right|^2 C(\theta)\, d\theta,$$

$$\text{where } \varphi(n,\theta) = d_n^{-1} e^{2\pi i n\theta} V(n,\theta).$$

Then

$$\mu_n = \sum_{j=1}^{h} \left| b_j^{(n)} \right|^2 \left| d_{n+j} \right|^2 = \sum_{j=1}^{h} \left| b_j^{(n)} \right|^2 V(n+j,0).$$

It is obvious that μ_n is a decreasing function of n and $\mu_n \to \mu$, where

$$\mu = \sum_{j=1}^{h} \left| b_j \right|^2 V(0). \text{Let } \delta_n = \mu_n - \mu, \text{ then } \delta_n \to 0 \text{ and } n \to \infty$$

We will now study the relationship between δ_n $(n \to \infty)$ and the spectral density function $C(\theta)$.

$$\delta_n = \int \left\{ \left| g_n^*(Z) \right|^2 - \left| g_\infty^*(Z) \right|^2 \right\} C(\theta)\, d\theta$$

$$= \int \left| g_n^*(Z) - g_\infty^*(Z) \right|^2 C(\theta)\, d\theta + 2 \operatorname{Re} \int \overline{\left(g_n(Z) - g_\infty^*(Z) \right)} g_\infty^*(Z)\, C(\theta)\, d\theta. \tag{13}$$

Since $g_\infty^*(Z)$ is the minimizing function, then

$$\int \left| g_\infty^*(Z) + \varepsilon e^{-2\pi i m\theta} \right| C(\theta)\, d\theta \geq \int \left| g_\infty^*(Z) \right|^2 C(\theta)\, d\theta$$

for all $m > 0$, and for all complex .

It follows that

$$\int \left| g_\infty^*(Z) \right|^2 C(\theta)\, d\theta + \left| \varepsilon \right|^2 C(\theta) + 2\mathrm{Re}\, \varepsilon \int g^*(Z)\, e^{2\pi i m\theta} C(\theta)\, d\theta$$

$$\geq \int \left| g^*(Z) \right|^2 C(\theta)\, d\theta .$$

So,

$$\left| \varepsilon \right|^2 C(\theta) + 2\,\mathrm{Re}\, \varepsilon \int g_\infty^*(Z)\, e^{2\pi i m\theta} C(\theta)\, d\theta > 0 \text{ for all complex}$$

ε and $m \geq 0$.

Consequently,

$$\int g_\infty^*(Z)\, e^{2\pi i m\theta} C(\theta)\, d\theta = 0 \text{ for } m > 0. \tag{14}$$

The corresponding result for the finite predictor is

$$\int g_n^*(Z)\, e^{2\pi i m\theta} C(\theta)\, d\theta = 0,\ 0 < m < n. \tag{15}$$

Using (15) in (13) we get

$$\delta_n = \int \left| g_n^*(Z) - g_\infty^*(Z) \right|^2 C(\theta)\, d\theta . \tag{16}$$

In the following we will assume $C(\theta)$ to be a positive continuous function and $\alpha > 1$, unless otherwise specified. From the first part we ge $0 < M < C(\theta) \leq M_2 < \infty$.

Now suppose that $C(\theta) = \sum_{k=-\infty}^{+\infty} C(K)\, e^{2\pi i k\theta}$, and that $\sum_{k>1n1} \left| C(K) \right|^2 = o(n^{-\alpha})$. Then $C(\theta)\, \varepsilon\, \zeta(\alpha)$, where $\xi(\alpha)$ is a Banach Algebra of type B, (10).

So,

$$0 < \delta_n = \int |g_n^*(Z) - g_\infty^*.(Z)|^2 \, C(\theta) \, d\theta$$

$$\leqslant M_2 \left\{ \sum_{m=0} \left| a(,m) - a(m) \right|^2 \sum_{m=n+1}^{\infty} \left| a(m) \right|^2 \right\} \qquad (17)$$

Consider the functions

$$h^{(n)}(\theta) = \sum_{m=0}^{n} a(n,) \, e^{-2\pi i m\theta}$$

and, $H(\theta) = \sum_{m=0}^{\infty} a(m) \, e^{-2\pi i m\theta}$.

Let $H^{(n)}(\theta) = \sum_{m=0}^{n} a(m) \, e^{-2\pi i m\theta}$

From (14) and (15) we have

$$\int h^{(n)}(\theta) \, e^{2\pi i k\theta} \, C(\theta) \, d\theta = C(-h-k), \, 0 \leqslant K \leqslant n,$$

$$\int H(\theta) \, e^{2\pi i k\theta} \, C(\theta) \, d\theta = C(-h-K), \, 0 \leqslant K .$$

Therefore,

$$\int \left[H^{(n)}(\theta) - h^{(n)}(\theta) \right] e^{2\pi i k\theta} \, C(\theta) \, d\theta$$

$$= \mu_k = \int \left[H^{(n)}(\theta) - H(\theta) \right] e^{2\pi i k\theta} \, C(\theta) \, d\theta, \, 0 \leqslant k \leqslant n .$$

Since $C(\theta)$ is a positive continuous function, the conditions for theorem 2 in (7) are satisfied and there exist constants K_c, N_c, depending only on C, such that

$$\left\{ \sum_{m=0}^{n} \left| a(m) - a(n,m) \right|^2 \right\}^{1/2} \leqslant K_c \left\{ \sum_{k=0}^{n} \left| \sum_{k=0}^{n} \left| \mu_k \right|^2 \right\}^{1/2}$$

$$\leqslant \left\| (H^{(n)} - H) \, C(\theta) \, K_c \right\| 2$$

$$\leqslant K_c \, M_2 \left\| H^{(n)} - H \right\|_2, \, n \geqslant N_c ;$$

i.e.,

$$\sum_{m=0}^{n} \left| a(n,m) - a(m) \right|^2 \leq M_3 \sum_{m=n+1}^{\infty} \left| a(m) \right|^2 , n \geq N_c . \qquad (18)$$

Using (18) in (17) we get

$$0 < \delta_n \leq M_2 (1 + M_3) \sum_{m=n+1}^{\infty} |a(m)|^2, n > N_c .$$

$$\text{Since } g_{\infty}^{*}(Z) \varepsilon \xi(\alpha), \text{ then } \sum_{m=n+1}^{\infty} |a(m)|^2 = o(n^{-\alpha})$$

which implies $\delta_n = o(n^{-\alpha})$.
To summarize, we proved the following theorem.

Theorem 2:

If $C(\theta)$ is a positive continuous function, $\alpha > 1$, and
If $C(\theta) \varepsilon \xi(\alpha)$, then $\delta_n = o(n^{-\alpha})$.
Now suppose that $\delta_n = o(n^{-\alpha})$. Then,

$$\delta_n = \int | g_n^{*}(Z) - g_{\infty}^{*}(Z) |^2 C(\theta) \, d\theta$$

$$\geq M_1 \left[\sum_{m=0}^{n} |a(n, m) - a(m)|^2 + \sum_{m=n+1}^{\infty} |a(m)|^2 \right.$$

$$\geq M_1 \sum_{m=n+1}^{\infty} |a(m)|^2 > 0.$$

So $\delta_n = o(n^{-\alpha})$ if and only if $\sum_{m=n+1}^{\infty} |a(m)|^2 = o(n^{-\alpha})$ if and only if $g^{*}(Z) \varepsilon \xi(\alpha)$.

If we assume that $E^{+}(-h+1)\, 1/V(\theta) \neq 0 \; \forall \theta$, then by the Wiener-Le´vy theorem we have

$$1/V(\theta) = 1 / \left[g_{\infty}^{*}(Z) / Z^{h} \left[E^{+}(-h+1)\, 1/V(\theta) \right] \right] \varepsilon \, \xi(\alpha).$$

Consequently,

$C(\theta) = (d^2 / |V(\theta)|^2) \, \varepsilon \, \xi(\alpha)$, and we proved the following result.

Theorem 3:

Let $C(\theta)$ be positive continuous function and $\alpha > 1$. If $E^+ (-h+1)\, 1/V(\theta) \neq 0$ for all θ, then $\delta_n = o(n^{-\alpha})$ if and only if $C(\theta)\, \varepsilon \xi(\alpha)$.

Remarks

It is worth noting here that this condition is always true in the lag 1 case since $E^+(0)\, 1/V(\theta) = 1/V(0) \neq 0$. Also, for large h, this condition will hold because of the continuity of $C(\theta)$ and $V(\theta) \neq 0$.

4. The additional error of prediction

It is often easier to find the a (m)'s than the a (n, m)'s, so in this section we will consider the additional error introduced if we use the values $\{ a(m) \}_0^n$ instead of $\{ a(n,m) \}_{m=0}^n$ in the finite predictor.

The additional error is given by

$$\Delta_n = \int \left\{ |g_n(Z)|^2 - |g_n^*(Z)|^2 \right\} C(\theta)\, d\theta \qquad (19)$$

where

$$g_n(Z) = Z^h - \sum_{m=0}^{n} a(m)\, Z^{-m}.$$

Then,

$$\Delta_n = \int |g_n(Z) - g_\infty^*(Z)|^2\, C(\theta)\, d\theta - \int |g_n^*(Z) - g_\infty^*(Z)|^2\, C(\theta)\, d\theta = \Delta_n^{(1)} - \delta_n$$

Theorem 4:

Let $C(\theta)$ be a positive continuous function and $\alpha > 1$. Then $C(\theta)\, \varepsilon \xi(\alpha)$ if and only if $\Delta_n^{(1)} = o(n^{-\alpha})$.

To prove this result we will use the formula for $\Delta_n^{(1)}$ which is

$$\Delta_n^{(1)} = \int |g_n^*(Z) - g_n(Z)|^2\, C(\theta)\, d\theta$$

where

$$0 \leqslant \Delta_n^{(1)} \leqslant M_2 \sum_{m=0}^{n} |a(n,m) - a(m)|^2 .$$

Using (18) we get

$$0 \leqslant \Delta_n^{(1)} \leqslant M_2 M_3 \sum_{m=n+1}^{\infty} |a(m)|^2 .$$

Now, $C(\theta)\, \varepsilon\, \xi(\alpha)$ implies that $V(\theta)\, \varepsilon\, \xi(\alpha)$ which implies that $g_\alpha^*(Z)\, \varepsilon\, \xi(\alpha)$ .. consequently, $\Delta_n^{(1)} = o(n^{-\alpha})$.

Theorem 5:

Let $C(\theta)$ be a positive continuous function, $\alpha > 1$, and $E^{+}(-h+1)\, 1/V(\theta) \neq 0$. Then,

$\Delta_n^{(1)} = o(n^{-\alpha}) \to C(\theta)\, \varepsilon\, \xi(\alpha)$.

To prove this theorem, we see that since

$$\Delta_n^{(1)} = \int |g_n(Z) - g_\infty^*(Z)|\, C(\theta)\, d\theta,$$

then

$$\Delta_n^{(1)} \geq M_1 \sum_{m-n+1}^{\infty} |a(m)|^2 > 0.$$

So,

$\Delta_n^{(1)} = o(n^{-\alpha}) \to g_\infty^*(Z)\, \varepsilon\xi(\alpha)$. Since $E^{+}(-h+1)\, 1/V(\theta) \neq 0$,

then, $V(\theta)\, \varepsilon\xi(\alpha) \to C(\theta)\, \varepsilon\xi(\alpha)$.

ACKNOWLEDGEMENTS

The author would like to thank Professor G. E. Baxter for suggesting the problem. Additionally, thanks goes to Professor H. Salehi for the important contributions made to this work through discussions.

I wish to thank my colleagues Professor E. K. Bowen, Professor J. C. Saber, and Professor A.A. Shah for their editing remarks. Finally, the author is deeply grateful to Miss Janet Manter whose good humor was tried by the typing requirements of this paper.

REFERENCES

1. G.E. Baxter; Polynomials Defined by Difference System, BAMS (1960).
2. G.E. Baxter, Polynomials Defined by a Difference System, J. Math. Anal Applic. (1961).
3. G.E. Baxter, A Convergence Equivalence Related to Polynomials Orthogonal on the Unit Circle, TAMS (1961).
4. G.E. Baxter, A Norm Inequality for a "Finite-Section", Wiener-Hopf Equation, Ill., J. Math. (1963).
5. G.E.Baxter, An Asymptotic Result for the Finite Predictor, Math. Scand, (1962).
6. A. Devinatz, Asymptotic Estimates for the Finite Predictor, Math. Scand. (1974).
7. Linear Operators, Part 1, Dunford and Schwartz, Interscience Publishers, Inc., 1958.
8. U. Grenander and G. Szego, Toeplitz Forms and Their Application, Berkeley and Los Angeles (1958).
9. Helson and Szego, Theory of Prediction Theory.
10. I.I. Hirschman, Jr., J. Math. Anal. and Applic. (1965).

SHORT NOTE ON THE APPLICATION OF HOCKING AND SMITH'S PROCEDURE IN SELECTION INDEX ESTIMATION

Abdul Majid H. Al-Nasir* and Nawal Majid G. Al-Wasiti*

Received, 10th April, 1976

INTRODUCTION

Practicing statisticians are faced with the task of analyzing incomplete data, such data may arise by chance or there may be economical or physical reasons for collecting the data in an incomplete form.

In 1968 Hocking and Smith[1] developed a method for estimating the parameters in a multivariate normal distribution with missing data.

This research applies the Hocking and Smith technique to the selection index problem. Incidently, estimates of phenotypic means and covariance matrix are also obtained.

Hocking and Smith Technique

Hocking and Smith technique[1] can be summarized as follows;

1. Group the data according to the missing variates.
2. For each group construct the best unbiased estimates of the parameters using only the data in that group.
3. Beginning with the estimates obtained for the full data group (i.e, the group whose observation vector have no missing variates) adjoin optimally the other estimates sequentially by the addition of linear combinations of estimates based on the sufficient statistics and having zero expectation.

As an illustration of this technique, assume a sample of size n consisting of n_1 observations from $N_p({}_1\mu, {}_1\Sigma)$ with likelihood function L_1 and n_2 observations from $N_q({}_2\mu, {}_2\Sigma)$, $q < p$ with likelihood function L_2. Denote by ${}_1\hat{\mu}_i$, $i = 1,...,p$ and ${}_1\hat{\sigma}_{ij}$, $i,j = 1,...,p$ the maximum likelihood estimates of the parameters based on the n_1 complete observations. Denote by $2\hat{\mu}_r$, $r = 1,...,q$ and $2\hat{\sigma}_{rt}$, $r, t = 1,...,q$ the maximum likelihood estimates of the parameters based only on the n_2 q-variate observations. Then the general estimates are:-

* Faculty of Science, Al-Mustansiriyah University, Baghdad-IRAQ.

$$\tilde{\mu}_i = {}_1\hat{\mu}_i + \sum_{r=1}^{q} \alpha_r \, ({}_1\hat{\mu}_r - {}_2\hat{\mu}_r) \ldots\ldots\ldots \quad (1)$$

$$i = 1,\ldots,p$$

$$\tilde{\sigma}_{ij} = {}_1\hat{\sigma}_{ij} + \sum_{r \leq t=1}^{q} \alpha_{rt} \, ({}_1\hat{\sigma}_{rt} - {}_2\hat{\sigma}_{rt}) \ldots \quad (2)$$

$$i,j = 1,\ldots,p$$

By choosing α_r and α_{rt} optimally (so as to minimize the variance), equations (1) and (2) give a minimum variance unbiased estimates of the desired parameters.

Suppose that we have other observations n_3 from N_s $({}_3\mu, {}_3\Sigma)$, $s < p$ with likelihood function L_3.

Denote by ${}_3\hat{\mu}_r$, $r = 1,\ldots,s$ and ${}_3\hat{\sigma}_{rt}$, $r, t = 1, \ldots, s$, which are the maximum likelihood estimate of parameters based only on the n_3, s-variate observations.

Then by adjoining this additional information to the estimates obtained in equations (1) and (2) we get

$$\mu_i^* = \tilde{\mu}_i + \sum_{r=1}^{s} \beta_r \, (\tilde{\mu}_r - \hat{\mu}_r), \; i = 1,\ldots,p \quad \ldots\ldots(3)$$

$$\sigma^*_{ij} = \tilde{\sigma}_{ij} + \sum_{r \leq t=1}^{s} \beta_{rt} \, (\tilde{\sigma}_{rt} - \hat{\sigma}_{rt}), \; i,j = 1,\ldots,p \ldots \quad ..(4)$$

where β_r and β_{rt} are chosen optimally as before.

Selection Index Estimation

The selection index is a well known procedure for grading individuals in large groups and has been applied to animal breeding programs.

Define

$$I_j = b, X_j \quad (5)$$

where I_j is a composite index value associated with the j^{th} member of the population, b is the n x 1 vector of the unknown coefficients denoting the value of the n traits and X_j is the n x 1 vector of the phenotypic values (observations) on the j^{th} member of the population. Following Smith and Pfaffenberger[3] we let

$$b = p^{-1} G \alpha \quad \ldots.(6)$$

where P is the n x n covariance matrix of phenotypic values, G is the n x n matrix of genotypic values, and α is the n x 1 vector of economic weights associated with the n traits.

Assuming that G and α are known, we obtained the estimate of the vector μ of the phenotypic means by using the technique of Hocking and Smith. Our procedure can be best illustrated by the following artificial example.

Example

Consider the following situation.

Traits	X_1	X_2
Observations	9	13
	7	8
	11	12
	12	
	8	
		9
		13

The data can be divided into three groups.
In group 1, we have $n_1 = 3$ observations on (x_1, x_2)
In group 2, we have $n_2 = 2$ observations on x_1
In group 3, we have $n_3 = 2$ observations on x_2

Now, within each group we can obtain the best unbiased estimate of the parameters.
In Group 1, we have

$$\begin{pmatrix} {}_1\hat{\mu}_1 \\ {}_1\hat{\mu}_2 \end{pmatrix} = \begin{pmatrix} 9 \\ 11 \end{pmatrix} \quad , \quad \text{and} \quad \begin{pmatrix} {}_1\hat{\sigma}_{11} \\ {}_1\hat{\sigma}_{12} \\ {}_1\hat{\sigma}_{12} \end{pmatrix} = \begin{pmatrix} 4 \\ 4 \\ 7 \end{pmatrix}$$

In group 2, we have

$${}_2\hat{\mu}_1 = 10 \quad , \quad {}_2\hat{\sigma}_{11} = 8$$

In group 3, we have

$${}_3\hat{\mu}_2 = 11 \quad , \quad {}_3\hat{\sigma}_{22} = 8$$

To combine the estimate obtained from groups 1 and 2, we use equations (1) and (2) and obtain

$$\tilde{\mu}_i = \begin{pmatrix} 9.4 \\ 11.4 \end{pmatrix} \quad , \quad \text{and} \quad \tilde{\sigma}_{ij} = \begin{pmatrix} 5.32 \\ 5.32 \\ 8.32 \end{pmatrix}$$

Adjoining the information in group 3 using equations (3) and (4) we obtain

$$\mu_i^* = \begin{pmatrix} 9.34 \\ 11.264 \end{pmatrix} \quad , \quad \text{and} \quad \sigma_{ij}^* = \begin{pmatrix} 5.206 \\ 5.2688 \\ 8.221 \end{pmatrix}$$

Therefore, the final estimates of the phenotypic covariance matrix and the phenotypic mean vector are given by

$$\hat{p} = \begin{pmatrix} 5.21 & 5.27 \\ & 8.22 \end{pmatrix} \text{and} \quad \hat{\mu} = \begin{pmatrix} 9.34 \\ 11.26 \end{pmatrix}$$

Let us take the matrix of the genotypic values, and the economic weights vector as

$$G = \begin{pmatrix} 2 & 0.75 \\ & 3 \end{pmatrix}, \text{ and } \alpha = \begin{pmatrix} 1 \\ 1 \end{pmatrix}.$$

Using equation (6) we estimate

$$\hat{b} = \begin{pmatrix} 0.19 \\ 0.34 \end{pmatrix}$$

and then, it can be determined from equation(5).

CONCLUSION

The estimation procedure developed by Hocking and Smith for the case of missing data can be extend to other situations if the covariance matrix required is available for the calculation of the coefficients. In this research we show that the above technique can be used in the selection index.

REFERENCES

1. Hocking,.R.R. and Smith W.B., "Estimation of parameters in the multivariate normal distribution with missing observation" *JASA*, 1968. pp. 159-173.

2. Nasir, A.M., "Prior distribution and order relations in the estimation of multivariate normal parameters with partial data" M.S. Thesis 1968, Texas.

3. Smith W.B. and Pfaffenberger, R.C., "Sélection index estimation from partial multivariate normal data", *Biometrics*,vol. 26, 1970, pp. 625-639.

المقـدمـة

يسر هيئة تحرير « مجلة علوم المستنصرية » أن تقدم العدد الأول من المجلة الى المجتمع العلمي في العراق وفي الوطن العربي . وتأمل أن تكون هذه المجلة العلمية مساهمة ايجابية من الجامعة المستنصرية لأجل تطور وتقدم بحوث العلوم الأساسية في وطننا العربي .

وتعني المجلة بنشر البحوث الأصيلة والنشرات القصيرة والرسائل الى المحرر في فروع العلوم المختلفة . ويجب أن تكون البحوث المقدمة للنشر جديدة وسيعني تقديمها أنه لم يسبق نشرها بأي لغة وأنها لم ترسل للنشر الى جهة أخرى . هذا وترسل البحوث الى محكمين من داخل أوخارج العراق للمساعدة في اختيار البحوث المناسبة .

ان نجاح وديمومة المجلة يعتمد في الأساس على دعم كافة العاملين في الحقل العلمي في العراق وفي الوطن العربي ، والأمل عظيم أن يساهم الجميع في مساعدة هذه المجلة حتى تحقيق أهدافها المكرسة لخدمة العلم والتقدم في الأمة العربية .

« هيئة التحرير »

مجلة علوم المستنصرية

طالب

المجلد ١ كانون الأول ١٩٧٦

مؤسسة دار الكتب للطباعة والنشر
جامعة الموصل

مجلة علوم المستنصرية

المجلد ١ كانون الأول ١٩٧٦

كلية العلوم — الجامعة المستنصرية — بغداد — العراق —

تعليمات للمؤلفين

١. تقدم ثلاث نسخ من البحث مطبوعة على الآلة الكاتبة وعلى ورق ابيض صقيل وتترك مسافة ٢,٥ سم على يسار كل صفحة .
٢. تقدم خلاصة باللغة العربية وأخرى باللغة الانكليزية وتطبع كل منهما على ورقة منفصلة .
٣. يطبع عنوان البحث وكذلك اسم المؤلف (او المؤلفين) وعنوانه على ورقة منفصلة ويكتب اسم المؤلف كاملا كان يكتب (احمد م. علي) .
٤. تقدم الرسوم التوضيحية منفصلة عن مسودة البحث وترسم بالحبر الصيني الاسود على ورق شفاف وترفق ثلاث صور لكل رسم وتكتب عناوين الرسوم على نفس الورقة .
٥. تنظم الجداول باسلوب تجعلها مفهومة دون اللجوء الى النص وذلك باعطاء كل جدول وكل عمود وصفا واضحا .
٦. لايجوز اعطاء المعلومات ذاتها بالرسم وبالجدول في وقت واحد الا اذا اقتضت ضرورة النقاش ذلك .
٧. يشار الى المصدر برقم ضمن قوسين [بعد الجملة مباشرة وتطبع كافة المصادر على ورقة منفصلة ويتوجب عند ذكر مختصرات اسماء المجلات اتباع اسلوب
٨. من المحبذ حيثما كان ممكنا ان يتسلسل البحث ليتضمن المقدمة ، طرق التجربة ، النتائج ، المناقشة.

مجلة علوم المستنصرية

طالب

المجلد ١ كانون الأول ١٩٧٦

مؤسسة الكتب الطباعة والنشر